Adina Friedl

Establishment of qRT-PCR for the analysis of the time dependent expression profile of microRNA-451 in hippocampus following severe traumatic brain injury in rat

To obtain the degree of

Master of Science

(MSc)

at Graz University of Technology

Supervised by:

Univ.-Prof. Dr. Ute Schäfer

Head of the Research Unit for Experimental Neurotraumatology

at Institute of Neurosurgery, Medical University of Graz

February 2014

Eidesstattliche Erklärung

Ich, Adina Friedl, erkläre ehrenwörtlich, dass ich die vorliegende Arbeit mit dem Thema *„Establishment of qRT-PCR for the analysis of the time dependent expression profile of microRNA-451 in hippocampus following severe traumatic brain injury in rat“* selbstständig und ohne fremde Hilfe verfasst habe, andere als die angegebenen Quellen nicht verwendet habe und die den benutzen Quellen wörtlich oder inhaltlich entnommenen Stellen als solche kenntlich gemacht habe. Die Arbeit hat in gleicher oder ähnlicher Form noch keiner anderen Prüfungsbehörde vorgelegen und wurde auch noch nicht veröffentlicht.

Ort, Datum	Mag. Adina Friedl

Acknowledgements

My special gratitude goes to everyone that contributed to the successful outcome of this work:

First and foremost, I would like to thank to my supervisor, *Univ.-Prof. Dr. Ute Schäfer*, for this interesting topic, the valuable guidance and advice, her trustful support and best working atmosphere.

I would like to gratefully acknowledge the enthusiastic advice of *Univ.-Ass. Dr. Silke Patz*, and to express my gratitude to all my colleagues for the stimulating discussions, help with experimental setup and general advice during this work, especially *MSc Muammer Ücal*, *MSc Mag. Christa Trattnig*, *Mag.(FH) Ulrike Fasching*, *Mag. Klaus Kraitsy*, *Verena Weiss, BMA Gerda Grünbacher*, *MSc Stefan Haubenwallner.*

I am forever grateful to my family for permanent affection, understanding and encouragement.

Last but not least I thank to my husband, *Karl*, for his kindness and patience during my entire study and especially throughout this time-consuming work, offering me support in every sense, always.

Zusammenfassung

Gehirnverletzungen als Hauptursache für Morbidität und Mortalität, induzieren multiple zelluläre pathologische Veränderungen, einschließlich Entzündung, Exzitotoxität und oxidativen Stress, Apoptosis, gestörter Plastizität und Regeneration, durch Änderung der Gen- und Proteinexpression, was zu langfristigen neurologischen Defiziten führt.

Da die bestehenden Behandlungen noch ineffizient sind, sind weitere Studien notwendig, um die genauen molekularen und zellulären Mechanismen der zugrunde liegenden neuronalen Schäden nach Hirntrauma zu verstehen und bessere therapeutische Strategien zu entwickeln.

MiRNAs als wichtige Regulatoren der Genexpression befinden sich reichlich im Nervensystem und sind bei der Aufrechterhaltung der neuronalen normalen Funktion und Homöostase beteiligt, welche mit der neuronalen Entwicklung, Differenzierung, Neurogenese, synaptischen Plastizität und Gedächtnis verbunden sind.

Bisherige Studien zeigten wesentliche Änderungen der miRNAs im Hippocampus nach Hirnschädigung, besonders für miR-451, was auf seiner wichtigen regulatorischen Rolle in Trauma-bezogenen zellulären Ereignissen schließen lässt.

Die vorliegende Arbeit konzentrierte sich auf die posttraumatischen Änderungen der miR-451-Expression im Hippocampus, welcher als wesentliche Gehirnregion für Gedächtnis, Kognition und Emotion, beim Hirntrauma besonders gefärdet ist.

Das temporale miR-451 Expressionsniveau nach induziertem schweren Hirntrauma in einem "Fluid Perkussion Schädigung" Rattenmodell, wurde über die qRT-PCR Analyse des ipsilateralen hippocampalen Gewebes bestimmt und als Änderung des ct-Wertes, im Vergleich zum Schein-Trauma dargestellt.

miR-451 wurde am Tag 1 post-trauma über-exprimiert gefunden, am Tag 4 invariant, nach 1 Woche ($p=0,0016$) und nach 2 Wochen ($p=0,0015$) statistisch signifikant unter-exprimiert und nach 3 Wochen nur leicht unter-exprimiert.

Abstract

Traumatic brain injuries are a major cause of morbidity and mortality, inducing multiple cellular pathological changes, including inflammation, excitotoxicity and oxidative stress, apoptosis, impaired plasticity and regeneration, by altering the gene and protein expression patterns, resulting in long term neurological deficits.

Since the existing treatments are still inefficient, further studies are request to elucidate the exact molecular and cellular mechanisms underlying the neuronal damage following TBI, for to develop better therapeutic strategies.

Abundant in the nervous system, miRNAs as gene expression key regulators are involved in the maintaining of neuronal normal function and homeostasis that is related to neuronal development, differentiation, neurogenesis, synaptic plasticity and memory.

Studies revealed post-TBI altered hippocampal miRNAs, particularly miR-451, suggesting its critical regulatory role in injury-related cell events.

The present work was focused on post-injury miR-451 expression changes in hippocampus, as an essential brain region for memory, cognition and emotion, vulnerably to TBI.

After induced severe TBI in a rat “fluid percussion injury” (FPI) model, miR-451 temporal expression level, determined by qRT-PCR analysis of ipsilateral hippocampal tissue, presented as change in threshold cycle (ct), compared to sham operated animals, was found up-regulated at day 1, invariant at day 4, statistically significant down-regulated at 1 week ($p=0.0016$) and 2 weeks ($p=0.0015$), being less decreased at 3 weeks’ time point.

Table of contents

List of abbreviations

ADAR	Adenosine Deaminase Acting on double stranded RNA
AGO	Argonaute proteins
ATP	Adenosin triphosphate
BBB	Blood brain barrier
BDNF	Brain derived neurotrophic factor
CA3 region	from Cornu Ammonis / hippocampus has CA1-CA4 regions
CCI	controlled cortical impact
CBF	Cerebral blood flow
CD133	prominin-1, cholesterol-binding glycoprotein
cDNA	Complementary DNA
CNS	Central nervous system
CSF	Cerebrospinal fluid
cp	crossing point
ct	threshold cycle
DCX	Doublecortin
DEPC	Diethyl pyrocarbonate
DG	Dentate gyrus
DGCR8	DiGeorge syndrome critical region 8 protein
DNA	Deoxyribonucleic acid
dsRBD	double-stranded RNA-binding domain
ECT	Electroconvulsive shock therapy
FA	Formaldehyde
FGFR1	Fibroblast growth factor receptor 1
FPI	Fluid Percussion Injury
GCL	Granule cell layer
GCS	Glasgow Coma Scale
GFAP	Glial fibrillary acidic protein
GTP	Guanosin triphosphate
HSP	Heat Shock Protein
ICP	Intracranial pressure

IL-1	Interleukin-1
IPC	Ischemic preconditioning
KD	Knock-down
KO	Knock-out
LNA	locked nucleic acid
Loqs	Loquacious [Drosophila melanogaster (fruit fly)]
MAPK	Mitogen-activated protein kinases
miRNA	MicroRNA
ML	Molecular layer
MM	Mastermix
MP	Microparticle
ND	NanoDrop
NSC	Neural Stem Cells
nNOS	neuronal Nitric Oxide Synthase
OB	olfactory bulb
ORF	open reading frame
PACT	Protein ACTivator of the interferon-induced protein kinase
PCR	Polymerase Chain Reaction
Pre-miRNA	precursor miRNA
Pri-miRNA	primary miRNA
qRT-PCR	quantitative Real Time-PCR
Ran-GTP	Ras-related GTP-binding nuclear protein
RBP	Ribonucleotid binding protein, RNA-binding proteins
RISC	RNA-induced silencing complex
RMS	Rostral migratory stream
RNA	Ribonucleic acid
RNase	ribonuclease
RG	RiboGreen
RT-PCR	Reverse Transcription Polymerase Chain Reaction
SEM	Standard error of the mean
SD	Standard deviation
sev	severe

SGZ	Subgranular zone of dentate gyrus
sh	sham
shRNA	small hairpin RNA
siRNA	small interfering RNA
snoRNA	small nucleolar RNA
SVZ	Subventricular zone of the lateral ventricle
T-ALL	T cell acute lymphoblastic leukemia
TBI	Traumatic brain injury
TE-buffer	Tris-EDTA buffer
TF	Transcription factor
TNF	Tumor necrosis factor
TRBP	TAR (Trans-activation-responsive) RNA-binding protein
Tuj	neuron specific β II tubulin
UTR	untranslated region
Ywhaz	Tyrosine 3-Monooxygenase/Tryptophan 5-Monooxygenase Activation Protein, Zeta Polypeptide; gene product belongs to 14-3-3 family of proteins

List of figures

List of tables

1. THEORETICAL BACKGROUND

1.1. Traumatic brain injury

Traumatic brain injury (TBI) as an insult to the brain due to an external physical force to the cranium causes structural and functional impairment of the brain, still representing the leading cause of death and disability in individuals under the age of 50 worldwide (1). Each year occur in the U.S. about 1.7 million TBI-related deaths, hospitalizations, and emergency department visits (2).

Upon Glasgow coma scale (GCS) score after resuscitation, TBI is graded in *mild*, *moderate* and *severe* (Tab.1). Mild TBI (GCS 13–15) corresponds to a concussion with full neurological recovery. In moderate TBI (GCS 9–13) the patient is exhausted or stuporous, and in severe TBI (GCS 3–8) the patient is comatose, incapable to open the eyes or follow demands, having an increased risk of death due to hypotension, hypoxemia (low oxygen level in the blood), and edema (brain swelling), if these are not adequately treated (3).

Table 1: Glasgow coma scale, based on the level of TBI patient consciousness

Eye opening		Motor response		Verbal response	
Spontaneous	4	Obeys	6	Oriented	5
To speech	3	Localises	5	Confused	4
To pain	2	Withdraws	4	Inappropriate	3
None	1	Abnormal flexion	3	Incomprehensible	2
		Extensor response	2	None	1
		None	1		

1.1.1. TBI pathophysiology

TBI pathophysiology comprises numerous complex mechanisms that are interconnected and can be succinctly described by the following three stages:

(a) The **first stage** or **primary insult** (mechanical damage) occurring at the moment of impact, being *"ischemia-like",* is described by direct tissue damage with succeeding impairment of *cerebral blood flow* (CBF) and metabolism, and can't be therapeutically influenced.

(b) The **second stage** or **secondary insult** (non-mechanical, delayed damage) named also "*catabolic-* or *self-digesting-like*" is represented through a pathophysiological cascade (Fig.1), which is triggered by *cerebral ischemia* along with inadequate *intracranial pressure* (ICP) and is sensitive to therapeutic interventions.

(c) The **third stage** or **brain specific recovery stage** includes endogenous restorative brain plasticity processes like *neurogenesis*, *angiogenesis*, *axonal remodeling* and *synaptogenesis*, which can be also subject of curative intervention.

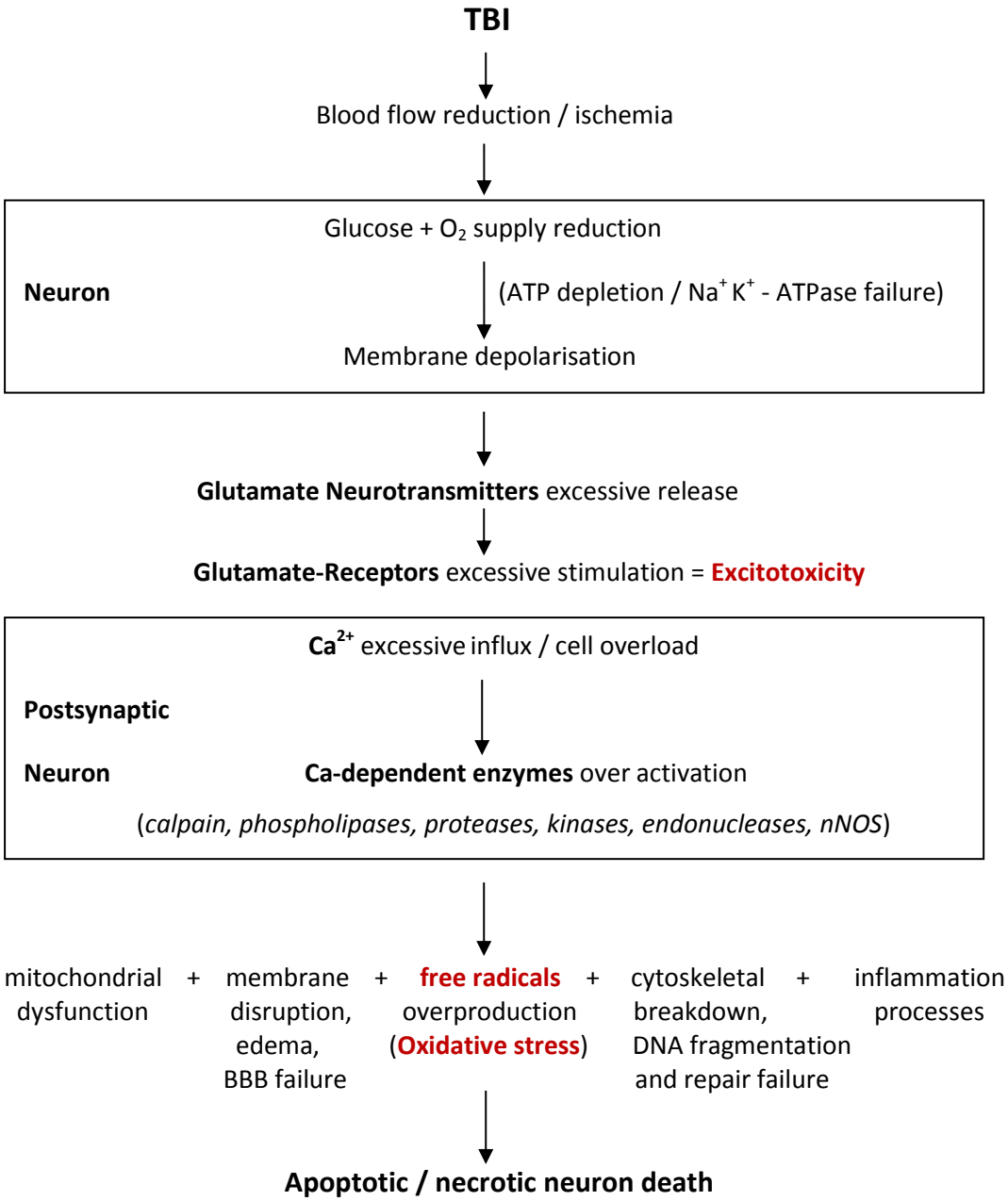

Figure 1: TBI pathophysiological cascade leading to neuron death

The TBI pathophysiology is reviewed in Fig.1 as an imbalance between the *cerebral blood flow* (CBF) and metabolism processes (4, 5) with subsequent neurotoxic cascade that finally leads to the membrane degradation of brain vascular and cellular structures in addition to the two forms of cell death: *necrosis*, as premature cell death in living tissue and *apoptosis*, as gene-directed "cell suicide" that affects only individual cells, leaving adjacent cells intact (6, 7). Acute trauma to the brain initiates a blood-flow reduction and consequent ischemia along with glucose and oxygen supply reduction. Therefore the ATP-stores decrease and energy-dependent membrane ion pumps fail with subsequent cell membrane depolarisation, thus compromising the brain homeostasis (8 , 9, 10).

After TBI astrocytes become "reactive" through phenotypic changes like: cytoplasm enlargement, elongation of the processes, up-regulation of glial fibrillary acidic protein (GFAP). Reactive astrocytes stimulate proinflammatory cytokines expression, swell and contribute to cerebral edema, failing to regulate the extracellular glutamate (11).

Excitotoxicity is due to the toxic action of massive release of glutamate excitatory neurotransmitters, which affects neurons and astrocytes through over-stimulation of glutamate receptors.

The succeeding down-stream neurotoxic cascade includes: an excessive Ca^{2+} influx and the over-activation of Ca-dependent enzymes along with free radicals overproduction and subsequent *oxidative stress*, mitochondrial dysfunction, membrane disruption, *edema* formation, blood brain barrier (BBB) integrity failure, *inflammation processes*, cytoskeletal break-down, DNA fragmentation and repair failure, leading after all to cell death and tissue destruction (12, 13, 14, 15).

1.1.2. TBI treatment strategies

As previously mentioned, beside the pathophysiological cascade, TBI induces also endogenous restorative brain plasticity processes like: *neurogenesis* (new neurons generation), *angiogenesis* (new capillaries from pre-existing vessels) and *vasculogenesis* (de novo blood vessels formation), *axonal remodelling* (axonal sprouting and pruning), *synaptogenesis* (new synapses formation). These processes provide promising treatment opportunities by amplifying them to promote post-TBI functional recovery (16, 17).

During life the neurogenesis generates continuously new neurons, mainly in two regions of the mammalian brain (A): ***subventricular zone*** **(SVZ)** of lateral ventricles (B) and ***subgranular zone*** **(SGZ)** within the **dentate gyrus of hippocampus** (C), Fig.2 (16, 18, 19).

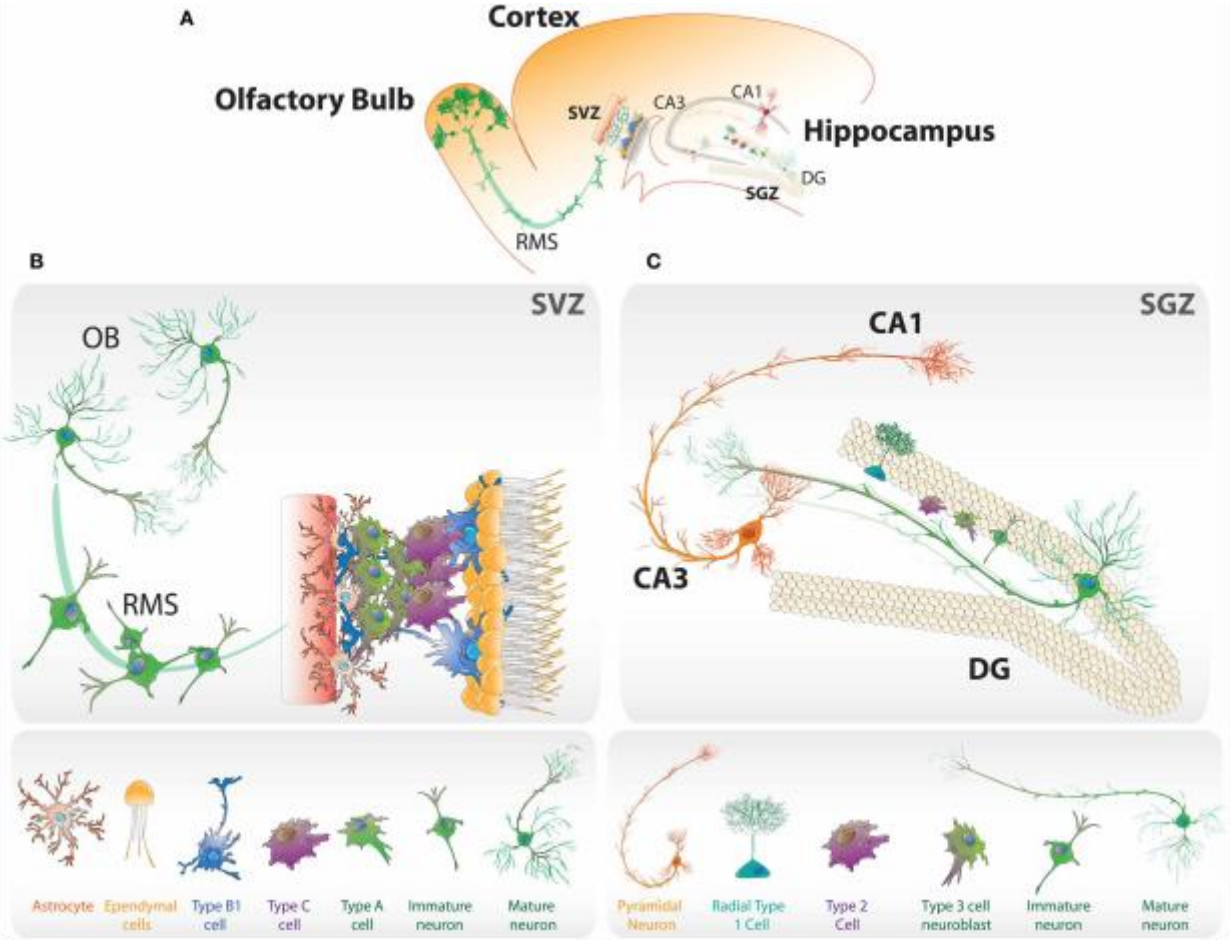

Figure 2: Schematic representation of the neurogenic niches in adult rodent brain (18)

In **SVZ** the ***astrocyte-like neural stem cells*** (NSC) called ***type B1 cells*** generate ***type C cells*** that rapidly proliferate producing ***type A neuroblasts***, which migrate through the **rostral migratory stream** (RMS) to the **olfactory bulb** (OB) where they mature into ***interneurons***.

Within **SGZ** the ***radial glial-like NSC,*** *progenitors, undifferentiated precursors* or ***type 1 cells,*** located at the bordure between **hilus** and **granule cell layer** (GCL), having a single radial process toward **molecular layer** (ML), give rise to **"fast proliferating"** ***type 2 cells*** that develop to neuronal lineage, differentiating into ***type 3 neuroblasts*** that become ***immature neurons*** extending dendrites toward molecular layer (ML), projecting their axons through hilus toward **CA3 region** and maturing during several weeks into ***dentate granule neurons*** that integrate into pre-existing hippocampal circuitry of GCL.

In rats was observed that TBI stimulates cell proliferation in hippocampus, where most of the new-born neurons of subgranular zone (SGZ) that survive 10 weeks after TBI can differentiate into mature neurons, contributing to cognitive recovery. Moreover, neuroblasts of sub ventricular zone (SVZ) migrate into "injured areas" instead into rostral migratory stream (RMS) and differentiate into neurons and glia (16).

To improve post-TBI functional recovery, experts suggest a combination of *neuroprotective* with *neurorestaurative* therapies, including drugs that reduce acute and delayed effects of TBI, stem cell-based along with pharmacological therapies for brain repair and brain cooling to stabilize the cerebral metabolism (16, 17, 20-27).

1.2. microRNAs

microRNAs are a class of small, 20-25nt long, single-stranded, highly conserved, non-coding RNA transcripts that negatively regulate the protein synthesis by targeting mRNAs at post transcriptional level (1, 28-37).

miRNAs play an important role in diverse biological processes such as cell cycle, development, cell proliferation and differentiation, apoptosis, metabolism, angiogenesis as well as immunity. Hence their dysregulation is associated with inflammation, autoimmunity, viral infections, heart diseases, neurodegeneration, and cancer (37-39).

In central nervous system (CNS) miRNAs are abundant, acting as key modulators of development and plasticity (30, 32, 39), therefore their altered expression is linked to the pathology of various neurological and neurodegenerative disorders (28, 32, 37, 39-42).

1.2.1. miRNAs biogenesis

Most of the miRNAs genes are located in intergenic regions, but some are found also in introns or exons of non-coding genes or inside of introns of protein-coding genes (32).

miRNA genes are typically transcribed by *RNA polymerase II* (few human miRNAs by *polymerase III*) to an "up to several thousand nt long" initial RNA transcript, the so-called **primary miRNA (pri-miRNA)**, which possesses a characteristic "stem-loop structure" that can be recognized and cleaved by *ribonuclease III (RNase III) endonuclease* **Drosha** within the nucleus (28, 40).

The cleavage product, named **precursor miRNA (pre-miRNA)**, is a -70nt long hairpin RNA with a 2nt 3'-overhang, which is recognized by ***Exportin-5*** and transported from nucleus to the cytoplasm in a Ran/GTP-dependent manner.

For an efficient cleavage **Drosha** requires a protein partner, **Pasha/DGCR8** that has a double-stranded RNA-binding domain (dsRBD) (35). **DGCR8** (DiGeorge syndrome critical region 8) protein increases eight fold Drosha activity and DGCR8 or Drosha knockdown (KD) induces pri-miRNAs accumulation, whereas pre-miRNAs amount decrease (32).

Some miRNAs bypass Drosha/DGCR cleavage: *miRtrons* as a subclass of miRNAs, encoded in introns of protein-coding genes, small hairpin shRNA-derived miRNAs, endogenous small interfering siRNA and also small nucleolar snoRNAs with a miRNA-related function outside of nucleolus (32, 39).

In cytoplasm **Dicer,** another conserved *RNase III enzyme*, together with its dsRBD protein partners, *TAR RNA-binding protein* (TRBP) and *PACT*, further process pre-miRNA into a **miRNA-miRNA* duplex**, consisting of the ~21nt mature miRNA strand and its star sequence, which is then unwound by the **helicase armitage**.

The mature miRNA strand (guide strand) is incorporated into a protein complex that include **Argonaute (AGO)** proteins, known as **RNA-induced silencing complex (RISC)**, whereas the other stand (passenger strand) is destroyed.

miRNA guide strand within RISC complex can bind in two ways: with imperfect complementarity to 3'UTR (untranslated region) of target mRNA, inducing translational repression or with perfect complementarity to ORF (open reading frame) causing target cleavage.

Dicer knock-out (KO) in *C. elegans* and mammalian cell lines leads to cytoplasmic pre-miRNA accumulation, first proved for **let-7**, a highly conserved miRNA, with role in developmental timing and involved in many forms of cancer.

As Fig.3 illustrates, most of miRNAs are processed from precursors with hairpin-structure by the consecutive action of the two RNase III enzymes: Drosha and Dicer. An exception to this makes **miR-451**, at which the processing is Dicer-independent and its cleavage is mediated by the endonuclease **Ago2** (32, 40, 43, 44, 46, 47).

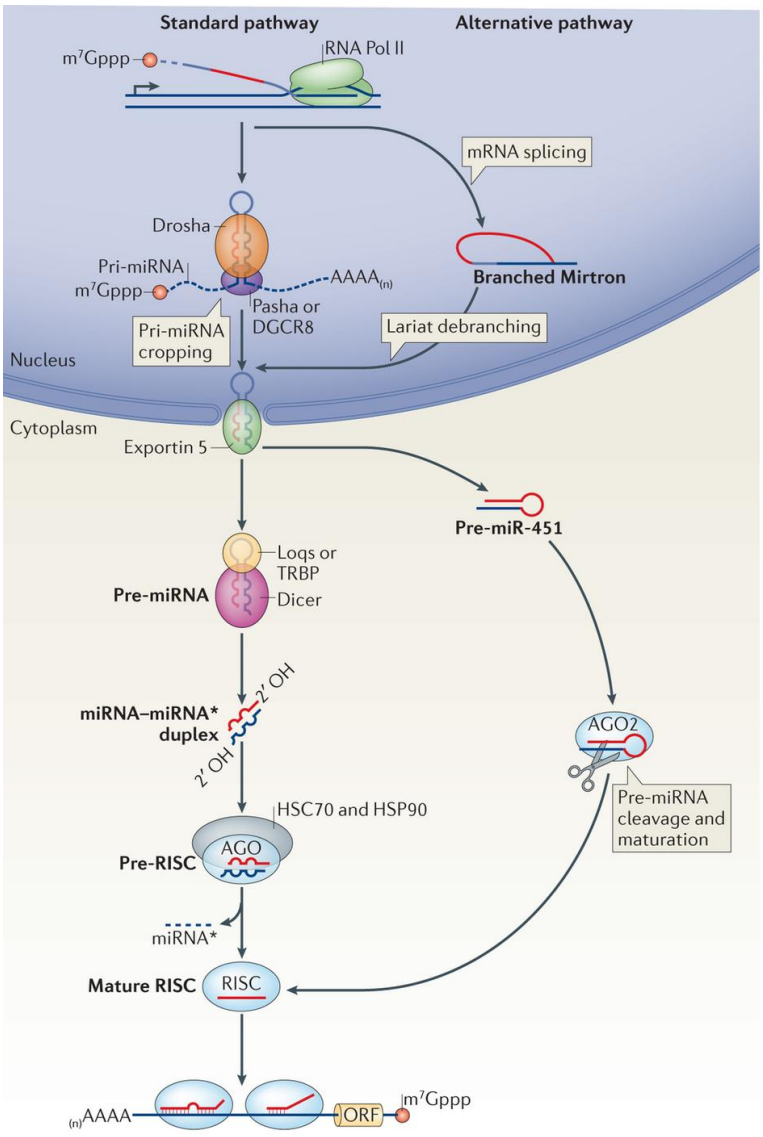

Figure 3: microRNA biogenesis pathway*

Fig. 3 illustrates the miRNA genes transcription by **RNA Pol II** to generate *pri-miRNAs*, whose hairpin structures are cleaved by **Drosha/Pasha, DGCR8** to release *pre-miRNAs*, which are then exported from nucleus into cytoplasm by **Exportin-RanGTP**, where they are further processed by **Dicer/Loqs (Loquacious), TRBP** to form an *~22 nt duplex*. The guide strand is next selected into the **RISC** protein complex to function as mature miRNA; the other strand is degraded. Mostly miRNA imperfect complementarity to target mRNA induces translational repression by binding to 3'-UTR, whereas a perfect complementarity causes target cleavage through binding to ORF. As exception, **miR-451** has a Dicer-independent processing, being cleaved by **Ago2** endonuclease.

* Ameres SL, Zamore PD, Diversifying microRNA sequence and function, Nature Reviews Molecular Cell Biology, Vol. 14, 475–488 (2013)

1.2.2. miRNA gene expression regulation

In animals, miRNA silencing of gene expression is mainly mediated by translational inhibition, which sometimes appears to be reversible, ensuring a dynamic miRNA mediated regulation, sensitive to specific cellular needs.

Since the mRNA target complementarity to miRNA seed region is only partial, one miRNA can potentially have hundreds of targets and conversely individual mRNAs can be regulated by many miRNAs, allowing vast combinatorial possibilities, providing the genetic complexity, associated with a multitude of essential biological processes (28, 32, 39, 45).

Compared with other tissues, the brain shows enriched ADAR (Adenosine Deaminase Acting on double stranded RNA) activity, that affect miRNA processing by the conversion of adenosine (A) to inosine (I), which then will be read as guanine (G). As consequence might appear changes in stem-loop stability of pri-miRNAs or in target mRNA selection, supposing to facilitate brain-specific expression (40).

1.2.3. miRNAs in CNS

The mammalian CNS is an amazingly complex system, particularly in humans with around 10^{18} synapses deriving from only about 10^{4} protein-coding genes (48) and requires a similarly complex network of molecular pathways to control its huge amount of various cellular processes and permanent adaptation to environmental signals (49).

It is postulated that around 50% of mammalian mRNAs are regulated by miRNAs in concerted action with transcription factors (TF) (50).

The miRNAs specificity for particular mRNAs depends on the intracellular concentrations, which in turn reflect the balance between protein degradation and biosynthesis (50, 51).

About 70% of all miRNAs, ubiquitous and brain-specific, are expressed in human nervous system to regulate its normal development and function (52, 53), in addition their misexpression is associated with diverse neurological diseases (51, 52, 54-62).

The *Dicer* gene deletion and subsequent failure of mature miRNAs expression showed: loss of stem cells populations with embryonic lethality (53), drastic myelination reduction via impaired oligodendrocytes differentiation (56, 58, 63, 64), as well as neurological and

neurodegeneration disorders as a result of abnormal morphology, loss of branching, disturbed axonal pathfinding and cell death of neurons subpopulations in distinct brain regions, including midbrain, cerebellum, hippocampus and cortex (28, 32, 65, 66).

Mature miRNAs lack in mice forebrain neurons by Dicer knock-out revealed learning improvement, due to better translation of "synaptic mRNAs", proved by increased levels of proteins that are translated in dendrites, known to affect plasticity, like BDNF (brain derived neurotrophic factor) etc. (67).

Able to regulate simultaneously many target genes, miRNAs show distinct profiles that are associated with various cellular processes like: neural stem cell (NSC) *self-renewal* and development, proliferation of NSC and progenitors, neuronal differentiation, maturation, synaptogenesis, dendrite remodelling and synaptic plasticity (50, 51, 53-58, 60-62, 68-72).

Current research proved miRNAs conserved role in the precise regulation of mammalian CNS proper development and maintenance (50, 53, 56).

Even in adult brains (*dentate gyrus* of hippocampus) is needed a tightly controlled *neurogenesis* for a normal cerebral function, including proliferation, fate specification, neuronal maturation, targeting, synaptic integration and survival of new-born neurons, confirming the structural plasticity in mature CNS (73, 74).

CNS injury produces profound molecular and cellular changes through tissue disturbance and consequent dysregulation of signalling pathways and regulatory mechanisms, including injury-associated miRNAs (46, 75-78).

Structural changes in Hippocampus are the most frequent consequences of TBI, confirmed by the about 60% TBI-patients with hippocampal atrophy, as well as cognitive and memory deficits (46).

Studies on TBI animal models revealed altered miRNAs expression, which during the post-injury *acute phase* were associated with cell pathology and stress management, targeting genes involved in apoptosis, protein folding and aerobic respiration and by contrast during the *chronic phase* were predicted to regulate genes of brain repair mechanisms, linked to cytoskeletal organisation and intracellular trafficking (46).

Injury-specific miRNAs may serve as *plasma biomarkers* to monitor brain injury since their expression profiles in rat brain (hippocampus) and in whole-blood correlate, showing more than 1.5 fold changes (79), and because of their abundance, specificity and stability in plasma (34, 46, 63, 78, 80). As example *miR-21* was reported to be modulated in all types of injury serving as "common cell-death regulator" in stroke, spinal cord and brain injury and studies with TBI patients revealed three miRNAs as promising diagnostic biomarkers for severe injury: *miR-16*, *miR-92a* and *miR-765* (34).

1.3. miR-451

Brain cells respond to traumatic injury through multiple pathological changes, including inflammation, excitotoxicity and oxidative stress, apoptosis, impaired plasticity and regeneration, by altering their gene and protein expression patterns, resulting in long term neurological deficits.

Abundant in the nervous system, miRNAs as gene expression key regulators are involved in maintaining of normal neuronal function and homeostasis that is related to neuronal development, differentiation, neurogenesis, synaptic plasticity and memory (34, 42, 81).

The present work was focused on **miR-451** in relation with its hypothesised key functions in TBI pathophysiology, as next described.

1.3.1. TBI related functions of miR-451

miR-451 is one of the well-known miRNAs that showed substantial change in expression after experimental TBI, as following studies (chronologically listed) reported:

- ***Redell et al. 2009*** (34) found miR-451 significantly up-regulation ($P<0.01$) at 3h and 24h post-TBI, in rat *ipsilateral hippocampus*, after controlled cortical impact injury (CCI), by microarray analysis. Using an independent set of animals by RT-PCR analysis, miR-451 was found down-regulated at 3h, up-regulated at 24h and invariant at 3 days post-TBI, but not significantly, maybe as a result of animal-to-animal responses variation. The RT-PCR analysis for the *contralateral hippocampus* indicated a miR-451 down-regulation at all three time points, statistically significant at 3 days' time point.

- ***Lei et al. 2009*** (82) inform about a more than two times down-regulation of miR-451 at 6h and 48h post injury in rat *brain cortex*, by microarray analysis.

- ***Truettner et al. 2011*** (83) presented the cytoprotective effect of therapeutic hypothermia and miRNA profiles in rat cerebral cortex after fluid percussion injury (FPI), where miR-451 appeared up-regulated by both methods: microRNA array and RT-PCR analysis.

  In RT-PCR results miR-451 at 7hours post-TBI was increased ~ 2.84 fold in normotherapia animals, but appeared at sham levels in hypothermia group. At 24h, mir-451 was at sham levels for normotherapia, but ~ 3.16 fold increased for hypothermia animals.

- ***Hu et al. 2012*** (29) reported distinctive miRNAs expression profiles in hippocampus after 24h and 7 days, in rat controlled cortical impact (CCI) model, where miR-451 was found up-regulated at 24h time point.

- ***Truettner et al. 2013*** (84) inform that miR-451-overexpression, induced by stretch injury, leads to increased stress and vulnerability in transfected neurons.

  qRT-PCR of "uninjured cells" overexpressing miR-451 showed the most rise in the expression of 6 analysed genes, which respond to cellular pathologies like trauma and ischemia, as example both cytokines *IL1-β* (11 fold, $p<0.05$) and *TNF-α* (24 fold, $p<0.05$), pro-apoptotic gene *Caspase 11* (7 fold, $p<0.01$).

  qRT-PCR of "stretch injured" cells overexpressing miR-451 compared to non-injured controls showed significant high expression levels ($p<0.001$) for the genes *IL1-β*, *TNF-α* and molecular chaperone *HSP70*, which respond to miss-folded proteins or other cellular stress.

- ***O'Connor et al. 2013*** (85) investigate the "early-life stress" induced changes to multiple hippocampal miRNA and their role in depressive pathology. They found that antidepressant treatments (with selective serotonin reuptake inhibitor *fluoxetine*, rapid acting NMDAR antagonist *ketamine* and electroconvulsive shock therapy (ECT) reversed the stress-induced changes to miR-451.

- ***Patz et al. 2013*** (86) examined the cerebrospinal fluid (CSF), detecting firstly more abundance of *microparticles*[1] (MPs) in brain-injured vs. non-injured subjects. Only in isolated CSF-MPs of brain-injured patients was found a significant amount of miR-451, suggesting its key role in the adaptive response to TBI.

1.3.2. Other known key functions of miR-451

The miR-451 essential functions have been identified in a variety of biological contexts as numerous publications reported:

a) miR-451 as an erythroid specific miRNA (87), highly up-regulated during erythropoiesis (88), induces basolateral epithelial cell polarity (89), acting as an enhancer of normal erythroid differentiation (88, 90-94), being required for homeostasis (95). It protects against erythroid oxidant stress by repressing 14-3-3zeta (96, 97). Haemolysis caused miR-451 overexpression in plasma, without haemolysis miR-451 is sufficiently constant to serve as normaliser (98). miR-451 was recommended to be used in the artificial blood production technique, as well as in gene therapy of hemoglobinopathies (88).

b) miR-451 is involved in response to pathogen infection (99) and is increased significant in blood exposed to Gram-positive bacteria (100).

Viral infection specifically induces miR-451 that directs a negative regulatory cascade to adjust *dendritic cells*[2] cytokine production (101).

c) miR-451 was found significantly overexpressed in diseased gingival tissues (102), in rheumatoid arthritis and systemic lupus erythematosus (103) and became significantly down-regulated in *hyperplastic scars*[3] (104).

---

[1] *Microparticles* are cell-derived membrane-sheathed structures that shuttle proteins, mRNA, miRNA to adjacent and distant cells.

[2] *Dendritic cells* are immune cells, present in skin, blood, inner lining of nose, lungs, stomach, intestines, which activated, migrate to lymph nodes, interacting with T and B cells to initiate adaptive immune responses.

[3] *Hyperplastic scars* and keloids appear in aberrant wound healing causing skin deformities.

d) miR-451 was early elevated in hypertrophic cardiomyopathy (105); its overexpression improves cardiomyocyte survival (106) and induces *IPC*[4]-mediated cardioprotection (107).

e) miR-451 is widely dysregulated, having a critical role in tumor genesis and progression that can be used for diagnosis, prognosis, and treatment of cancer diseases (108):

- miR-451 over-expression represses 14-3-3ζ promoting excessive apoptosis (109).
- miR-451 is in fact down-regulated in *glioma*[5] cells, but re-introduced to glioma cells acts as tumor-suppressor by inhibiting cell growth, proliferation and inducing cell apoptosis (110-112). miR-451 expression showed a direct proportionality with the glucose level, controlling glioma cells ability to "go or grow", elevated miR-451 and glucose levels were associated with poorer prognosis (113, 114).
- miR-451 was significantly up-regulated in saliva of esophageal cancer patients (115). Over-expressed miR-451 induced apoptosis and suppressed cell proliferation, invasion and metastasis in esophageal carcinoma, and injection of miR-451 inhibited tumor growth in a xenograft model of esophageal cancer (116). Other group reveals also its important role in regulating xenograft rejection (117).
- miR-451 was significantly up-regulated in thyroid cancer with lymph node metastasis (118) and considered as suppressor of oncogenesis of T cell acute lymphoblastic leukemia (T-ALL) (119).
- miR-451 over-expression is associated with strong poor prognosis for recurrence and survival of gastric cancer (120) and plasma miR-451 was proposed as blood-based biomarker for screening gastric cancer (121). miR-451 were also found significantly elevated in pancreas cancer patients (122).
- miR-451 repress colorectal carcinoma cells by inhibiting cell growth (123) and caused a decrease in self-renewal, tumorigenicity, and chemoresistance, being suggested as candidate to circumvent recurrence and drug resistance (124)

[4] *IPC (Ischemic preconditioning)* is an intrinsic process, whereby repeated short ischemia protects myocardium against a subsequent ischaemic insult; and an experimental technique for producing resistance to the loss of blood supply, and thus oxygen to tissue.

[5] *Glioma* is a high aggressive, malignant, lethal brain tumor, with median survival of about 6 months if untreated.

- miR-451 was found significantly high and as suppressor in human lung cancer (125, 126) moreover was significantly up-regulated during the development of pulmonary hypertension (127).
- miR-451 was considered as tumor-suppressor through its down-regulation in hepatocellular carcinoma associated with high proliferation (128) along with its significantly decreasing in renal cell carcinoma serum (129). miR-451 growth-inhibitory effect was described in diabetic nephropathy by induced suppression of Ywhaz and p38 MAPK signalling (130).
- miR-451 was reported as significantly up-regulated in human *osteosarcoma*[6] cells (131), in contrast miR-144/miR-451 cluster was down-regulated (132). miR-451 over-expression in osteosarcoma correlates with subsequent positive response to chemotherapy (133).
- miR-451 was found significantly up-regulated having tumor-suppressor function in breast cancer (134) and as best biomarker ($p < 0.0001$) in combination with miR-145 in discriminating breast cancer from healthy controls and all other types of cancer (135).

1.3.3. miR-451 typical features

miR-451 is expressed as "miR-144/451 cluster" (95, 97, 106, 107) from a highly conserved bicistronic locus in the vertebrate genome (44, 136).

A microRNA pathway bypassing Dicer cleavage was described firstly for miR-451 (43, 136). Even though miR-451 processing in nucleus requires Drosha to create a short *pre-mir-451-hairpin* of about 42nt (136, 137), in contrast to other miRNAs, this hairpin is directly loaded into Ago2, as sole vertebrate "Slicer" Argonaute (136) that cut it into a *30nt intermediate*, whose 3'end will be resected to create a ~ *23nt mature miR-451* (136, 138).

Dicer KO cells can produce matures miR-451 but no other miRNAs, whereas Ago2 KO cells reconstituted with wild-type Ago2, excluding Slicer-deficient Ago2, can process miR-451 (137, 139).

[6] *Osteosarcoma* is a malignant bone tumour that usually develops in teenagers.

Studies confirmed that miR-451 gene and the endonucleolytic activity of animal Ago proteins are highly conserved, suggesting their evolutionary meaning in gene regulation. Therefore Ago2 is exclusively required for viability in mice, where homozygous mutants died shortly after birth due to anemia (138).

In addition the expression of miR144/451 cluster is strictly Ago2 dependent and is required for erythroid homeostasis, along with the fact that mice deficient of it result in erythroid hyperplasia, splenomegaly and anemia, miR-451 having a greater impact than miR-144 on target gene expression (95).

1.4. Hypothesis / Aims

As a major cause of morbidity and mortality, brain injuries induce profound molecular and cellular alterations due to tissue damage and disturbance of cellular mechanisms and signalling pathways, where miRNAs play key regulatory roles (39, 41, 46, 75-78, 82).

Since the existing treatments are still inefficient (29, 46) and many survivors must live with neurological deficits (14, 15), further studies are demanded to elucidate the exact molecular and cellular mechanisms underlying neuronal damage following TBI, aimed to develop better therapeutic strategies (4, 39).

Hippocampus is an essential brain region for memory, cognition and emotion, vulnerably to TBI that produces major pathophysiological changes like: cell loss, disturbed neural circuits, impaired synaptic transmission and plasticity, leading to long-term post-TBI neurological deficits (29, 34, 140).

The hypothesis that miR-451 could play an essential role in post-TBI molecular and cellular changes in hippocampus, is based on already published results, along with the findings of our own research group, for instance:

- miR-451 presence only in CSF-MPs (cerebrospinal fluid microparticles) of brain-injured patients vs. non-injured patients, discovered first of all by our research group, suggesting its key role in the adaptive response to TBI (86)

- miR-451 up-regulation during “in vitro” neuronal differentiation of NTera2 (Fig.19*), “in situ hybridisation” marked miR-451 expression in the dentate gyrus of hippocampus at healthy controls, but a down-regulation at moderate brain injured rats (Fig.20*) (unpublished results of our research group)

- post-TBI altered hippocampal miRNAs, including miR-451 (29, 34), suggesting its critical regulatory role in injury-related cell events and miR-451 substantial change in expression after experimental TBI (34, 82-85)

- miR-451 key function in a variety of biological processes, like: erythropoiesis (87-98), cell differentiation (89), infections (99-101), autoimmune diseases (103), cardiomyopathy (104-106)

- miR-451 widely dysregulation and critical role in numerous cancer types, concerning tumor genesis and progression (107-135), mostly being up-regulated and acting as tumor-suppressor (esophagus, thyroid, lung, liver, bone, breast)

Owing to these reasons the aim of this work was to contribute at the investigation of miR-451 as a potential key modulator of molecular and cellular mechanisms implicated in TBI pathophysiology, by analysing of miR-451 expression changes in hippocampus in a rat “fluid percussion injury” (FPI) model.

For this purpose was used the real-time PCR (qRT-PCR) to detect miRNA-451 expression in ipsilateral hippocampal tissue, isolated from the brain of healthy or sham control animals and from severe damaged brains at 1 day, 4 days, 1 week, 2 weeks and 3 weeks.

2. MATERIAL AND METHODS

2.1. Fluid Percussion Injury (FPI) trauma model

In the present study were used small RNAs samples isolated with mirVana™ PARIS™ KIT from frozen (-70°C) hippocampal tissue of rats after "severe trauma" (pressure values more than 2.5 atm) obtained by Fluid Percussion Injury (FPI) on Sprague Dawley rats as trauma model, available from my colleague MSc Muammer Ücal.

In the Tab.2 are pointed the five experimental sets used in these experiments, therefore 5 animals for each condition, "sham" and "severe" trauma, for day 1, day 4, 1 week, 2 weeks and 3 weeks after TBI. As "healthy" controls were used 3 animals.

Table 2: Five experimental sets and corresponded animal codes

	healthy	**sham d1**	**severe d1**	**sham d4**	**severe d4**	**sham 1w**	**severe 1w**	**sham 2w**	**severe 2w**	**sham 3w**	**severe 3w**
set 1	*1450*	*1101*	*763*	*1080*	*723*	*1146*	*991*	*1148*	*985*		*983*
set 2	*1451*	*1100*	*1188*	*1083*	*1258*	*1147*	*993*	*1150*	*987*	*1119*	*976*
set 3	*1452*	*1103*	*1189*	*1082*	*1245*	*1288*	*1229*	*1151*	*1239*	*1120*	*1207*
set 4	*1451*	*1032*	*1187*	*1038*	*1256*	*1458*	*1238*	*1283*	*1456*	*1152*	*1305*
set 5	*1450*	*1102*	*765*	*1081*	*1242*	*1459*	*1465*	*1284*	*1460*	*1121*	*1206*

For the pressure recordings was used a pressure sensor connected to both: a fluid percussion device (Scien Instruments, NY, USA) and a computer for the standardization of primary physical damage.

Tab. 3 presents the pressure values used to produce a "severe" trauma to the animals of the five sets.

Table 3: Pressure values of "severe" traumas for the five experimental sets

	set 1	pressure [atm]	set 2	pressure [atm]	set 3	pressure [atm]	set 4	pressure [atm]	set 5	pressure [atm]
severe d1	*763*	2,59	*1188*	2,82	*1189*	2,63	*1187*	2,56	*765*	2,53
severe d4	*723*	2,89	*1258*	2,56	*1245*	2,73	*1256*	2,70	*1242*	2,82
severe 3w	*983*	2,63	*976*	2,53	*1207*	2,70	*1305*	2,54	*1206*	2,97
severe 1w	*991*	2,67	*993*	2,63	*1229*	3,12	*1238*	2,74	*1465*	2,74
severe 2w	*985*	2,56	*987*	2,72	*1239*	2,82	*1456*	2,94	*1460*	2,72

2.2. RNA concentration measurement

The RNA content of the small RNAs samples, which were isolated from the ipsilateral hippocampal tissue of rats ("healthy controls", "sham" and "severe trauma" animals), was measured with Quant-iT™ RiboGreen® RNA Assay Kit (Invitrogen).

This method use advanced fluorophores that bind to RNA and become fluorescent. The intensity of the emitted fluorescence of the resulting complex is directly proportional to the amount of RNA target molecules in the sample.

Because RiboGreen Reagent binds only to intact miRNA molecules, and doesn't interfere with molecules of free nucleotides or contaminants, the results obtained by RiboGreen method are more accurate than those obtained with UV absorbance readings by NanoDrop ND-1000 Spectral photometer.

Therefore RiboGreen method was at the end the method of choice to measure the miRNA concentration of all samples.

2.2.1. NanoDrop method description

The NanoDrop spectral photometer allows the quantification of RNA by measuring the optical density (OD) or absorbance at 260 and 280 nm wavelengths and calculating the concentration using Beer-Lambert law, which indicates a direct proportionality of the absorbance with the concentration.

Generally the ratio of absorbance 260/280 of pure RNA samples is about 2.0, while a lower ratio of absorbance than 2.0 means a contamination with protein, phenol or other compounds that absorb at 280 nm wavelengths.

The absorbance ratio 260/230 of pure RNA samples is expected to be in the range of 2.0 – 2.2 and a ratio value lower than 1.8 may mean contaminants which absorb at 230nm.

This measurement was done by direct pipetting of undiluted 2µl miRNA sample. Because the pH of the sample influences the absorbance, as blank on the Nanodrop should be used the solvent, not water.

2.2.2. RiboGreen method description

RNA samples were treated with fluorochrom RiboGreen® reagent, which bound only to RNA intact molecules as previous explained. The amount of RNA in the sample was calculated using a RNA standard curve as a serial dilution of ribosomal RNA standard (rRNA) in 1x TE-Buffer, obtained as described above.

The RiboGreen® RNA reagent was diluted 200fold, therefore 7.5µl RiboGreen® RNA reagent were added to 1492.5µl 1x TE-Buffer to obtain 1.5ml diluted Ribogreen reagent, which was protected from light in dark eppis.

2.2.3. Preparation of standard solutions

The standard curve was prepared as a serial dilution using 7 decreasing concentrations of rRNA standard in 1x TE-Buffer, which are showed in the Tab. 4.

The first tube contained 245µl TE buffer and 5µl rRNA standard and the every other 6 tubes 120µl TE buffer. The serial dilution was provided by taking of 120µl from the first tube after properly vortexing and passing to the second, then vortexing the second tube,

taking again 120µl and passing them to the third tube and so on in order to obtain the standard concentrations.

Table 4: rRNA concentration of the standards

Standard	Standard concentration [ng/µl]	1x TE-Buffer [µl]	rRNA [µl]
1. Std	2	245	5
2. Std	1	120	120
3. Std	0.5	120	120
4. Std	0.250	120	120
5. Std	0.125	120	120
6. Std	0.0625	120	120
7. Std	0.03125	120	120

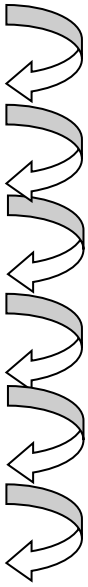

2.2.4. Preparation of sample solutions

The sample solutions were prepared by adding of 2.4µl from original isolated miRNA to 117.6µl 1x TE buffer for to obtain 120µl miRNA (1:50) sample solution.

2.2.5. POLARstar optima fluorometer Analysis

The seven prepared standard solutions (in decreasing concentrations: 2, 1, 1.5, 0.250, 0.125, 0.0625 and 0.03125 ng/µl) and the 1:50 diluted miRNA sample solutions were passing in duplicates, 50µl each, to the black 96 well fluoroplate.

Then 50µl Ribogreen RNA reagent (1:200) was added onto each well, excepting the two wells for blank, each consisting of 100µl 1x TE buffer.

The black fluoroplate was shacked 3 min. with 300 rpm, covered with aluminium foil and then analysed by POLARstar optima fluorometer (emission: blue, excitation: yellow).

2.3. Formaldehyde Agarose Gel Electrophoresis

After the determination of miRNA concentration, from each sample are prepared 50ng miRNA, solved in 20 µl, in order to use then 30 ng for "formaldehyde agarose gel electrophoresis" and 20ng for the "cDNA synthesis".

1.2% formaldehyde (FA) agarose gel electrophoresis was performed to check the results of the RNA concentration measurement, expecting that all the bands on the gel will show the same intensity, with other words each band will contain 30 ng miRNA, like Fig.15 illustrates at Chapter 3.2.2.

2.3.1. Preparation of 1.2 % formaldehyde agarose gel

The 1.2% formaldehyde agarose gel (1.2% agarose) of size 10 x 14 x 0.7 cm (a small gel) was prepared from 1.2 g agarose mixed with 10 ml 10x formaldehyde agarose gel buffer (see composition below) and 100 ml RNase-free water, followed by heating to melt the agarose and cooling to 65°C in a water bath.

Then 1.8 ml of 37% (12.3 M) formaldehyde (toxic) and 1 µl Gel Red were added, mixed thoroughly and put onto gel support. The gel was equilibrated in 1x FA agarose gel running buffer for 30 min. before running.

Table 5: Composition of the formaldehyde agarose gel buffers

10x FA agarose gel buffer	1x FA agarose gel running buffer	5x RNA loading buffer
▪ 200 mM 3-[N-morpholino] propane sulfonic acid (MOPS) ▪ 50 mM sodium acetate ▪ 10 mM EDTA ▪ pH to 7.0 with NaOH	▪ 100 ml 10x FA agarose gel buffer ▪ 20 ml 37% (12.3 M) FA ▪ 880 ml RNase-free water	▪ 16 µl saturated aqueous bromophenol blue solution ▪ 80 µl 500 mM EDTA, pH 8.0 ▪ 720 µl 37% (12.3 M) FA ▪ 2 ml 100% glycerol ▪ 3084 µl formamide ▪ 4 ml 10x FA agarose gel buffer ▪ RNase-free water to 10 ml ▪ Stability 3 months at 4°C

2.3.2. RNA samples preparation for electrophoresis

The RNA sample preparation for FA agarose gel electrophoresis consisted in adding 1 volume of 5x loading buffer per 4 volumes of RNA sample (in the present work 3µl of loading buffer and 12µl of RNA), mixing, incubating 3min. at 65°C, chilling on ice and loading onto the equilibrated 1.2 % FA agarose gel.

2.3.3. Gel running conditions

The gel was run at 150V for 15min. in 1x FA agarose gel running buffer.

2.4. cDNA synthesis

2.4.1. Reverse transcription by Qiagen

The conversion of miRNA into cDNA (first strand cDNA synthesis from RNA template) performed using miScript II RT Kit from Qiagen utilised HiFlex Buffer in the reverse transcription reaction and all RNA species were converted into cDNA (Fig. 4).

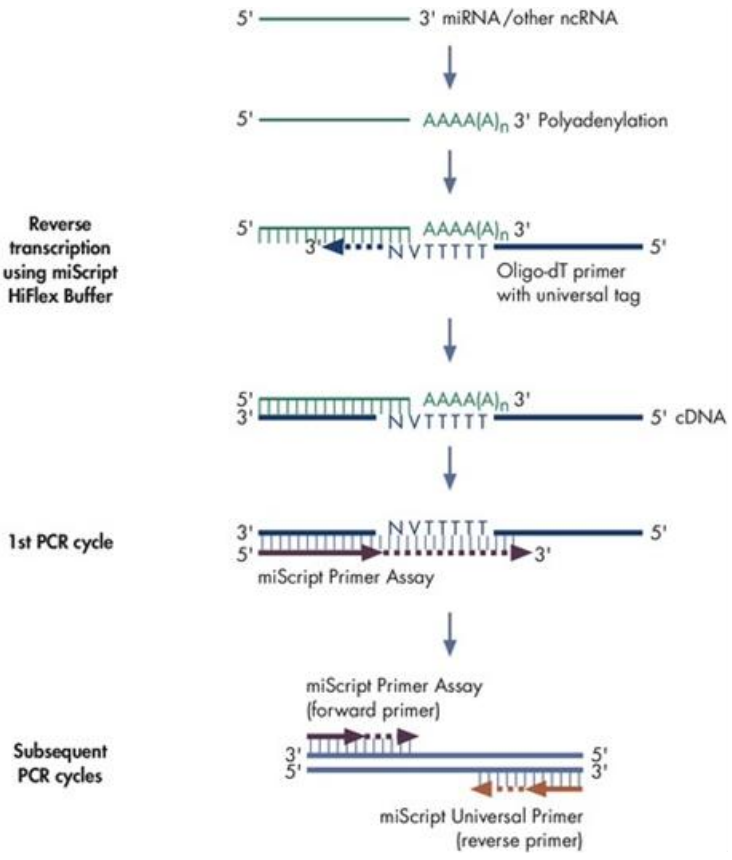

Figure 4: Conversion of miRNA into cDNA using HiFlex Buffer by Qiagen Kit (141)

Both reactions, polyadenylation, in which mature miRNAs are polyadenylated by poly(A) polymerase, and subsequent reverse transcription into cDNA, are carried out in the same tube in parallel. The oligo-dT primers with a 5'-universal tag and a 3'-degenerate anchor allowed the recognizing and amplification of mature miRNA later in the RT-PCR step, excluding a detection of genomic DNA (141).

The cDNA synthesis is a reverse transcription reaction, which includes incubation of the reaction components (Tab. 6) for 1 hour at 37°C, followed by the reaction inactivation for 5 min. at 95°C.

Table 6: Reverse transcription reaction components, by Qiagen

Component	**Volume / reaction**
HiFlex Buffer	4µl
Nucleic Mix	2µl
RNase free water	4µl
Reverse Transcriptase	2µl
Template RNA	8µl
Total volume	**20µl**

A mastermix (MM) was prepared on ice, as sum of the components visible in Tab. 6 (excepting "template RNA"), multiplied by the number of reactions. A "no template control" or RT(-) reaction, with RNase free water instead of template RNA, was also included.

MM was mixed gently and 12µl MM was dispensed into the tubes containing 8µl RNA template (20ng miRNA). The total volume of the reaction mix was 20µl for each reaction. Samples were incubated 1h at 37°C, then 5min at 95°C and finally were stored a -20°C.

2.4.2. Reverse transcription by Exiqon

The conversion of miRNA into cDNA performed using Universal cDNA Synthesis kit II from Exiqon, by which microRNA polyadenylation and reverse transcription occurred in a single reaction step.

Analog to cDNA synthesis previous described, the reverse transcription reaction comprises the incubation of the reaction components (Tab.7) for 1h at 42°C followed by an inactivation step for 5 min. at 95°C.

Table 7: Reverse transcription reaction components, by Exiqon

Component	Volume / reaction
Reaction Buffer	4µl
RNase free water	6µl
Enzyme mix	2µl
Template RNA	8µl
Total volume	**20µl**

A mastermix (MM) was prepared also on ice, as sum of the components of Tab.7 (excepting “template RNA”), multiplied by the number of reactions.

A “no template control” or RT(-) reaction, with RNase free water instead of template RNA, was also included.

MM was mixed gently and 12µl MM was dispensed into the tubes containing 8µl RNA template (20ng miRNA). The total volume of the reaction mix was 20µl for each reaction. Samples were incubated 1h at 42°C, then 5min at 95°C and finally were stored a -20°C.

2.5. Quantitative Real Time-PCR (qRT-PCR)

The detection of mature miRNAs in samples was done by subsequent quantitative real time-PCR (qRT-PCR) of cDNAs prepared before in reverse transcription reaction, by using miScript SYBR Green PCR Kit from Qiagen, which contains miScript Universal reverse primer and QuantiTect SYBR Green PCR.

For accurate and reproducible results, U6 was used as normalisation control (reference gene), excluding possible variations of input RNA amount, eventual RNA degradation, inhibitors in RNA samples or differences in sample handling.

2.5.1. qRT- PCR cycling conditions

The real-time PCR reactions were performed using "Roche Light-Cycler 480" at corresponding cycling conditions: Qiagen (Tab.7) or Exiqon (Tab.8).

Table 8: RT- PCR cycling conditions / Qiagen

Steps	Time	Temperature	Additional comments
PCR activation	**15min**	**95°C**	HotStarTaq DNA polymerase activation
3 step cycling:			
Denaturation	15s	94°C	
Annealing	30sec	55°C	
Extension	30s	70°C	Perform fluorescence data collection Acquisition mode: single
Melting curve:			
	10s	95°C	
	1min	50°C	
	continuous	95°C	10 acquisitions per °C
cooling	**10s**	**40°C**	
Cycle number	**45**		**using Roche LC 480**

Table 9: RT- PCR cycling conditions / Exiqon

Process step	Settings, LC 480 instrument
Polymerase Activation / Denaturation	10min, 95°C
Amplification	10s, 95°C 1min, 60°C Ramp-rate 1.6 C/s 45 amplification cycles
Melting curve analysis	yes

After establishing of RT-PCR for miR-451 (Chapter 3.3.), in all experiments were used Qiagen cycling conditions, where the annealing requirements were modified according to the optimal annealing conditions for Exiqon primers (1min., 60°C).

2.5.2. qRT-PCR Workflow

Prior to RT-PCR, cDNA samples were diluted 1:80 (Exiqon) or 1:60 (Qiagen). Then two mastermix (MM) were prepared on ice, using the first three reaction components according to Tab.9: **5µl** SYBR Green + **1µl** 10xUP + **1µl** Primer = **7µl** per PCR reaction, multiplying by number of reactions, in duplicate, as well as a "blank", RT(-) and MM-control (no fluorescence signal denotes no contamination in MM).

Table 10: Reaction setup for real-time PCR

Components / Qiagen	Vol / rxn	Components / Exiqon	Vol / rxn
2x QuantiTect SYBR Green PCR Master Mix	5µl	SybrGreen Master Mix	5µl
10x miScript Universal Primer	1µl	Exiqon forward primer (1:4)	0.5µl
Exiqon Primer (miR-451 or U6)	1µl	Exiqon reverse primer (1:4)	0.5µl
cDNA template (1:60)	3µl	cDNA template (1:80)	4µl
Total volume	**10µl**	**Total volume**	**10µl**

For a better understanding Fig.5 displays a "96-well white plate" of a RT-PCR experiment from 08.05.20143 as example.

Date: 08.05.2013 **Experiment / Plate:** qRT-PCR_set 4

U6 (Exiqon)	A1 *H*	A2 *sh d1*	A3 *sev d1*	A4 *sh d4*	A5 *sev d4*	A6 *sh 3w*	A7 *sev 3w*	A8 *RT(-)*	A9 *blank*	A10 *MM*	A11	A12
	B1 *H*	B2 *sh d1*	B3 *sev d1*	B4 *sh d4*	B5 *sev d4*	B6 *sh 3w*	B7 *sev 3w*	B8	B9	B10	B11	B12
miR-451 (Exiqon)	C1 *H*	C2 *sh d1*	C3 *sev d1*	C4 *sh d4*	C5 *sev d4*	C6 *sh 3w*	C7 *sev 3w*	C8 *RT(-)*	C9 *blank*	C10 *MM*	C11	C12
	D1 *H*	D2 *sh d1*	D3 *sev d1*	D4 *sh d4*	D5 *sev d4*	D6 *sh 3w*	D7 *sev 3w*	D8	D9	D10	D11	D12

Figure 5: 96-well white plate of a RT-PCR experiment

In blue are marked the well's positions (A1-A12, B1-B12 etc.), in green sample's names. Lines A and B belong to U6 reference gene, lines C and D belong to miR-451 target gene.

On the white plate are visible 17 reactions (R) for each gene. Therefore 18 R (one supplementary) were necessary to calculate the component amounts for each MM as Tab.11 presents.

Table 11: qRT-PCR Mastermix preparation

MM / U6	**MM / miR-451**
18 R x 5µl = **90µl** *SYBR Green*	18 R x 5µl = **90µl** *SYBR Green*
18 R x 1µl = **18µl** *10xUP*	18 R x 1µl = **18µl** *10xUP*
18 R x 1µl = **18µl** *U6 primer*	18 R x 1µl = **18µl** *miR-451*
126µl total volume	**126µl** total volume

First of all, were dispensed 7µl MM into the wells of the white plate, kept on ice: from MM/U6 (A1 to A10, B1 to B7) and MM/miR-451 (C1 to C10, D1 to D7) respectively. Then were added 3µl of the correspondent cDNA template, RT(-) or RNase free water for blank. After mixing and spin down the prepared plate was measured at Light Cycler.

2.5.3. Data analysis by ΔΔCt method

The threshold cycle (ct) values for both genes, miR-451 target gene and U6 reference gene, provided from Light Cycler were imported into an Excel sheet and for each sample was calculated the "mean ct" of the duplicates.

The expression of miR-451 target gene was then normalized to U6 reference gene, calculating Δct for each sample, as following difference:

$$\Delta ct = \text{mean ct (miR-451)} - \text{mean ct (U6)} \qquad \text{(a)}$$

Changes in miR-451 expression level due to "severe trauma" were represented as change in Δct value of "severe" from "sham" by the formula:

$$\Delta\Delta ct = \Delta ct \text{ (sham)} - \Delta ct \text{ (severe)} \qquad \text{(b)}$$

A positive difference or positive ΔΔct value denotes an increase in abundance of miR-451 target gene after severe trauma, while negative difference reveals a decrease in miR-451 abundance (34).

2.5.4. Statistical analysis

All RT-PCRs were repeated at least two times in duplicates. Data were presented as "mean ΔΔct ± SEM" for five animal sets, corresponding to each investigated time point (see Tab. 15 and 16).

Standard error of the mean (SEM) defines the error of the mean of the sample with respect to the mean of the population, giving an idea about how far the found mean differs from the real mean and was calculated using the formula (142):

$$SEM = SD/\sqrt{n}, \text{ where SD = standard deviation} \qquad \text{(c)}$$

The comparison between groups was performed by statistical Student's t- test, in Excel.

P-values less than 0.05 indicate *statistically significant differences*. A p-value of 0.05 means 5% chance that null hypothesis ("no difference") is true (142).

3. RESULTS

3.1. Establishment of miRNA concentration measurement

In prior experiments, the concentration of miRNA samples was measured by NanoDrop spectral photometer, easy to execute by directly measurement of 2µl miRNA.

Changeable results by repeated application of the Nanodrop (ND) measurement, in addition to unequal bands on the gel and much more amount necessary for the measurement, suggested that this method is inadequate to measure miRNA concentration, especially when samples are provided from sacrificed animals.

3.1.1. Comparison between ND and RG concentration measurement

Numerous trials indicated that the spectral photometer seams to measure all molecules inside the miRNA sample, also the molecules of free nucleotides or contaminants, resulting in inaccurate concentration values.

Following results were selected to justify why finally RiboGreen (RG) was preferred to measure the miRNA concentration of all samples.

For instance Fig.6 presents a gel of three different miRNA samples (notated by animal codes), measured by ND, indicating that 30ng/slot were insufficient, being undetectable; the bands were visible using 150ng/slot, but 4 and 5 seemed to be overloaded.

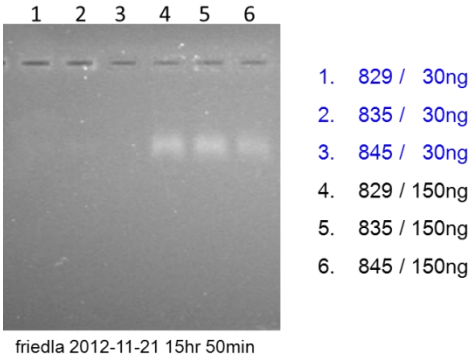

Figure 6: 1.2 % FA agarose gel; ND measurement, 30ng/slot (blue) and 150ng/slot (black)

In the next trial were used 100ng miRNA /slot, like Fig.7 presents. On this gel some bands were undetectable (1, 9, 10, 11, 12), and the others dissimilar, indicating an inexact concentration measurement by ND method.

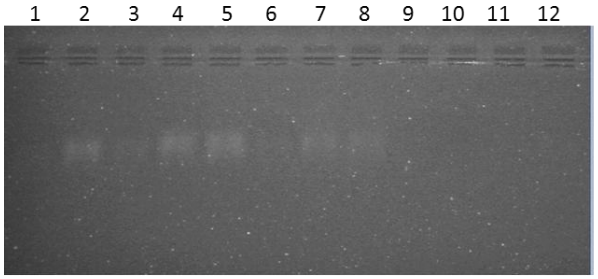

1.	629	7.	1076
2.	1100	8.	1089
3.	1084	9.	717
4.	1192	10.	1075
5.	1188	11.	1095
6.	651	12.	1083

Figure 7: 1.2 % FA agarose gel; ND measurement, 100ng/slot

This experiment was repeated to get sure, that no handling imperfections occurred before. On the next gel (Fig. 8) could be remarked a similar profile of the bands as before, so it seems that the measured concentrations by ND were inexact.

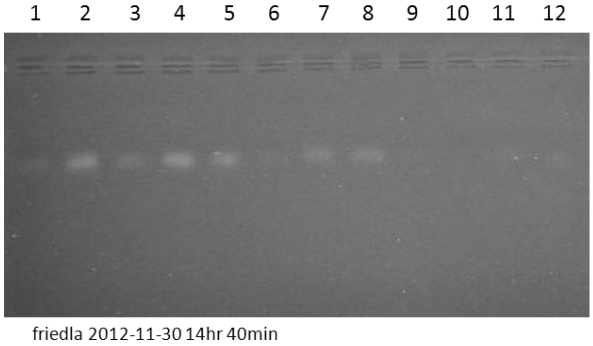

1.	629	7.	1076
2.	1100	8.	1089
3.	1084	9.	717
4.	1192	10.	1075
5.	1188	11.	1095
6.	651	12.	1083

Figure 8: 1.2 % FA agarose gel; ND measurement, 100ng/slot

Preceding miRNA samples were measured then by RG, showing a better accuracy of this method through similar bands on the gel of Fig.9.

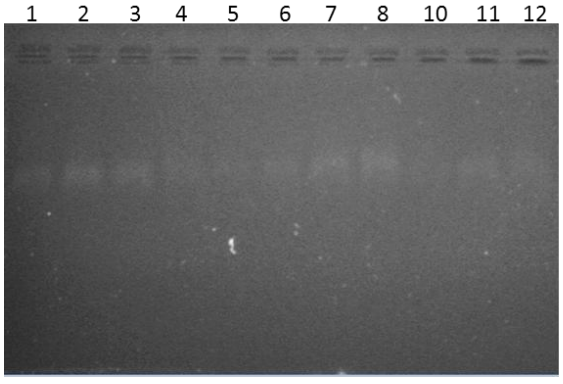

1.	629	7.	1076
2.	1100	8.	1089
3.	1084	9.	717
4.	1192	10.	1075
5.	1188	11.	1095
6.	651	12.	1083

Figure 9: 1.2 % FA agarose gel; RG measurement, 30ng/slot, sample 9 vacant (blue)

Tab.12 enables a comparison between the two methods, ND and RG, by listing the measured concentrations of miRNA samples, presented on the previous gels (Fig.7-9).

Table 12: Comparison of concentration values using both methods (ND and RG)

	miRNA samples	Conc. by ND [ng/µl]		Conc. by RG [ng/µl]
		28.11.2012	29.11.2012	03.12.2013
1.	629	64.0	49.0	16.7
2.	1100	34.0	27.0	26.8
3.	1084	36.0	31.0	14.5
4.	1192	62.0	59,0	64.8
5.	1188	31.0	24.0	24.9
6.	651	44.0	45.0	18.0
7.	1076	56.0	47.0	28.0
8.	1089	53.0	45.0	22.0
9.	717	98.0	73.0	-
10.	1075	21.0	15.0	3.1
11.	1095	66.0	64.0	18.6
12.	1083	62.0	51.0	17.6

In Tab.12 is notable that concentration values obtained by ND are generally higher, suggesting the measurement of all existing molecules in the miRNA sample, including also molecules of free nucleotides or contaminants, as already mentioned.

Although ND measurement was identical operated, it can be observed their instability from a day to another, causing irreversible loss of miRNA amount during repeated measurements.

3.1.2. Accuracy of RG concentration measurement

The next gels, where miRNA samples were measured by RG method, indicated mostly similar bands, 30ng miRNA/slot were detectable.

For instance on the gel of Fig.10, from twelve miRNA concentrations, only three appeared inadequate (red circle), band 6 being imperceptible, 5 and 7 too strong, suggesting more than 30ng/slot. Only miRNA samples, which denoted similar bands, could be converted into cDNA.

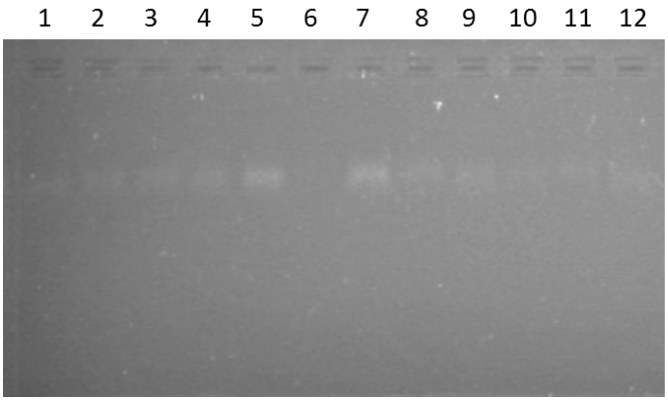

1. 1068
2. 1090
3. 713
4. 1002
5. 671
6. 663
7. 1072
8. 1093
9. 731
10. 997
11. 645
12. 637

Figure 10: 1.2 % FA agarose gel; RG measurement, 30ng/slot

On following gel (Fig.11) only one miRNA sample was undistinguishable (at line 9); all the other bands seemed to be alike and could be converted into cDNA.

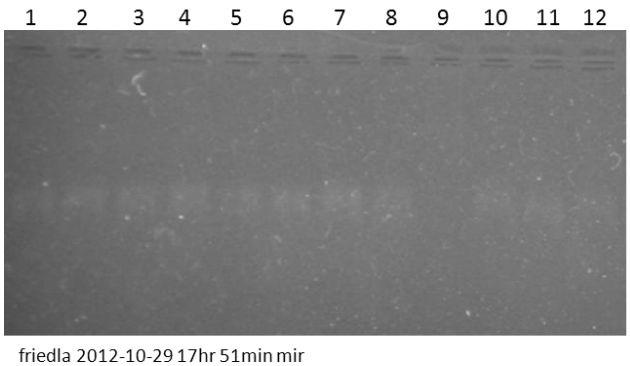

1. 1102
2. 1086
3. 1070
4. 1091
5. 715
6. 1094
7. 1081
8. 1097
9. 725
10. 1103
11. 1087
12. 729

Figure 11: 1.2 % FA agarose gel; RG measurement, 30ng/slot

Definitely the gel of Fig.12 displayed similar bands, proposing RG method to measure miRNA concentration.

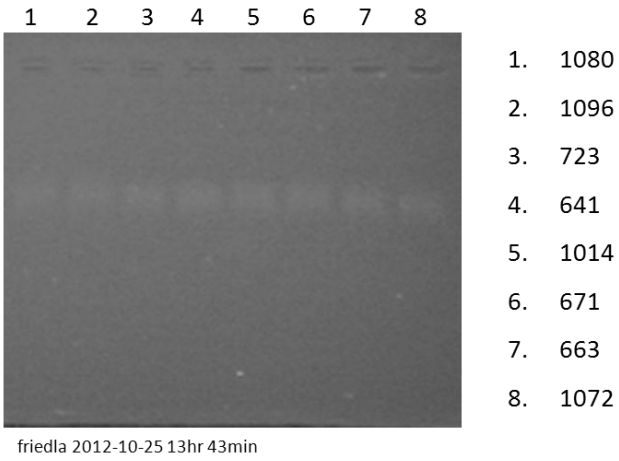

Figure 12: 1.2 % FA agarose gel; RG measurement, 30ng/slot

Considering afore presented results, could be concluded that ND method is not adequate to measure miRNA concentration, but RG method offer high accuracy and reproducibility, needing small miRNA amounts and saving important miRNA quantities.

Therefore RG method was the method of choice to measure miRNA concentration of all our samples, although this method is more expensive and considerably time-consuming.

3.2. miRNA concentration by Ribogreen method

3.2.1. Standard curves and appropriate miRNA concentration values

A correct standard curve was especially important to measure exact concentrations by RG method, as described at Chapter 2.2.2.

As example, Fig.13 illustrates the experiment from 25.04.2013, showing an exact standard curve, where the measured standards were almost precisely located on the linear slope.

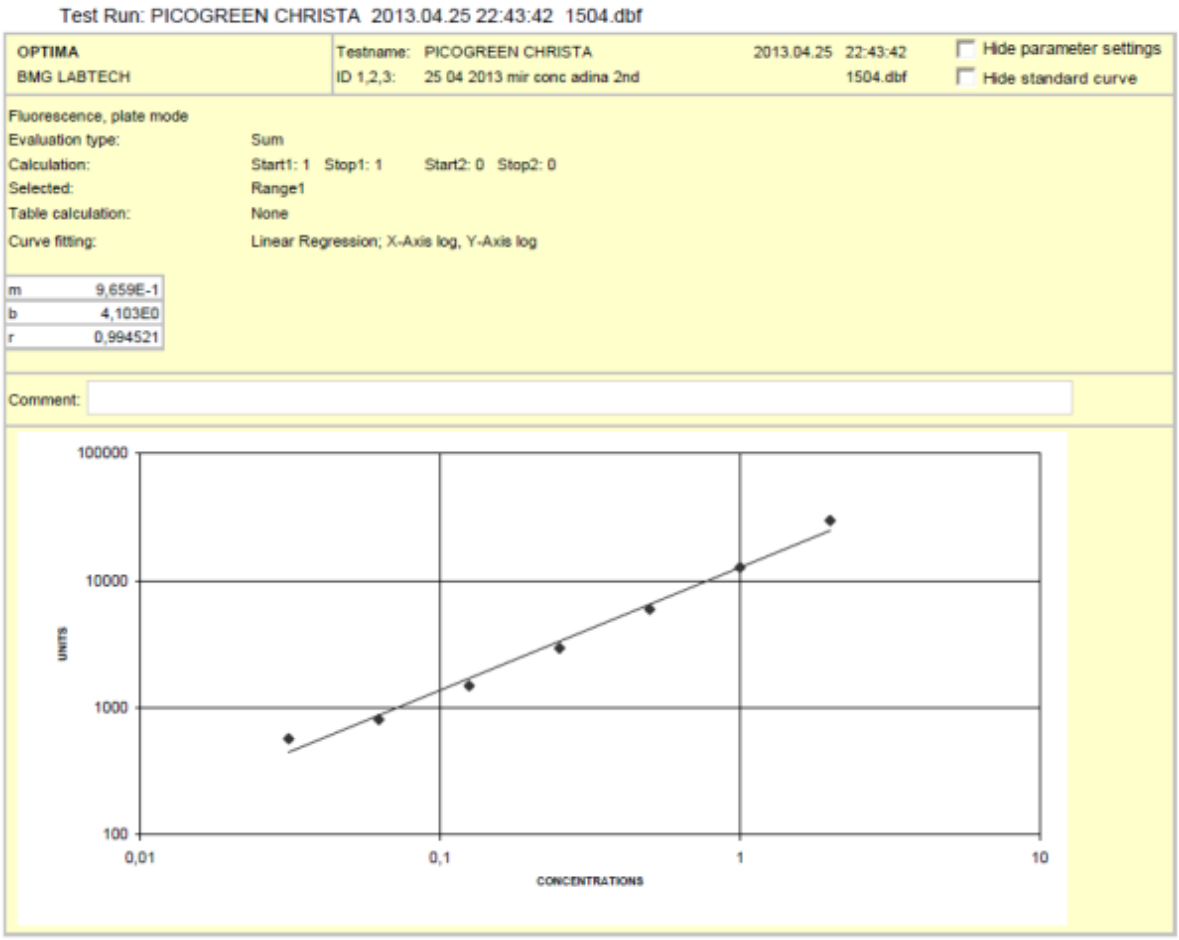

Figure 13: Standard curve of miRNA concentration measurement by RG method

Accordingly to this correct standard curve, the measured miRNA concentrations resulted in similar values of the duplicates (Fig.14).

In Fig. 14 can be remarked comparable values of the duplicates: at standards (red) and samples (black). This is visible at fluorescence (raw data) and respectively at the concentration values.

Test Run: PICOGREEN CHRISTA 2013.04.25 22:43:42 1504.dbf

Sort contents Up	Sort contents Down	Sort sample IDs Up	Sort sample IDs Down	Sort rows Up	Sort rows Down	Sort columns Up	Sort columns Down	Avg of replicates	Use dilution factor		
Content	Sample ID	Well	Dilution factor	Raw data	Avg of replicates	SD of replicates	%CV	Calculated concentr.			
B		A08	1,000	35	38	3	7,9	2,24E-3			
B		B08		41				2,64E-3			
S1		A01	1,000	28971	29618	647	2,2	2,350			
S1		B01		30265				2,459			
S2		A02	1,000	13016	12690	326	2,6	1,027			
S2		B02		12364				0,973			
S3		A03	1,000	5988	5954	35	0,6	0,460			
S3		B03		5919				0,454			
S4		A04	1,000	2962	2940	23	0,8	0,222			
S4		B04		2917				0,218			
S5		A05	1,000	1514	1486	28	1,9	0,111			
S5		B05		1458				0,106			
S6		A06	1,000	787	809	22	2,7	56,22E-3			
S6		B06		830				59,40E-3			
S7		A07	1,000	593	570	23	4,0	41,94E-3			
S7		B07		547				38,57E-3			
X1		C01	1,000	4398	4253	146	3,4	0,334			
X1		D01		4107				0,311			
X2		C02	1,000	2275	2404	129	5,4	0,169			
X2		D02		2533				0,189			
X3		C03	1,000	4666	4752	86	1,8	0,355			
X3		D03		4837				0,368			
X4		C04	1,000	6112	5709	403	7,1	0,469			
X4		D04		5306				0,405			
X5		C05	1,000	5996	6051	55	0,9	0,460			
X5		D05		6106				0,469			
X6		C06	1,000	10774	10341	433	4,2	0,844			
X6		D06		9908				0,774			
X7		C07	1,000	6461	6266	195	3,1	0,497			
X7		D07		6071				0,466			
X8		C08	1,000	4685	4391	295	6,7	0,356			
X8		D08		4096				0,310			
X9		C09	1,000	8522	8117	406	5,0	0,662			
X9		D09		7711				0,597			
X10		C10	1,000	5605	5327	279	5,2	0,429			
X10		D10		5048				0,385			
X11		C11	1,000	18582	17351	1232	7,1	1,484			
X11		D11		16119				1,281			
X12		C12	1,000	8767	8934	167	1,9	0,682			
X12		D12		9100				0,709			

Figure 14: Fluorescence values and correspondent concentration of the standards (red) and miRNA samples (black)

3.2.2. Measurement precision test by electrophoresis

Accordingly to prior obtained exact concentration results, on the gel of Fig.15 could be achieved similar miRNA bands, proving an accurate miRNA concentration measurement by RG, permitting the conversion of all miRNA samples into cDNA.

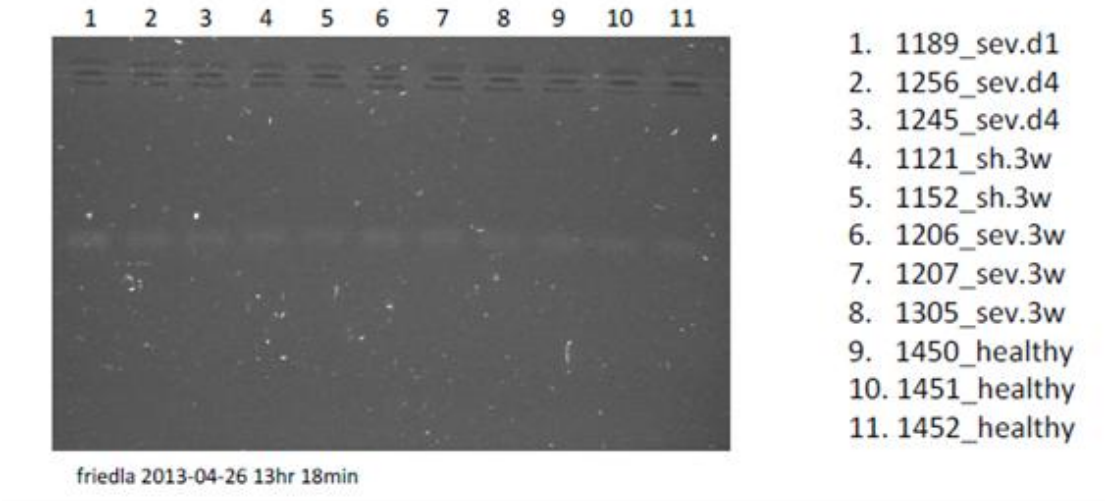

Figure 15: 1.2% FA agarose gel of miRNA samples, RG measurement, 30ng/slot

3.3. Establishment of qRT-PCR for miR-451 target gene

3.3.1. Accurate amplification plots and melting peaks

In a qRT-PCR amplification plot, the fluorescence is plotted against the number of cycles, producing sigmoidal-shaped plots, where the threshold cycle (ct) represents the cycle at which appears first detectable amount. Consequently a sample containing a higher amount of starting template appears earlier, having a lower ct value.

PCR products are double stranded at low temperature and SYBR Green can bind to them resulting in a high fluorescence. High temperatures denaturize the PCR products and therefore fluorescence decreases rapidly.

The melting peaks are produced by measuring continuously the fluorescence with slowly increasing temperature from a low value (65°C) to a high one (95°C) and plotting fluorescence values against temperature. The appearance of only one peak means the amplification of the specific PCR product. Supplementary peaks at a lower temperature appear sometimes as a result of primer-dimer co-amplification.

Fig.16-19 illustrate the amplification curves and related melting peaks for U6 reference gene and miR-451 target gene of the **qRT-PCR experiment from 8.05.2013** as example, showing adequate amplification curves and single melting peaks of specific amplification

products. No contamination was indicated via “green” (Fig.16 and 18) or “blue” lines (Fig 17 and 19) of the blank, RT(-) and MM samples.

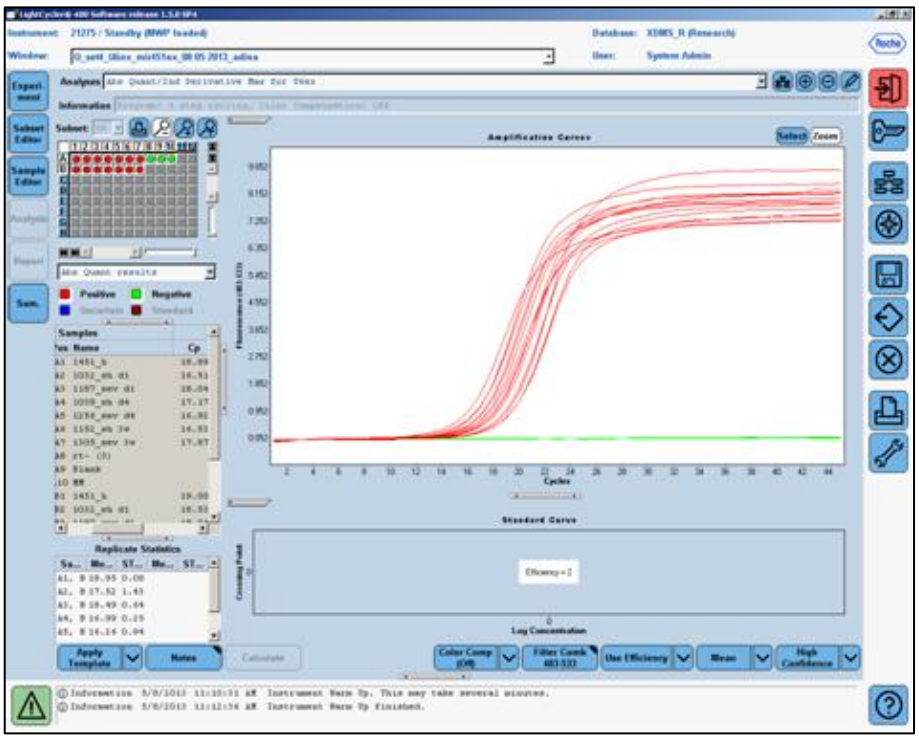

Figure 16: Amplification curves for U6 reference gene

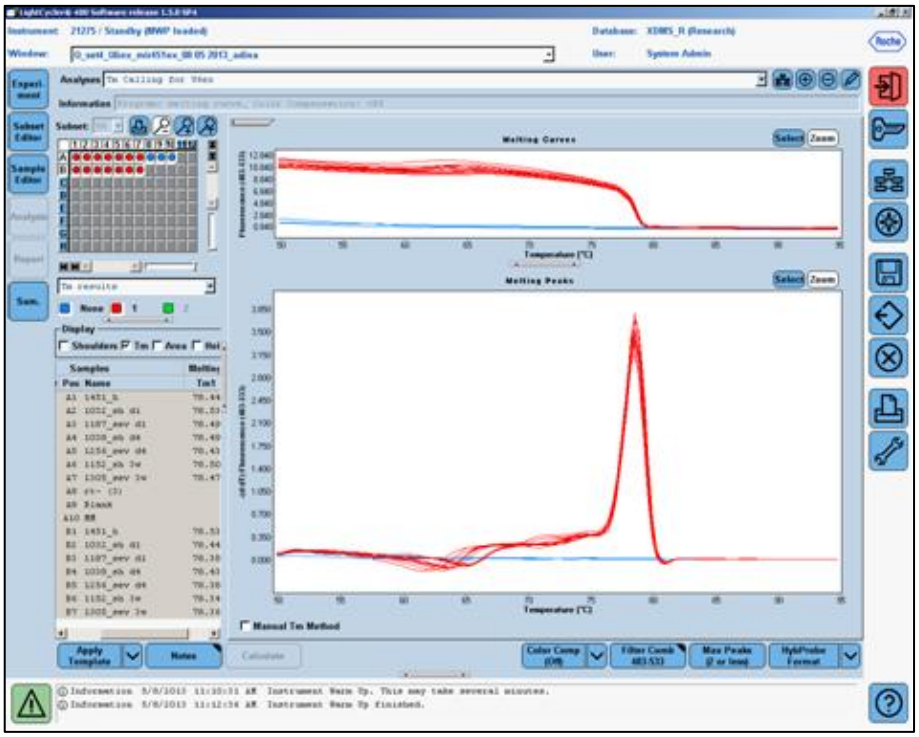

Figure 17: Melting peaks for U6 reference gene

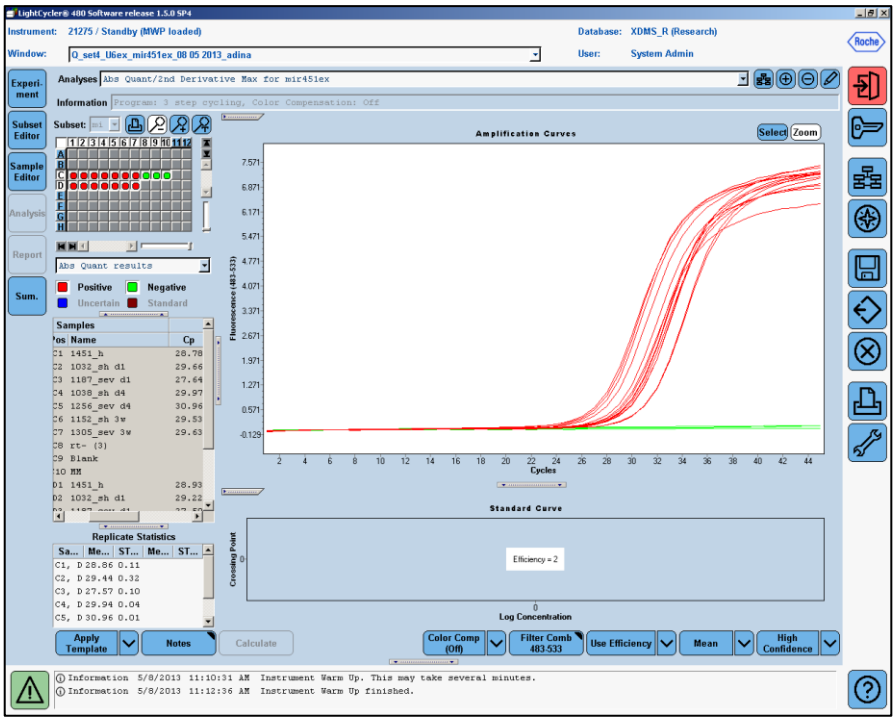

Figure 18: Amplification curves for miR-451

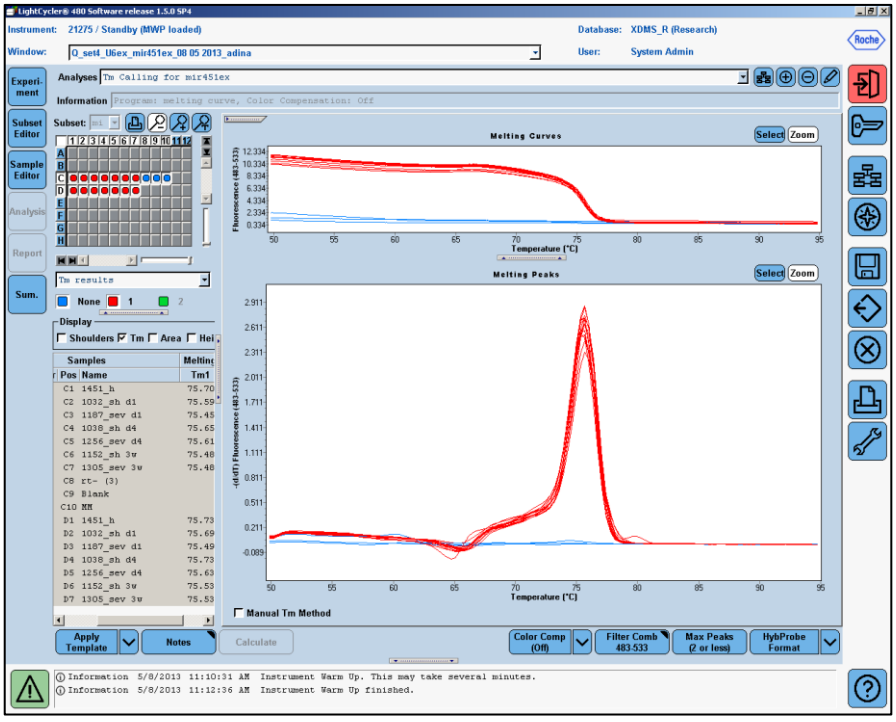

Figure 19: Melting peaks for miR-451

The amplification curves and related melting peaks of the RT-PCR experiments used for the post-TBI miR-451 expression profile (Fig.32) are presented at Chapter 5 (APPENDIX), Fig.50-62, as “raw data“.

3.3.2. qRT-PCR experiments by Exiqon

It is well-known that any relative RT-PCR needs a stable reference gene or endogenous control to correct eventual sample-to-sample and run-to-run variations.

As reference gene was used at the beginning a U6 primermix from Exiqon. At the beginning the RT-PCR trials were performed at Exiqon cycling conditions, but the experiments appeared many times contaminated and it was difficult to locate the errors or to relate them to some imperfections.

Fig.20 displays the results of the first RT-PCR, at which could be observed contaminations in Blank and MM (see arrows).

1. 1101_Sh d1
2. 763_Sev d1
3. 1080_Sh d4
4. 723_Sev d4
5. 1118_Sh 3w
6. 983_Sev 3w
7. Blank
8. MM

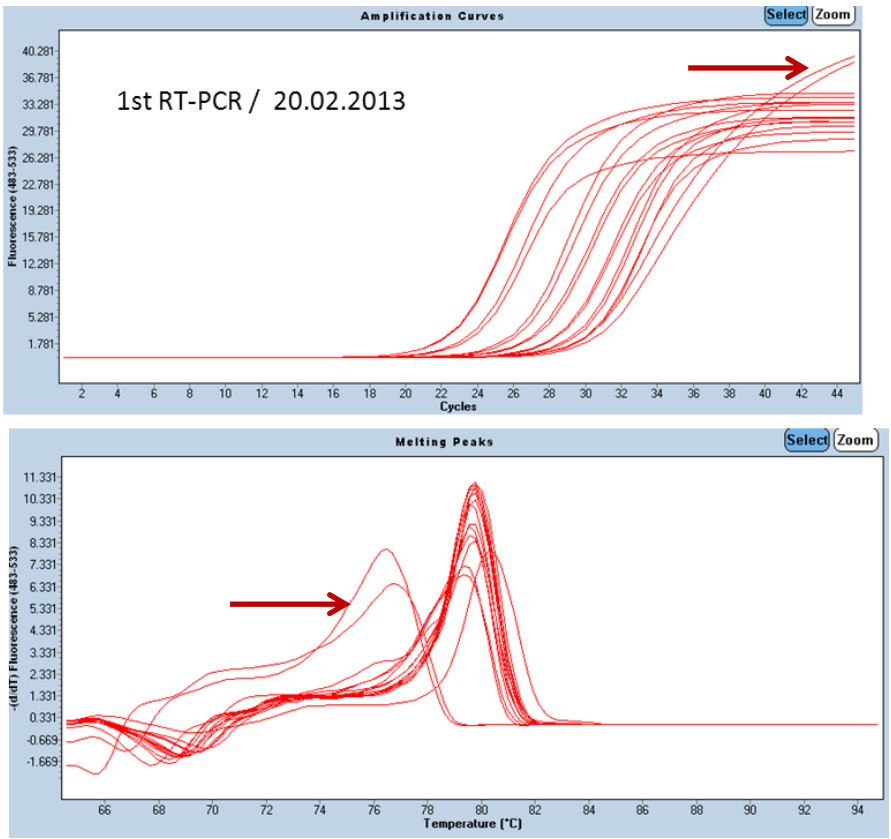

Figure 20: Amplification curves and melting peaks for U6 / 1st RT-PCR / 20.02.2013

The amplified samples were then charged on a 2% agarose gel, where the contaminations were confirmed through the presence of same PCR product (98bp) in blank and MM, as Fig.21 illustrates.

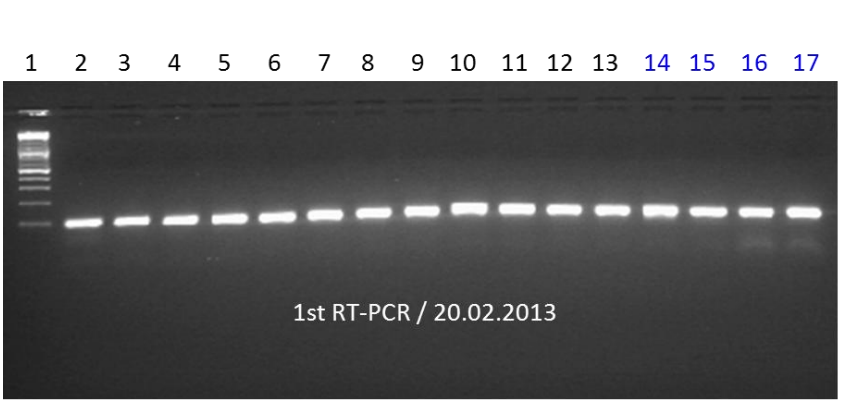

Figure 21: 2% agarose gel of the amplified samples of 1st RT-PCR / 20.02.2013

3.3.3. Contamination troubleshooting

The next RT-PCR experiments were set to determine the source of contamination, as point A) explained.

A) To check the water, in a second RT-PCR were used one miRNA sample (1101_sh d1) as positive control, a blank containing water from the water aliquot utilized in the previous RT-PCR, another blank with water took from our lab stock of RNase free water and also a master mix sample (Fig.22).

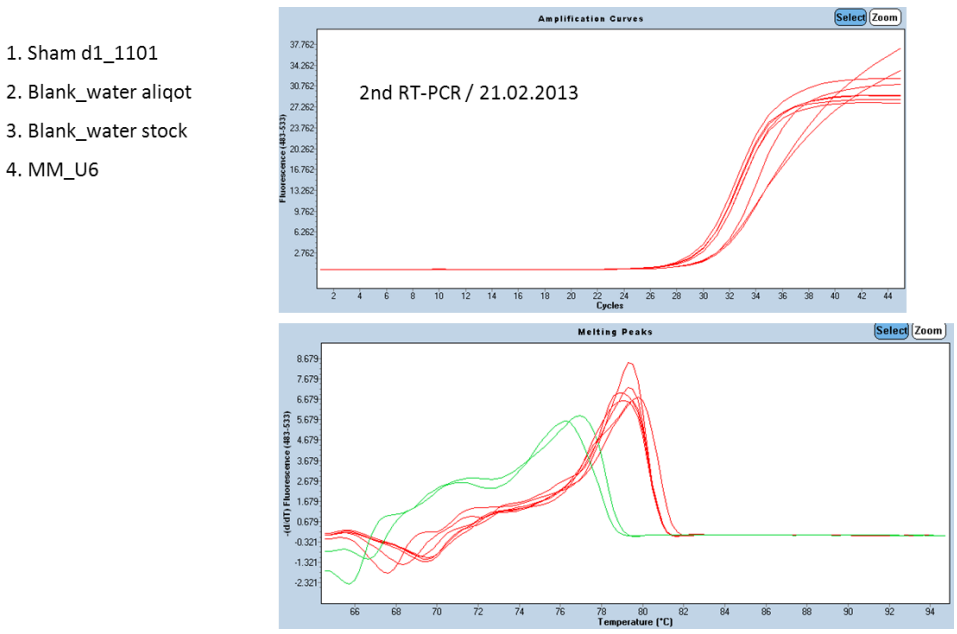

Figure 22: Amplification curves and melting peaks for U6 / 2nd RT-PCR / 21.02.2013

As Fig. 22 displays, contaminations appeared in both blanks and MM, suggesting two possibilities: either U6 primermix or Sybrgreen were contaminated.

Subsequently, to verify the source of contamination a third RT-PCR experiment with three parallel approaches was proposed, where again same contamination profile occurred (Fig.23).

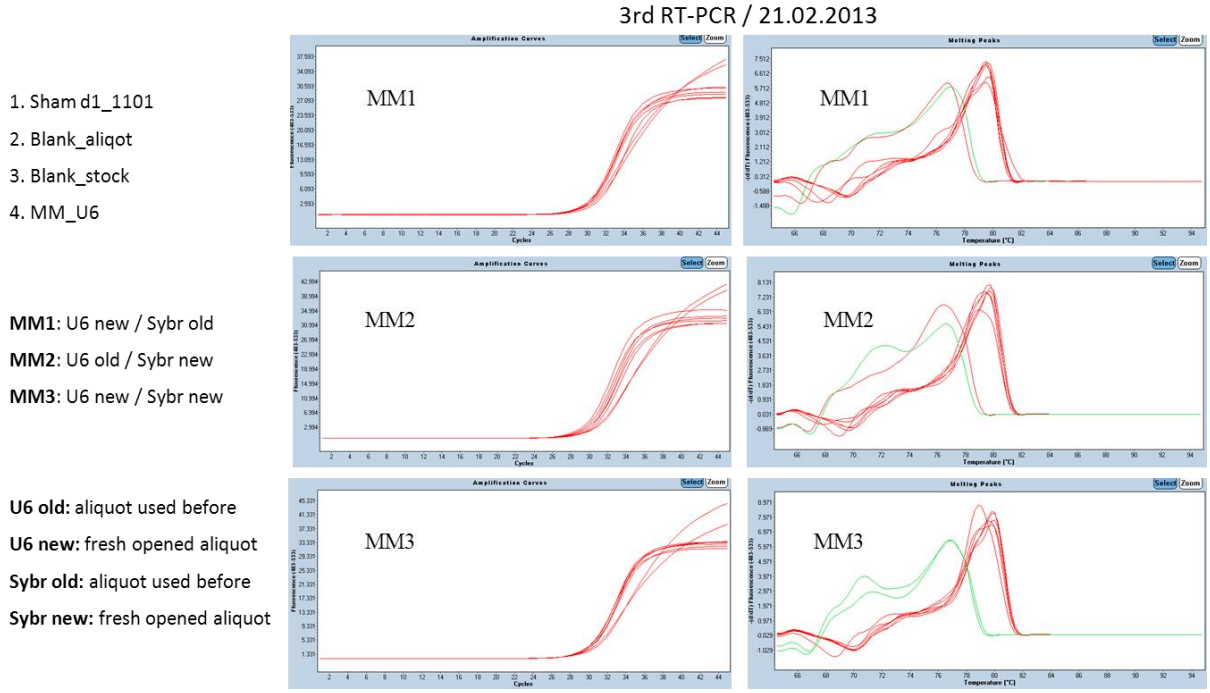

Figure 23: Amplification curves and melting peaks for U6 / 3rd RT_PCR / 21.02.2013

The contamination was also confirmed on the related gel, at which the PCR product appeared in all slots (Fig.24).

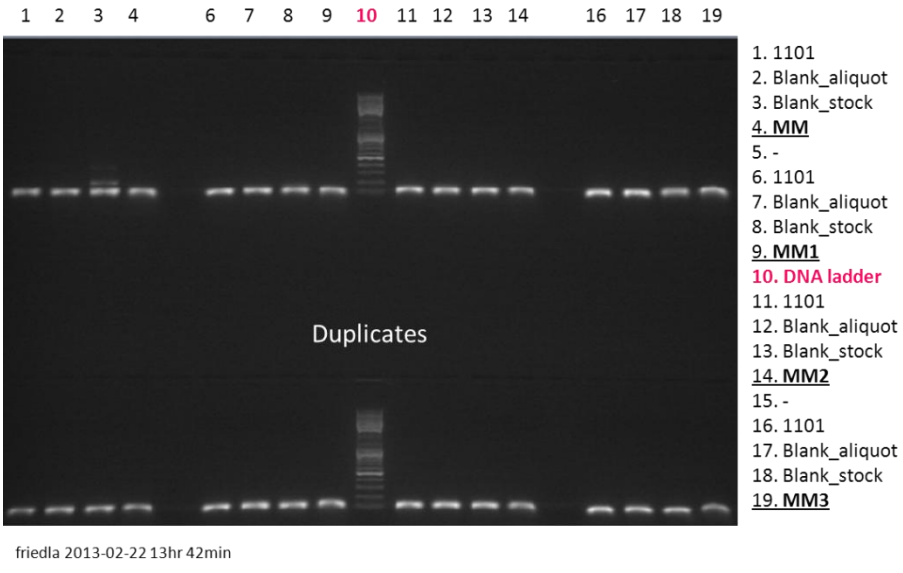

Figure 24: 2% agarose gel of the samples of 2nd and 3rd RT-PCR / 22.02.2013

Contaminations of blanks and MM at all three approaches of the 3rd RT-PCR, suggested a possible contamination of the water in which U6 primermix was initial diluted. Therefore a new U6 primermix was ordered, re-suspended in fresh RNase free water and the source of contamination was further followed up, as described at point B).

B) Following RT-PCRs tried to exclude any source of contamination, by preparing the PCR plate under lamina, using for the two MM the new ordered U6 primermix, with Sybr used before and also from a new original vial, like Fig. 25 presents.

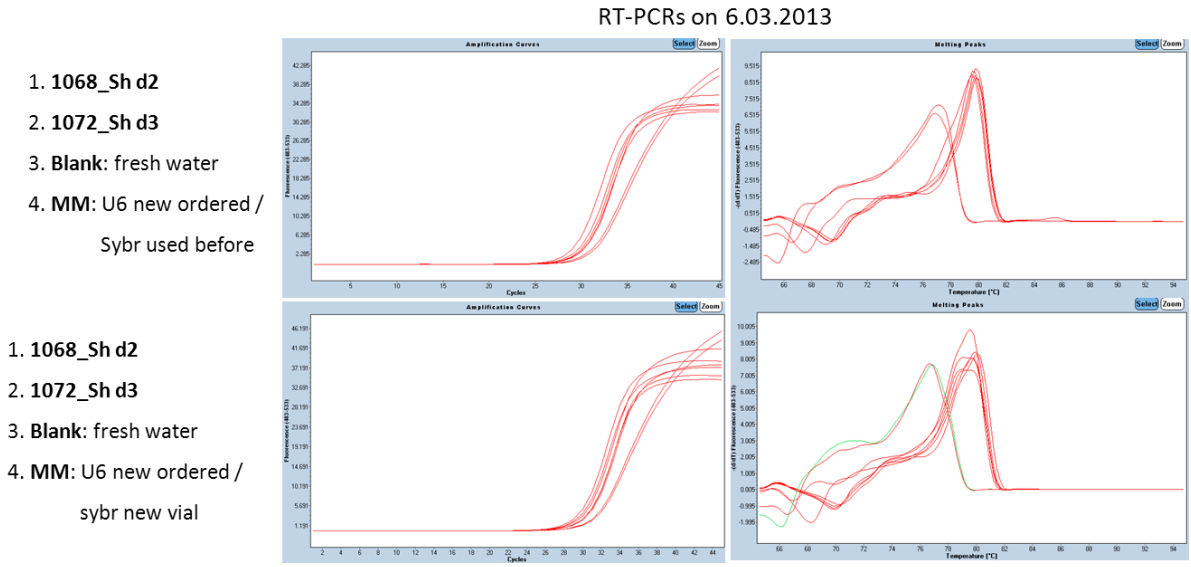

Figure 25: Amplification curves and melting peaks for U6 / RT_PCRs / 06.03.2013

The contamination visible in Fig.25 was also confirmed on subsequent gel, at which the same PCR product appeared in all slots (Fig.26).

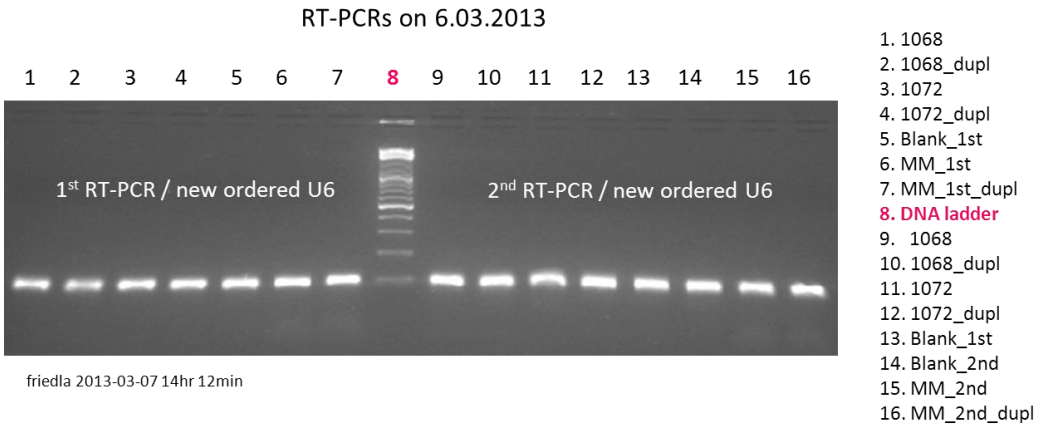

Figure 26: 2% agarose gel of the samples of RT-PCRs / 06.03.2013

After these RT-PCRs it was difficult to locate or relate errors to some imperfections and consequently Exiqon system was abandoned.

The following RT-PCRs were performed using a miScript PCR Starter Kit offered for free from Qiagen Company, as subsequent described.

3.3.4. qRT-PCR experiments by Qiagen

The miScript PCR starter Kit offered by Qiagen company, provided own cDNA synthesis compounds (which were used to prepare new cDNA by Qiagen) and two different reference genes: Hs_miR-15a_1 and U6 / RNU6-2-1.

First the miRNA samples of set 1 were converted into cDNA using Qiagen PCR starter kit. Next gel was executed to check the PCR results, proving similar bands as Fig.27 sshowed.

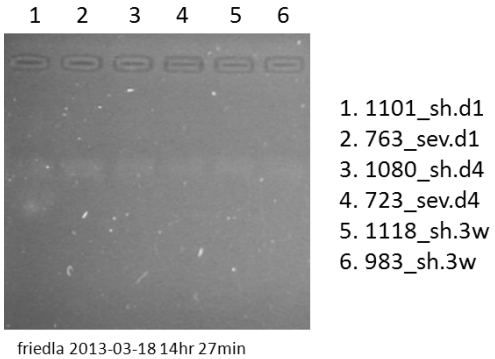

Figure 27: 1.2% FA agarose gel of miRNA samples measured by RG, 30ng/slot

RT-PCRs were performed then to test the before mentioned Qiagen reference genes (15a and U6), provided by miScript PCR starter kit, using the Qiagen cycling conditions (Tab.8).

Both trials looked ideal (similar duplicate amplification curves, single melting peaks of specific amplification products and no contaminations) (Fig.28-29).

1. 1101_Sh d1
2. RT-
3. Blank / Qiagen water
4. MM

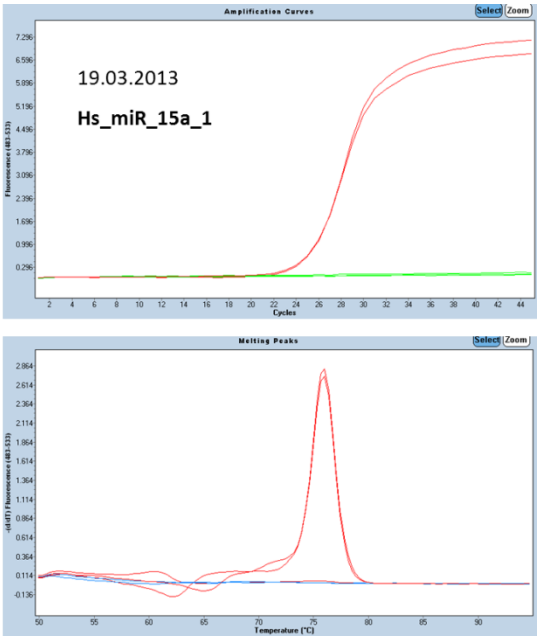

Figure 28: Amplification curves and melting peaks for “15a” gene / 19.03.2013

1. 1101_Sh d1
2. RT-
3. Blank / Qiagen water
4. MM

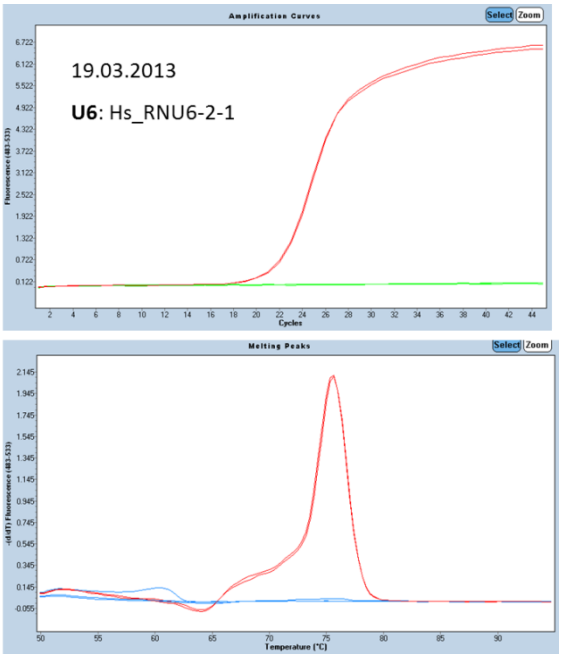

Figure 29: Amplification curves and melting peaks for “U6” gene / 19.03.2013

Afterwards in the following RT-PCR experiment was tested U6 reference gene from Qiagen for the set 1 (samples of Fig.27).

Besides a blank with water from Qiagen kit (sample 8.) was applied a blank containing RNase free water from our lab aliquots (sample 9.), which in previous RT-PCRs appeared contaminated and as Fig.30 illustrates, both blanks looked clean.

1. 1101_sh d1
2. 763_sev d1
3. 1080_sh d4
4. 723_sev d4
5. 1118_sh 3w
6. 983_sev 3w
7. RT(-)
8. Blank / Qiagen water
9. Blank / lab water aliqot
10. MM

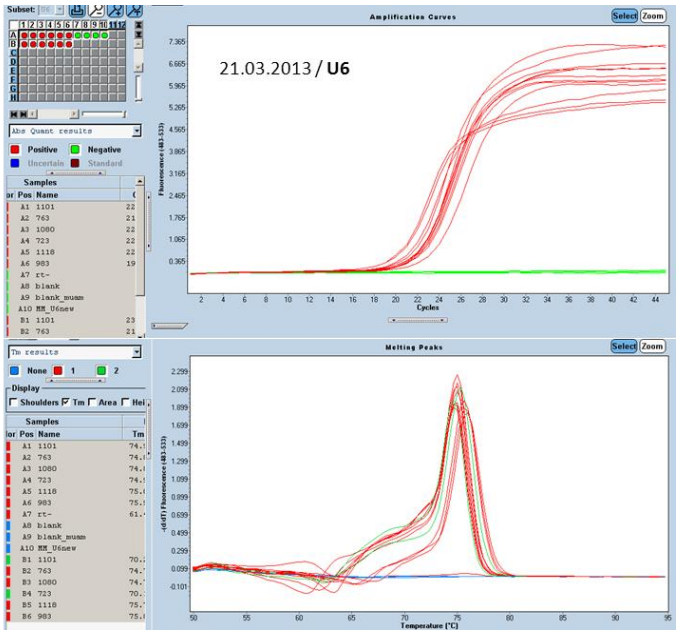

Figure 30: Amplification curves and melting peaks for "U6" / 21.03.2013

It is well-known that the melting peaks could be: red (one peak), blu (none), and green (two peaks). In this RT-PCR the duplicate of sample 1101 and of sample 723 appeared green (two peaks), indicating the presence of a primer dimer, besides the specific PCR product.

3.3.5. Qiagen cycling conditions optimisation

Because miRNAs possess highly conserved sequences, it was possible to use in the next RT-PCR experiments a "human miR-451 primer" from Exiqon, already available in our lab.

Since our lab water seemed to be clean, as proved before (Fig.30), was tested again the U6 primermix from Exiqon, used on 6.03.2013, which appeared to be contaminated at that time.

Consequently following RT-PCRs were performed at Qiagen cycling conditions, at which the annealing step was modified according to the optimal annealing requirements of Exiqon primers (1min, 60°C / Tab.9).

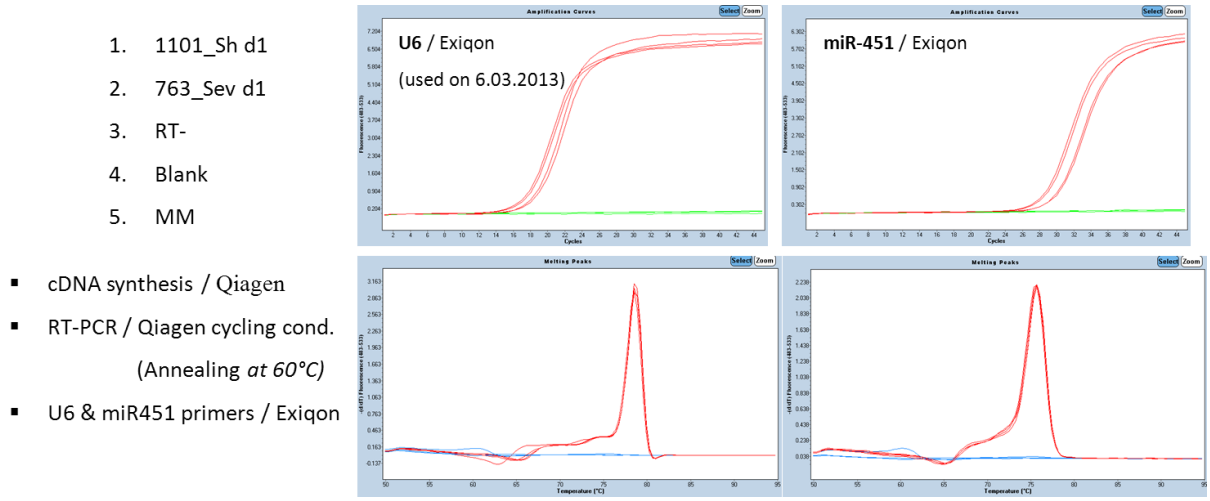

Figure 31: Amplification curves and melting peaks for "U6" / 08.04.2013

Fig. 31 illustrates proper amplification curves and corresponding melting peaks for the U6 reference gene and miR-451 target gene from Exiqon. No contaminations were indicated through green or blue lines of the blank, RT(-) and MM samples.

Consequently next RT-PCRs, whose results (ct values) were used to determine the post-TBI miR-451 temporal expression profile (Fig.32), were operated at prior established conditions:

- "U6 for rat" and "human miR-451", both from Exiqon, were used as primers.
- The real-time PCR reactions were performed using "Roche Light-Cycler 480" at Qiagen cycling conditions (Tab.8), at which the annealing step was modified, according to the optimal annealing settings for the Exiqon primers (1min, 60°C / Tab.9).

Raw data of qRT-PCR experiments used for the post-TBI miR-451 temporal expression profile graph (Fig.32) are showing at Chapter 5 (APPENDIX), Fig.50-62 and Tab.16-24.

3.4. miR-451 temporal expression profile post-TBI by qRT-PCR

The temporal expression profile of miR-451 after severe Fluid Percussion Injury (FPI), determined by qRT-PCR analysis of rat ipsilateral hippocampal tissue is shown in the graph of Fig 32.

Data is presented as change in threshold cycle of miR-451 post severe TBI, compared to sham operated animals, normalized to U6 reference gene, for the examined time points: 1 day, 4 days, 1 week, 2 weeks, and 3 weeks.

Changes of miR-451 expression after "severe TBI" are represented as "mean ΔΔct ± SEM" values of the five sets (see calculation at Tab.15 and 16 of Chapter 5), corresponding to each examined time point (1 day, 4 days, 1 week, 2 weeks, and 3 weeks).

The miR-451 expression level changes after "severe trauma" were statistically analysed as comparison between groups of the considered time points, using Student's t-test, performed in Excel, where significant differences were considered P-values less than 0.05 observable in Fig. 32.

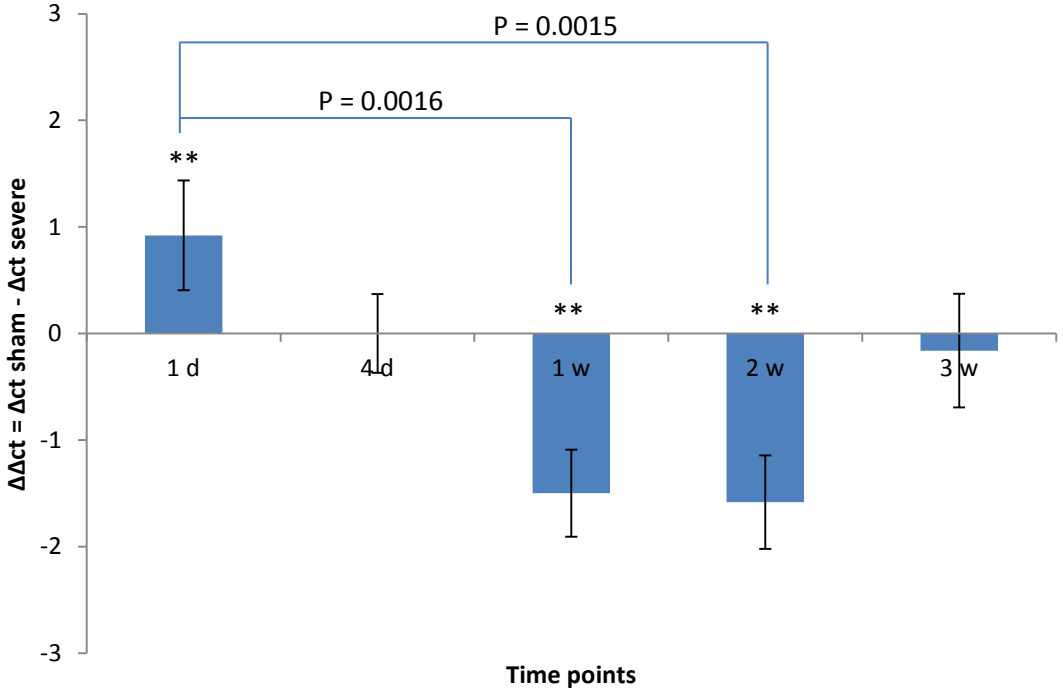

Figure 32: miR-451 temporal expression profile post-TBI, determined by qRT-PCR analysis of rat ipsilateral hippocampal tissue

As Fig. 32 illustrates, after severe TBI, miR-451 appears up-regulated in rat ipsilateral hippocampal tissue of day 1 comparing to sham, then at day 4 miR-451 expression returns to the sham level, but becomes significantly down-regulated after 1 week ($p=0.0016$) and 2 weeks ($p=0.0015$) relating to day 1, and later at 3 weeks' time point being less decreased, looking like returning to the sham level.

A p-value less than 0.001 denotes a 0.1% chance that „null hypothesis" or "no difference" between "day 1" group and "1 week" or "2 weeks" groups is true.

4. DISCUSSION

4.1. miR-451 expression changes after severe TBI

The miR-451 up-regulation at day 1 and the invariance at day 4 post-TBI correlate to the results of *Redell et al. 2009* (34), that found by microarray analysis a significantly up-regulation of miR-451 in rat ipsilateral hippocampus at 3h and 24h post-TBI and by RT-PCR an up-regulation at 24h and an invariance at 3 days post-injury.

A similar tendency was described by *Truettner et al 2011* (83), regarding miR-451 expression profiles in rat cerebral cortex with an increase of about 3 fold at 7h post-FPI in normothermia animals, by RT-PCR analysis.

Also *Hu et al. 2012* (29) reported an up-regulation of miR-451 at 24h time point, in rat controlled cortical impact (CCI) model.

On the other hand *Lei et al. 2009* (82) found out a more than two times down-regulation of miR-451 at 6h and 48h post injury in rat brain cortex by microarray analysis.

Truettner et al. 2013 (84) reported that miR-451-overexpression, induced by stretch injury, leads to increased stress and vulnerability in transfected neurons. “Stretch injured” cells overexpressing miR-451 compared to non-injured controls showed significant high expression levels for genes, which respond to miss-folded proteins (chaperone HSP70) or other cellular stress (cytokines IL-1β and TNF-α as well as pro-apoptotic gene Caspase 11).

MiR-451 implication in TBI is also supported by numerous experiments of our own research group, as next described.

Patz et al. 2013 (86) evidenced firstly that human cerebrospinal fluid (CSF) comprises membrane-sheathed microparticles (MPs) that shuttle proteins, mRNA and miRNA to local or distant target cells.

Along with this a significant miR-451 amount was reported only in CSF-MPs isolated from brain-injured vs. non-injured patients, but miR-451 was never detected in CSF-MPs derived from healthy subjects.

In addition the incubation of cultured *NTera2*[7] cells with CSF derived from brain-injured patients demonstrated a transfer of miR-451 to these cells through the down-regulation of specific target genes (*FGFR1*[8] or *CD133*[9]). But NTera2 cells incubated with CSF from healthy subjects (where no miR-451 was detected) showed no effect on the miR-451 target genes.

Moreover, CSF-MPs mediated down-regulation of miR-451 target genes was suppressed by adding "miR-451 antagomir" (miR-451 LNA inhibitor), in contrast to "miR-451 scrambled", suggesting that miR-451 specific sequence is critical for aforementioned target genes repression (Fig.33*).

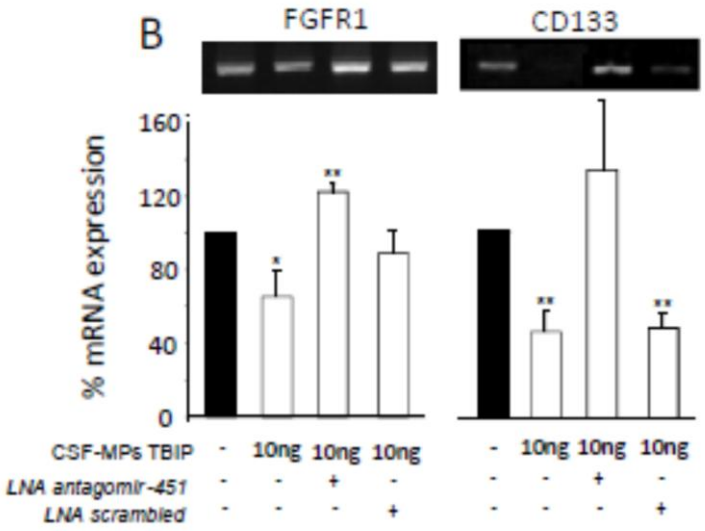

Figure 33*: Influence of CSF-MPs from TBI patients on NTera2 gene expression

CSF of TBI patients (TBIP) regulates FGFR1 and CD133 gene expression of NTera2 cells, through miR-451 contained in its MPs. The black column represents the mRNA expression without CSF-MPs of TBI patients, the second column indicates an mRNA down-regulation by adding of 10ng CSF-MPs from TBI patients, the third column suggests a repression of

[7] *NTera2*: human cell line with a phenotype resembling committed CNS neuronal precursor cells.

[8] *FGFR1*: fibroblast growth factor receptor 1, protein involved in cell division, regulation of cell growth and maturation, formation of blood vessels, wound healing, and embryonic development.

[9] *CD133*: protein localized to membrane protrusions on adult stem cells, is supposed to maintain stem cell properties by suppressing differentiation.

* Graph presented with friendly permission of Univ.-Prof. Dr. Ute Schäfer.

this down-regulation through "miR-451 antagomir" addition, and the last one shows an almost no effect on this down-regulation, when adding "miR-451 scrambled".

Experiments "in vitro" of our research group also reveal an increasing of miR-451 expression during neuronal differentiation, from a low expression in proliferating neuronal stem cells to highest expression at late differentiation stage (Fig. 34*).

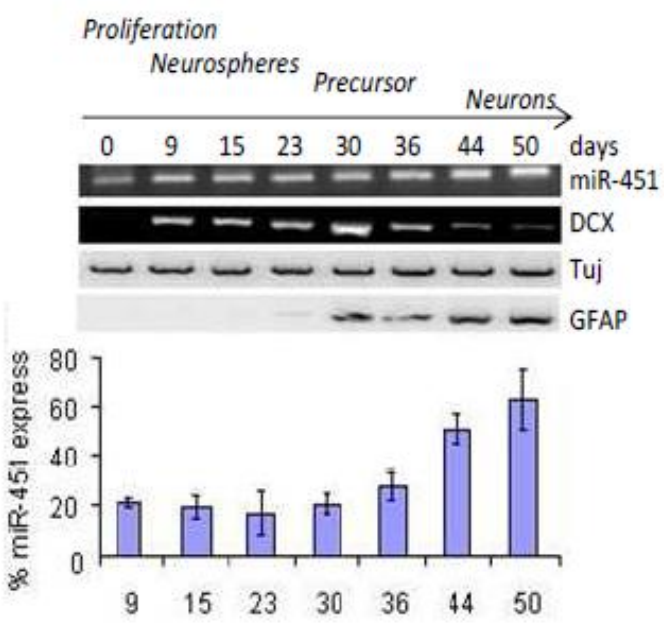

Figure 34*: miR-451 expression during "in vitro" cell differentiation of NTera2

During the 50 days neuronal differentiation of NTera2 cells "in vitro", can be observed a slowly miR-451 up-regulation with the highest level at late differentiation stage, along with expression changes of distinct target genes, for instance: *DCX* (doublecortin, a microtubule-associated protein, required for neuronal migration), *Tuj* (neuron specific β III tubulin, a neuronal marker), *GFAP* (glial fibrillary acidic protein, an intermediate filament protein).

The up-regulation of mir-451 at late neuronal differentiation stage, but not in the proliferating stage, correlates with the experimental attested miR-451 inhibition of cell-growth and proliferation in the field of numerous cancer types, acting as tumor-suppressor and its role in promoting cell differentiation, especially during erythropoiesis.

* Graph presented with friendly permission of Univ.-Prof. Dr. Ute Schäfer.

We could assume that miR-451-overexpression at day 1 post-TBI of the present work reflects a rapid adaptive response of the organism to the excessive cellular stress induced by severe brain trauma. This can be related to an elevated need of mature neuronal cells that can replace rapidly the damaged ones and subsequent acceleration of late neuronal differentiation stage and maturation, which is induced by high miR-451 level, linked to specific target genes expression changes, as Fig.33 illustrated before.

The described effect is also in accordance with the reported mir-451 high expression in other biological contexts:

- *erythropoiesis*, where elevated miR-451 induces basolateral epithelial cell polarity, acting as differentiation enhancer (87-94) and protector against oxidant stress (96, 97)
- *infections* (bacterial gram-positive, viral) inducing the cytokine production (99-101)
- *autoimmune diseases* like rheumatoid arthritis, systemic lupus erythematosus (103)
- *cardiomyopathy*, improving cardiomyocyte survival, having protective role (105-107)
- *tumors*, where its high expression promote excessive apoptosis, supressed cell proliferation and growth, invasion and metastasis (109-112, 116). Therefore was defined miR-451 as “tumor-supressor”.

However, miR-451 expression returns to the sham level at day 4 and becomes significant down-regulated at 1 week and 2 weeks post-TBI, then later at 3 weeks-time point being only less under-expressed, appearing to return to the sham-level (Fig.32).

The post-TBI miR-451 expression profile, at which the initial up-regulation at day 1 continues with a decrease to sham level at day 4 and furthermore a significant miR-451 down-regulation at 1 week – 2 weeks suggests a “neuronal proliferation period” (Fig.34) of about 2 weeks after the short initial phase of extreme cellular stress.

The mir-451 down-regulation linked to a neuronal proliferation phase could be connected to de-repression of genes like FGFR1 and CD133 (Fig.33) and processes as: neuronal proliferation (Fig.34), growth, blood vessels formation, wound healing.

This aspect can be correlated with the following results from “in situ hybridization”, obtained by our research group, as following described.

In this regard Fig.35* displays a marked miR-451 expression in the *dentate gyrus* of hippocampus at healthy rats (A, B, and B') in contrast to a down-regulation, indicated by no signal (C and C'), at moderate injured brain.

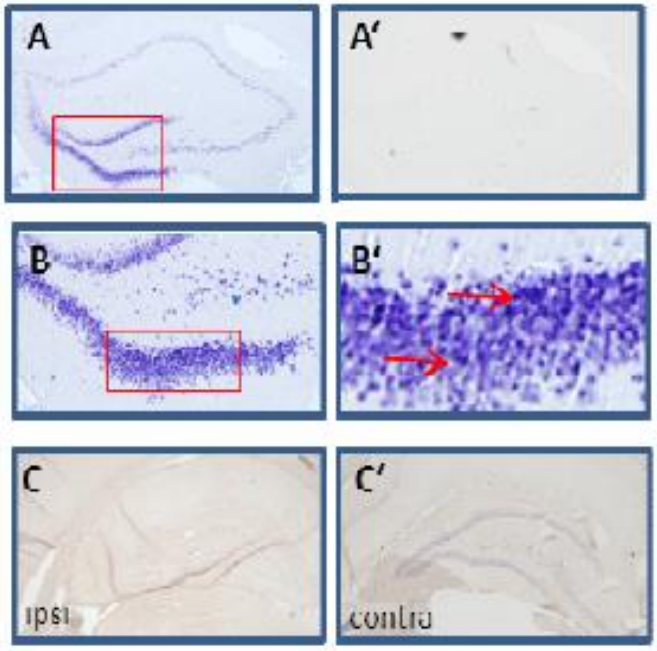

Figure 35*: miR-451 expression in rat hippocampal dentate gyrus

A-A' and B-B': healthy animal; C-C': moderate brain injured animal

In A, B and B' is noticeable a pronounced miR-451 expression, especially in the subgranular zone (SGZ) and granular cell layer (GCL) of the hippocampal dentate gyrus.

A' indicates no signal, by using of a "miR-451 scrambled" as a negative control.

C and C' suggest via negative signal a miR-451 down-regulation doing to a moderate trauma (by lateral fluid percussion of < 2.4 atm), 4 hours after TBI, mainly in the ipsilateral hippocampus (C).

As previous discussed, miR-451 overexpression is connected with intensive cell-differentiation, while its down-regulation is linked to neuronal cell proliferation (results of our research group) along with high tumor cell growth in different cancer types and poor prognosis (numerous published results).

* Graph presented with friendly permission of Univ.-Prof. Dr. Ute Schäfer.

Looking at the miR-451 temporal expression profile post-TBI in rat hippocampal tissue (Fig.32) can be supposed that TBI comprise a "initial short period" of about one day, with raised miR-451, linked to extreme cellular stress, apoptosis, neuronal maturation and growth, followed by a "proliferative period" of 2 weeks with significant miR-451 down-regulation and de-repression of genes as FGFR1 and CD133, related to intensive cell differentiation, proliferation and growth, increased DCX level along with neuronal migration, and a third period of "brain repair and regeneration", at which miR-451 level increases again in addition to adult neurogenesis and synaptic plasticity, strong neuronal maturation processes, apoptosis and wound healing.

Studies on TBI animal models associate *post-injury acute phase* with cell pathology and stress management, affecting genes involved in apoptosis, protein-folding, aerobic respiration, in contrast to *chronic phase*, particularly with regard to genes of brain repair mechanisms related to cytoskeletal organization and intracellular trafficking (46).

It was also published that TBI stimulates cell proliferation in rat hippocampus, where new-born neurons of subgranular zone (SGZ) surviving 10 weeks after TBI differentiate into mature neurons, contributing to cognitive recovery. Furthermore some *neuroblasts*[10] of subventricular zone (SVZ) migrate into "injured areas" instead of rostral migratory stream (RMS) and differentiate into neurons and glia (16).

As a consequence of all discussed facts, could be admitted that TBI comprises two distinct phases: an initial short **acute phase** as *"cell pathology and stress management phase"*, where miR-451 is up-regulated, promoting neurogenesis, neuronal maturation, apoptosis, followed then by a **chronic phase** as *"brain repair and regeneration mechanisms phase",* in which miR-451 becomes first significantly down-regulated about 2 weeks long, with subsequent de-repression of genes like FGFR1 and CD133, along with intensive cell differentiation, proliferation and growth, increased DCX level along with neuronal migration and then again a miR-451 increasing, linked to neurogenesis and synaptic plasticity, blood vessels formation, apoptosis and wound healing.

[10] *Neuroblasts* differentiate from neural stem cells and represent dividing cells that will develop into neurons, often after a migration phase. Neuroblasts can still undergo mitosis, whereas neurons are postmitotic.

4.2. Conclusion

This work was aimed to contribute at the elucidation of exact molecular and cellular mechanisms of traumatic brain injury, by analysing the miR-451 expression level of ipsilateral hippocampal tissue, after induced severe TBI in a rat "fluid percussion injury" (FPI) model at different time points: 1 day, 4 days, 1 week, 2weeks and 3 weeks.

This study might be considerate a novelty, since miR-451 expression level post-TBI at late time points (1 week, 2 weeks and 3 weeks) seems to be under-investigated.

The qRT-PCR analysis (Fig.32) showed that miR-451 temporal expression level, comparing to sham control animals, was up-regulated at day 1, invariant at day 4, statistically significant down-regulated at 1 week ($p=0.0016$) and 2 weeks ($p=0.0015$), being of some decrease at 3 weeks' time point, looking like returning slowly to the sham level.

Concluding the results of the present work, in addition to those from the literature, along with the unpublished results of our research group, thoroughly discussed in the previous chapter, TBI could be dividing in two phases:

- an initial short **acute phase** as *"cell pathology and stress management phase*", where miR-451 is up-regulated promoting neurogenesis, neuronal cell differentiation with predominant maturation, required by the high need of mature neuronal cells that can replace rapidly the damaged ones, strong apoptosis and fast removal of damaged cells, followed by
- a **chronic phase** as *"brain repair and regeneration mechanisms phase"*, in which miR-451 becomes first significantly down-regulated about 2 weeks, with subsequent de-repression of genes like FGFR1 and CD133, along with intensive cell proliferation and growth, increased DCX level along with neuronal migration and then again a miR-451 increasing, correlated mainly to neuronal differentiation and apoptosis, in addition to the continuance of neurogenesis, synaptic plasticity, blood vessels formation, wound healing and cognitive recovery. This chronic phase could be imagine as a "long time repair and regeneration phase", at which miR-451 is strong related to the complex adult neurogenesis processes and its expression will follow a "sinusoidal time profile" with up- and down-regulation periods, linked to prior discussed cellular mechanisms and processes of the brain.

5. APPENDIX

5.1. miRNA concentration values measured by RG

Tab.13 shows the concentration of miRNA samples of the five sets, measured by RiboGreen method, which were converted by Qiagen kit to cDNA, then used for RT-PCRs at Qiagen cycling conditions.

Table 13: Concentration of miRNA samples by RG, converted into cDNA by Qiagen, used for the post-TBI miR-451 temporal expression profile

	set 1	Conc. [ng/µl]	**set 2**	Conc. [ng/µl]	**set 3**	Conc. [ng/µl]	**set 4**	Conc. [ng/µl]	**set 5**	Conc. [ng/µl]
healthy	**1450**	20,40	**1451**	69,20	**1452**	34,80	**1451**	69,20	**1450**	20,40
sh d1	**1101**	21,00	**1100**	26,80	**1103**	9,50	**1032**	10,60	**1102**	24,40
sev d1	**763**	13,30	**1188**	24,90	**1189**	9,00	**1187**	11,50	**765**	10,00
sh d4	**1080**	18,20	**1083**	17,60	**1082**	15,30	**1038**	24,10	**1081**	15,70
sev d4	**723**	28,30	**1258**	44,60	**1245**	21,90	**1256**	17,90	**1242**	4,42
sh 1w	**1146**	3,44	**1147**	3,16	**1288**	4,03	**1458**	41,30	**1459**	52,80
sev 1w	**991**	6,63	**993**	5,18	**1229**	29,40	**1238**	44,30	**1465**	29,10
sh 2w	**1148**	4,75	**1150**	5,68	**1151**	5,03	**1283**	14,60	**1284**	4,90
sev 2w	**985**	3,02	**987**	2,17	**1239**	4,84	**1456**	33,80	**1460**	23,20
sh 3w			**1119**	13,30	**1120**	23,90	**1152**	40,50	**1121**	23,30
sev 3w	**983**	22,00	**976**	8,90	**1207**	16,70	**1305**	31,50	**1206**	24,10

As next Tab.14* presents the concentration of miRNA samples, measured by RG, which were converted into cDNA by Exiqon kit and are kept at -20°C, remaining to be used in future experiments.

* Concentration values are absent in case of miRNA samples deficit.

Table 14: Concentration of miRNA samples by RG, converted into cDNA by Exiqon

		Set 1	Conc. [ng/µl]	**Set 2**	Conc. [ng/µl]	**Set 3**	Conc. [ng/µl]	**Set 4**	Conc. [ng/µl]	**Set 5**	Conc. [ng/µl]
Day1	Sham+hbot	**1085**	20.6	**1086**	17.7	**1087**	16.4	**1084**	14.5	**1295**	35.0
	Moderate	**757**	16.3	**767**	3.5	**761**	-	**1192**	64,8	**1255**	34.6
	Mod+hbot	**657**	14.1	**653**	2.6	**659**	12.2	**1191**	31.0	**1190**	69.7
	Sev+hbot	**1040**	9.6	**1053**	9,6	**655**	20.0	**651**	18.0	**1303**	27.6
Day2	Sham	**1068**	24.7	**1070**	12.0	**1071**	9.8	**1076**	28.0	**1034**	19.6
	Sham+hbot	**1090**	27.8	**1091**	22.8	**1088**	41.1	**1089**	22.0	**1296**	24.8
	moderate	**713**	14.2	**715**	16.1	**711**	-	**717**	-	**1249**	29.1
	severe	**1002**	15.5	**719**	-	**1003**	16.5	**1204**	29.0	**1250**	18.0
	Mod+hbot	**671**	13.3	**667**	-	**669**	15.6	**1197**	38.0	**1201**	59.9
	Sev+hbot	**663**	14.0	**661**	3.0	**1195**	41.0	**1196**	45.0	**1200**	38.0
Day3	Sham	**1072**	14.7	**1073**	7.0	**1074**	12,0	**1075**	3.1	**1036**	26.4
	Sham+hbot	**1093**	42.6	**1094**	17.7	**1092**	33.0	**1095**	18.6	**1297**	24.0
	moderate	**751**	2.9	**753**	7.9	**998**	9.3	**1222**	53.0	**1223**	34.5
	severe	**997**	24.5	**733**	2.5	**1170**	29.8	**1216**	44.0	**1220**	36.5
	Mod+hbot	**645**	18,9	**643**	-	**647**	15.1	**1218**	53.0	**1214**	32.4
	Sev+hbot	**637**	15.0	**633**	-	**1012**	19.4	**1217**	42.0	**635**	30.1
Day4	Sham+hbot	**1096**	16.8	**1097**	20.0	**1098**	11.7	**1099**	20.5	**1298**	22.3
	Moderate	**731**	19.7	**727**	-	**729**	38.9	**1257**	50.0	**1254**	22.2
	Mod+hbot	**641**	19.8	**625**	-	**639**	26.5	**1253**	33.7	**1171**	17.7
	Sev+hbot	**1014**	15.8	**627**	2.6	**629**	16.7	**1259**	37.5	**631**	22.5

5.2. Raw data of standard curves and measured concentrations by RG

The standard curves together with appropriate concentrations of all RG measurements are visible in Fig. 36-49, where could be remarked: exact standard curves, standards almost precisely located on the linear slope, comparable values of the duplicates, observable at both, fluorescence and miRNA concentration values.

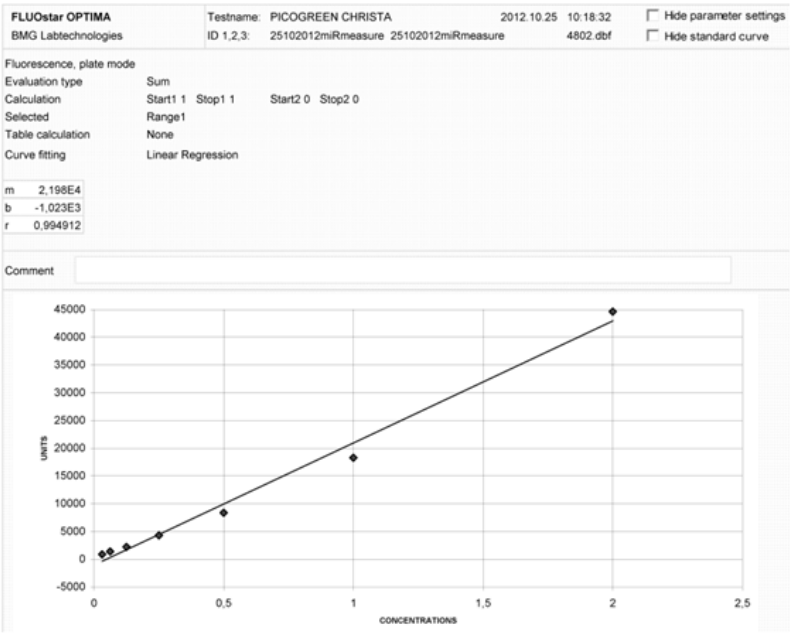

Sort contents: Up / Down | Sort sample IDs: Up / Down | Sort rows: Up / Down | Sort columns: Up / Down

Content	Sample ID	Well	Dilution factor	Raw data	Avge of replicates	SD of replicates	%CV	Calculated concentr.
B		A09	1,000	61	70	9	12,2	49,70E-3
B		B09		78				
S1		A01	1,000	45814	44608	1206	2,7	2,076
S1		B01		43402				
S2		A02	1,000	19144	18295	850	4,6	0,879
S2		B02		17445				
S3		A03	1,000	8204	8373	169	2,0	0,427
S3		B03		8541				
S4		A04	1,000	4311	4298	14	0,3	0,242
S4		B04		4284				
S5		A05	1,000	2432	2233	199	8,9	0,148
S5		B05		2034				
S6		A06	1,000	1452	1387	66	4,7	0,110
S6		B06		1321				
S7		A07	1,000	879	884	5	0,6	86,76E-3
S7		B07		889				
X1		C01	1,000	7048	6968	80	1,1	0,364
X1		D01		6888				
X2		C02	1,000	6586	6352	235	3,7	0,335
X2		D02		6117				
X3		C03	1,000	11686	11397	289	2,5	0,565
X3		D03		11108				
X4		C04	1,000	8618	7690	929	12,1	0,396
X4		D04		6761				
X5		C05	1,000	6354	5903	452	7,6	0,315
X5		D05		5451				
X6		C06	1,000	5021	4828	193	4,0	0,266
X6		D06		4635				
X7		C07	1,000	5397	5099	298	5,8	0,279
X7		D07		4801				
X8		C08	1,000	5854	5421	434	8,0	0,293
X8		D08		4987				

Figure 36: RG measurement on 25.10.2012

FLUOstar OPTIMA | Testname: PICOGREEN CHRISTA | 2012.10.24 11:53:06 | Hide parameter settings
BMG Labtechnologies | ID 1,2,3: 24102012miRmeasure 24102012miRmeasure | 4801.dbf | Hide standard curve

Fluorescence, plate mode
Evaluation type: Sum
Calculation: Start1 1 Stop1 1 Start2 0 Stop2 0
Selected: Range1
Table calculation: None
Curve fitting: Linear Regression

m	2,065E4
b	-6,545E2
r	0,994349

Comment

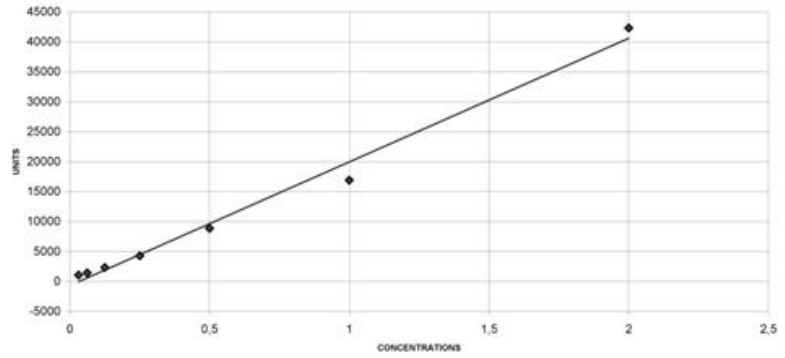

Sort contents: Up / Down | Sort sample IDs: Up / Down | Sort rows: Up / Down | Sort columns: Up / Down

Content	Sample ID	Well	Dilution factor	Raw data	Avge of replicates	SD of replicates	%CV	Calculated concentr.
B		A08	1,000	63	74	11	14,9	35,29E-3
B		B08		85				
S1		A01	1,000	40768	42320	1552	3,7	2,082
S1		B01		43872				
S2		A02	1,000	17486	16920	567	3,3	0,851
S2		B02		16353				
S3		A03	1,000	8621	8892	271	3,0	0,462
S3		B03		9162				
S4		A04	1,000	4380	4319	61	1,4	0,241
S4		B04		4258				
S5		A05	1,000	2336	2359	23	1,0	0,146
S5		B05		2382				
S6		A06	1,000	1427	1450	23	1,6	0,102
S6		B06		1473				
S7		A07	1,000	1156	1096	60	5,5	84,79E-3
S7		B07		1036				
X1		C01	1,000	9014	9540	526	5,5	0,494
X1		D01		10065				
X2		C02	1,000	10616	10795	179	1,7	0,555
X2		D02		10974				
X3		C03	1,000	5196	5195	2	0,0	0,283
X3		D03		5193				
X4		C04	1,000	5308	5728	420	7,3	0,309
X4		D04		6147				
X5		C05	1,000	80	3130	3050	97,4	0,183
X5		D05		6179				
X6		C06	1,000	11013	16802	5789	34,5	0,846
X6		D06		22591				
X7		C07	1,000	81	3451	3370	97,7	0,199
X7		D07		6821				
X8		C08	1,000	17624	16911	713	4,2	0,851
X8		D08		16198				
X9		C09	1,000	7288	7488	200	2,7	0,394
X9		D09		7687				
X10		C10	1,000	9469	9472	3	0,0	0,490
X10		D10		9475				
X11		C11	1,000	6809	7152	343	4,8	0,378
X11		D11		7494				
X12		C12	1,000	5192	5519	327	5,9	0,299
X12		D12		5845				

Figure 37: Raw data of RG measurement on 24.10.2012

FLUOstar OPTIMA
BMG Labtechnologies

Testname: PICOGREEN CHRISTA
ID 1,2,3: 29102012mir_2

2012.10.29 14:57:18
4806.dbf

Hide parameter settings
Hide standard curve

Fluorescence, plate mode
Evaluation type Sum
Calculation Start1 1 Stop1 1 Start2 0 Stop2 0
Selected Range1
Table calculation None
Curve fitting Linear Regression

m	2,922E4
b	-1,128E3
r	0,995331

Comment

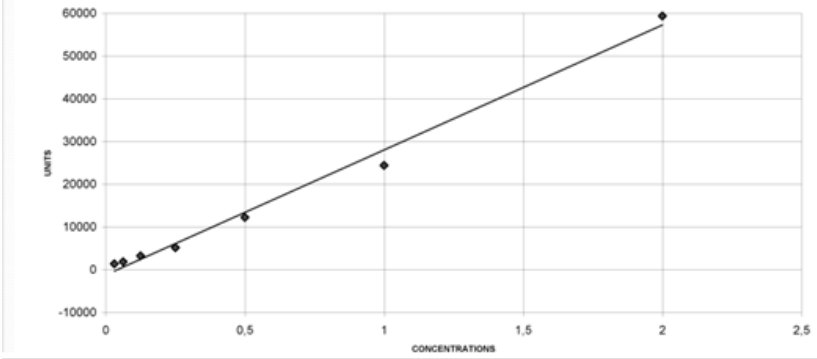

Sort contents: Up / Down | Sort sample IDs: Up / Down | Sort rows: Up / Down | Sort columns: Up / Down

Content	Sample ID	Well	Dilution factor	Raw data	Avge of replicates	SD of replicates	%CV	Calculated concentr.
B		E08	1,000	65	72	7	9,7	41,06E-3
B		F08		79				
S1		E01	1,000	62524	59418	3106	5,2	2,072
S1		F01		56312				
S2		E02	1,000	23555	24458	903	3,7	0,876
S2		F02		25360				
S3		E03	1,000	12195	12306	111	0,9	0,460
S3		F03		12416				
S4		E04	1,000	6114	5224	891	17,0	0,217
S4		F04		4333				
S5		E05	1,000	3522	3296	226	6,9	0,151
S5		F05		3070				
S6		E06	1,000	2036	1917	119	6,2	0,104
S6		F06		1798				
S7		E07	1,000	1282	1436	154	10,7	87,75E-3
S7		F07		1590				
X1		G01	1,000	12374	13108	734	5,6	0,487
X1		H01		13841				
X2		G02	1,000	9134	9188	54	0,6	0,353
X2		H02		9242				
X3		G03	1,000	5621	5852	231	3,9	0,239
X3		H03		6082				
X4		G04	1,000	12447	12156	292	2,4	0,455
X4		H04		11864				
X5		G05	1,000	8461	8245	216	2,6	0,321
X5		H05		8029				
X6		G06	1,000	9094	9221	127	1,4	0,354
X6		H06		9347				
X7		G07	1,000	7634	8030	396	4,9	0,313
X7		H07		8426				
X8		G08	1,000	10617	10559	58	0,5	0,400
X8		H08		10501				
X9		G09	1,000	60018	60983	965	1,6	2,126
X9		H09		61948				
X10		G10	1,000	4576	4414	162	3,7	0,190
X10		H10		4252				
X11		G11	1,000	8704	8464	240	2,8	0,328
X11		H11		8224				
X12		G12	1,000	21838	21579	260	1,2	0,777
X12		H12		21319				

Figure 38: Raw data of RG measurement on 29.10.2012

FLUOstar OPTIMA | Testname: PICOGREEN CHRISTA | 2012.12.03 11:32:05 | Hide parameter settings
BMG Labtechnologies | ID 1,2,3: 03 12 2012_miR | 4866.dbf | Hide standard curve

Fluorescence, plate mode
Evaluation type: Sum
Calculation: Start1 1 Stop1 1 Start2 0 Stop2 0
Selected: Range1
Table calculation: None
Curve fitting: Linear Regression

m	2,722E4
b	-3,502E2
r	0,999604

Comment

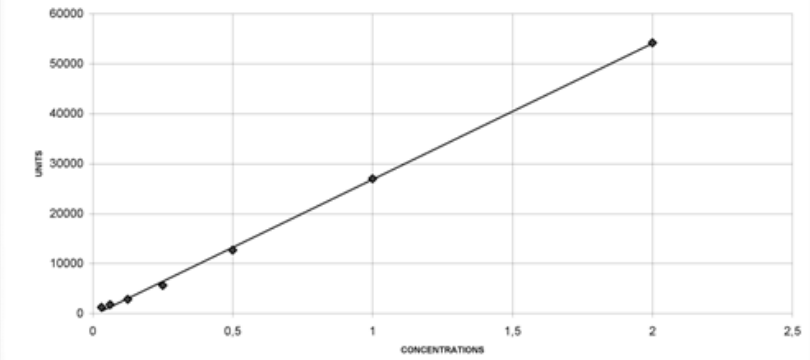

Sort contents		Sort sample IDs		Sort rows		Sort columns		
(•) Up	( ) Down	( ) Up	( ) Down	( ) Up	( ) Down	( ) Up	( ) Down	
Content	**Sample ID**	**Well**	**Dilution factor**	**Raw data**	**Avge of replicates**	**SD of replicates**	**%CV**	**Calculated concentr.**
B		A08	1,000	59	59	1	0,9	15,02E-3
B		B08		58				
S1		A01	1,000	43467	54234	10767	19,9	2,006
S1		B01		65000				
S2		A02	1,000	27433	27006	427	1,6	1,005
S2		B02		26579				
S3		A03	1,000	13123	12710	414	3,3	0,480
S3		B03		12296				
S4		A04	1,000	6265	5659	607	10,7	0,221
S4		B04		5052				
S5		A05	1,000	3079	2876	203	7,1	0,119
S5		B05		2673				
S6		A06	1,000	1877	1809	69	3,8	79,32E-3
S6		B06		1740				
S7		A07	1,000	1321	1271	50	3,9	59,57E-3
S7		B07		1221				
X1		C01	1,000	9355	8741	614	7,0	0,334
X1		D01		8127				
X2		C02	1,000	15243	14229	1014	7,1	0,536
X2		D02		13215				
X3		C03	1,000	7707	7541	167	2,2	0,290
X3		D03		7374				
X4		C04	1,000	36326	34908	1418	4,1	1,295
X4		D04		33490				
X5		C05	1,000	14384	13185	1200	9,1	0,497
X5		D05		11985				
X6		C06	1,000	10053	9460	593	6,3	0,360
X6		D06		8867				
X7		C07	1,000	15265	14889	377	2,5	0,560
X7		D07		14512				
X8		C08	1,000	12912	11634	1279	11,0	0,440
X8		D08		10355				
X9		C09	1,000	1060	1351	291	21,5	62,51E-3
X9		D09		1642				
X10		C10	1,000	10505	9767	738	7,6	0,372
X10		D10		9029				
X11		C11	1,000	9500	9222	278	3,0	0,352
X11		D11		8944				

Figure 39: Raw data of RG measurement on 03.12.2012

FLUOstar OPTIMA
BMG Labtechnologies

Testname: PICOGREEN CHRISTA 2012.12.04 13:17:52
ID 1,2,3: 04122012_miR 4871.dbf

☐ Hide parameter settings
☐ Hide standard curve

Fluorescence, plate mode
Evaluation type Sum
Calculation Start1 1 Stop1 1 Start2 0 Stop2 0
Selected Range1
Table calculation None
Curve fitting Linear Regression

m	3,201E4
b	-8,265E2
r	0,999036

Comment

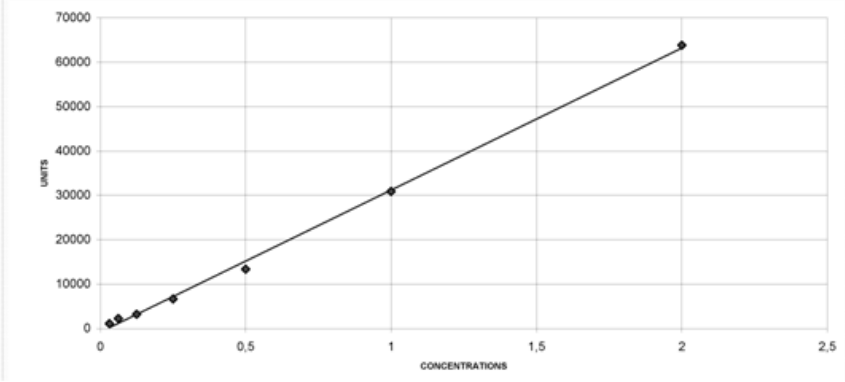

Sort contents		Sort sample IDs		Sort rows		Sort columns		
◉ Up	○ Down	○ Up	○ Down	○ Up	○ Down	○ Up	○ Down	
Content	**Sample ID**	**Well**	**Dilution factor**	**Raw data**	**Avge of replicates**	**SD of replicates**	**%CV**	**Calculated concentr.**
B		E08	1,000	50	58	8	13,8	27,63E-3
B		F08		66				
S1		E01	1,000	65000	63815	1186	1,9	2,019
S1		F01		62629				
S2		E02	1,000	34582	30891	3691	11,9	0,991
S2		F02		27200				
S3		E03	1,000	12311	13338	1027	7,7	0,442
S3		F03		14364				
S4		E04	1,000	6903	6664	239	3,6	0,234
S4		F04		6425				
S5		E05	1,000	3077	3219	142	4,4	0,126
S5		F05		3361				
S6		E06	1,000	2252	2243	9	0,4	95,89E-3
S6		F06		2234				
S7		E07	1,000	1138	1087	52	4,7	59,76E-3
S7		F07		1035				
X1		G01	1,000	12146	11972	174	1,5	0,400
X1		H01		11798				
X2		G02	1,000	5673	5429	244	4,5	0,195
X2		H02		5185				
X3		G03	1,000	23346	25541	2195	8,6	0,824
X3		H03		27736				
X4		G04	1,000	7628	6852	776	11,3	0,240
X4		H04		6076				
X5		G05	1,000	5251	5082	170	3,3	0,185
X5		H05		4912				
X6		G06	1,000	9153	8804	349	4,0	0,301
X6		H06		8455				
X7		G07	1,000	12407	11571	837	7,2	0,387
X7		H07		10734				
X8		G08	1,000	9432	8930	503	5,6	0,305
X8		H08		8427				
X9		G09	1,000	6461	6672	211	3,2	0,234
X9		H09		6883				
X10		G10	1,000	16844	16144	700	4,3	0,530
X10		H10		15444				

Figure 40: Raw data of RG measurement on 04.12.2012

FLUOstar OPTIMA
BMG Labtechnologies

Testname: PICOGREEN CHRISTA
ID 1,2,3: 07122012_mir_2

2012.12.07 10:55:39
4878.dbf

☐ Hide parameter settings
☐ Hide standard curve

Fluorescence, plate mode	
Evaluation type	Sum
Calculation	Start1 1 Stop1 1 Start2 0 Stop2 0
Selected	Range1
Table calculation	None
Curve fitting	Linear Regression

m	2,462E4
b	9,326E2
r	0,995045

Comment

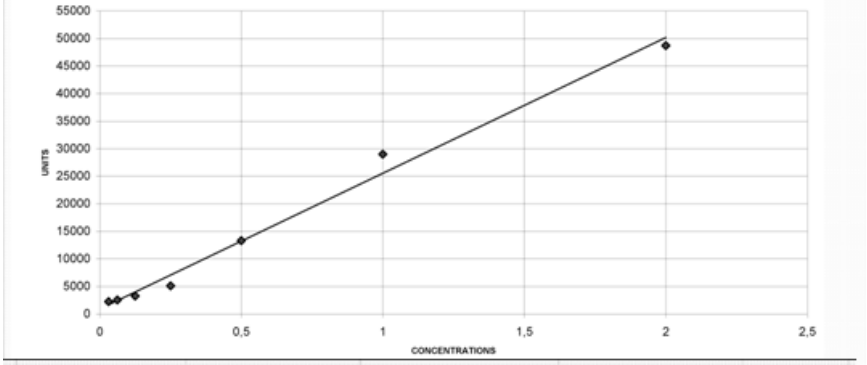

Sort contents		Sort sample IDs		Sort rows		Sort columns		
(•) Up	( ) Down	( ) Up	( ) Down	( ) Up	( ) Down	( ) Up	( ) Down	
Content	**Sample ID**	**Well**	**Dilution factor**	**Raw data**	**Avge of replicates**	**SD of replicates**	**%CV**	**Calculated concentr.**
B		E08	1,000	65	67	2	2,3	0
B		F08		68				
S1		E01	1,000	53583	48715	4869	10,0	1,941
S1		F01		43846				
S2		E02	1,000	26307	28989	2682	9,3	1,140
S2		F02		31671				
S3		E03	1,000	14035	13311	724	5,4	0,503
S3		F03		12587				
S4		E04	1,000	4165	5120	955	18,7	0,170
S4		F04		6075				
S5		E05	1,000	2983	3289	306	9,3	95,69E-3
S5		F05		3594				
S6		E06	1,000	1823	2548	725	28,4	65,59E-3
S6		F06		3272				
S7		E07	1,000	3653	2265	1389	61,3	54,10E-3
S7		F07		876				
X1		G01	1,000	20037	21181	1144	5,4	0,822
X1		H01		22325				
X2		G02	1,000	5904	5664	240	4,2	0,192
X2		H02		5424				
X3		G03	1,000	11675	11002	674	6,1	0,409
X3		H03		10328				
X4		G04	1,000	24984	25550	566	2,2	1,000
X4		H04		26115				
X5		G05	1,000	23396	22889	508	2,2	0,892
X5		H05		22381				
X6		G06	1,000	17469	17536	67	0,4	0,674
X6		H06		17603				
X7		G07	1,000	20758	19389	1370	7,1	0,750
X7		H07		18019				
X8		G08	1,000	6325	6155	170	2,8	0,212
X8		H08		5985				
X9		G09	1,000	18662	18166	496	2,7	0,700
X9		H09		17670				
X10		G10	1,000	18027	17944	84	0,5	0,691
X10		H10		17860				
X11		G11	1,000	6890	6574	316	4,8	0,229
X11		H11		6258				
X12		G12	1,000	36544	35263	1282	3,6	1,394
X12		H12		33981				

Figure 41: Raw data of RG measurement on 07.12.2012

FLUOstar OPTIMA
BMG Labtechnologies

Testname: PICOGREEN CHRISTA
ID 1,2,3: 29122012_miR

2012.12.29 11:01:30
4912.dbf

☐ Hide parameter settings
☐ Hide standard curve

Fluorescence, plate mode
Evaluation type Sum
Calculation Start1 1 Stop1 1 Start2 0 Stop2 0
Selected Range1
Table calculation None
Curve fitting Linear Regression

m	3,004E4
b	-2,224E3
r	0,990183

Comment

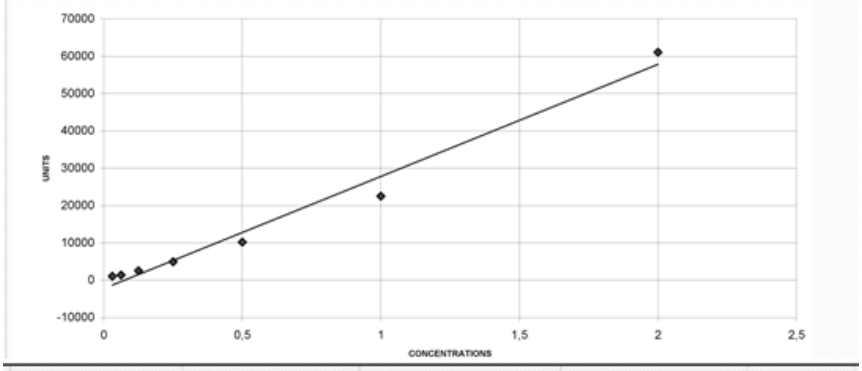

Sort contents: ◉ Up ○ Down | Sort sample IDs: Up Down | Sort rows: Up Down | Sort columns: Up Down

Content	Sample ID	Well	Dilution factor	Raw data	Avge of replicates	SD of replicates	%CV	Calculated concentr.
B		A08	1,000	84	96	12	12,0	77,20E-3
B		B08		107				
S1		A01	1,000	65000	61081	3920	6,4	2,107
S1		B01		57161				
S2		A02	1,000	24821	22478	2343	10,4	0,822
S2		B02		20135				
S3		A03	1,000	10559	10166	394	3,9	0,412
S3		B03		9772				
S4		A04	1,000	5228	4960	268	5,4	0,239
S4		B04		4692				
S5		A05	1,000	2544	2533	12	0,5	0,158
S5		B05		2521				
S6		A06	1,000	1439	1387	53	3,8	0,120
S6		B06		1334				
S7		A07	1,000	1135	1066	69	6,5	0,110
S7		B07		997				
X1		C01	1,000	14154	14325	171	1,2	0,551
X1		D01		14495				
X2		C02	1,000	10135	9523	612	6,4	0,391
X2		D02		8911				
X3		C03	1,000	12151	12656	505	4,0	0,495
X3		D03		13161				
X4		C04	1,000	16222	15220	1002	6,6	0,581
X4		D04		14218				
X5		C05	1,000	8845	8588	258	3,0	0,360
X5		D05		8330				
X6		C06	1,000	34071	33772	299	0,9	1,198
X6		D06		33473				
X7		C07	1,000	20417	20604	187	0,9	0,760
X7		D07		20790				
X8		C08	1,000	13520	13611	91	0,7	0,527
X8		D08		13702				
X9		C09	1,000	12678	12199	480	3,9	0,480
X9		D09		11719				
X10		C10	1,000	18941	18469	472	2,6	0,689
X10		D10		17997				
X11		C11	1,000	22234	19692	2542	12,9	0,729
X11		D11		17150				
X12		C12	1,000	18505	17227	1279	7,4	0,647
X12		D12		15948				

Figure 42: Raw data of RG measurement on 29.12.2012

FLUOstar OPTIMA
BMG Labtechnologies

Testname: PICOGREEN CHRISTA 2013.01.07 15:01:28
ID 1,2,3: 07012013_mir 4930.dbf

☐ Hide parameter settings
☐ Hide standard curve

Fluorescence, plate mode
Evaluation type Sum
Calculation Start1 1 Stop1 1 Start2 0 Stop2 0
Selected Range1
Table calculation None
Curve fitting Linear Regression

m	2,688E4
b	-1,913E3
r	0,994416

Comment

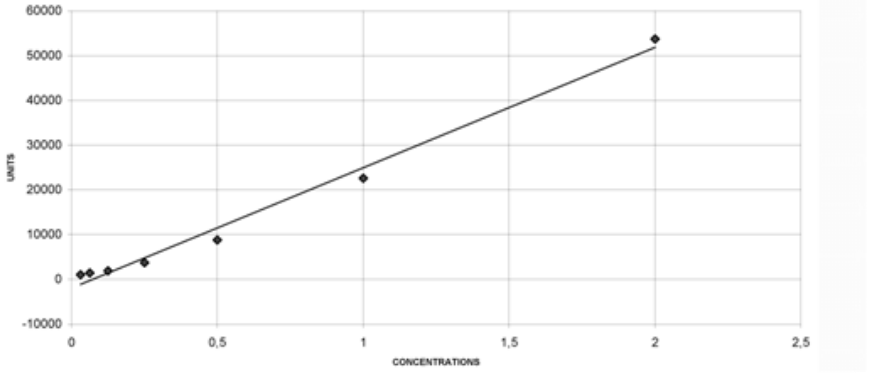

Sort contents: Up / Down | Sort sample IDs: Up / Down | Sort rows: Up / Down | Sort columns: Up / Down

Content	Sample ID	Well	Dilution factor	Raw data	Avge of replicates	SD of replicates	%CV	Calculated concentr.
B		A08	1,000	54	65	11	16,9	73,59E-3
B		B08		76				
S1		A01	1,000	47728	53730	6002	11,2	2,070
S1		B01		59731				
S2		A02	1,000	22198	22594	396	1,8	0,912
S2		B02		22990				
S3		A03	1,000	9178	8832	347	3,9	0,400
S3		B03		8485				
S4		A04	1,000	3844	3730	115	3,1	0,210
S4		B04		3615				
S5		A05	1,000	1974	1933	42	2,1	0,143
S5		B05		1891				
S6		A06	1,000	1495	1433	62	4,3	0,124
S6		B06		1371				
S7		A07	1,000	1337	1043	295	28,2	0,110
S7		B07		748				
X1		C01	1,000	14849	14272	577	4,0	0,602
X1		D01		13695				
X2		C02	1,000	12666	11021	1646	14,9	0,481
X2		D02		9375				
X3		C03	1,000	10163	10080	83	0,8	0,446
X3		D03		9997				
X4		C04	1,000	10531	10129	402	4,0	0,448
X4		D04		9727				
X5		C05	1,000	7960	7719	242	3,1	0,358
X5		D05		7477				
X6		C06	1,000	4436	4367	69	1,6	0,234
X6		D06		4298				
X7		C07	1,000	10827	10165	663	6,5	0,449
X7		D07		9502				
X8		C08	1,000	6688	6950	262	3,8	0,330
X8		D08		7211				
X9		C09	1,000	7480	6440	1040	16,1	0,311
X9		D09		5400				
X10		C10	1,000	13501	14077	576	4,1	0,595
X10		D10		14653				

Figure 43: Raw data of RG measurement on 07.01.2013

FLUOstar OPTIMA	Testname:	PICOGREEN CHRISTA	2013.01.10 15:31:56	Hide parameter settings
BMG Labtechnologies	ID 1,2,3:	10012013_mir	4941.dbf	Hide standard curve

Fluorescence, plate mode	
Evaluation type	Sum
Calculation	Start1 1 Stop1 1 Start2 0 Stop2 0
Selected	Range1
Table calculation	None
Curve fitting	Linear Regression

m	3,002E4
b	-1,582E3
r	0,994431

Comment

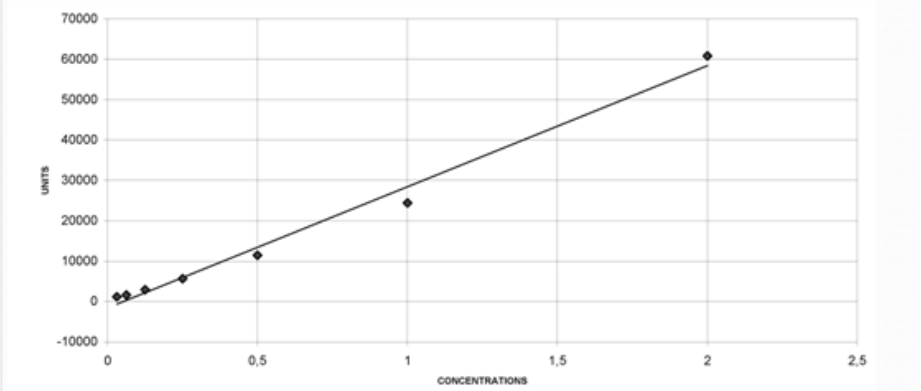

Sort contents		Sort sample IDs		Sort rows		Sort columns		
Up	Down	Up	Down	Up	Down	Up	Down	
Content	**Sample ID**	**Well**	**Dilution factor**	**Raw data**	**Avge of replicates**	**SD of replicates**	**%CV**	**Calculated concentr.**
B		A08	1,000	585	338	248	73,3	63,94E-3
B		B08		90				
S1		A01	1,000	64167	60866	3301	5,4	2,080
S1		B01		57565				
S2		A02	1,000	24921	24436	485	2,0	0,867
S2		B02		23951				
S3		A03	1,000	11320	11468	148	1,3	0,435
S3		B03		11616				
S4		A04	1,000	6331	5647	684	12,1	0,241
S4		B04		4963				
S5		A05	1,000	2974	2896	78	2,7	0,149
S5		B05		2818				
S6		A06	1,000	1603	1582	21	1,3	0,105
S6		B06		1561				
S7		A07	1,000	1033	1168	135	11,6	91,61E-3
S7		B07		1303				
X1		C01	1,000	14324	14216	109	0,8	0,526
X1		D01		14107				
X2		C02	1,000	6418	6458	40	0,6	0,268
X2		D02		6497				
X3		C03	1,000	10174	10186	12	0,1	0,392
X3		D03		10198				
X4		C04	1,000	14363	13910	453	3,3	0,516
X4		D04		13457				
X5		C05	1,000	12713	13042	329	2,5	0,487
X5		D05		13370				
X6		C06	1,000	21936	21053	884	4,2	0,754
X6		D06		20169				
X7		C07	1,000	17175	16704	471	2,8	0,609
X7		D07		16233				
X8		C08	1,000	13798	13690	108	0,8	0,509
X8		D08		13582				
X9		C09	1,000	15655	15297	359	2,3	0,562
X9		D09		14938				

Figure 44: Raw data of RG measurement on 04.12.2012

Test Run: PICOGREEN CHRISTA 2013.02.05 21:34:24 1431.dbf

OPTIMA BMG LABTECH	Testname: PICOGREEN CHRISTA ID 1,2,3: 05022013_miRconc_(2)		2013.02.05 21:34:24 1431.dbf		Hide parameter settings Hide standard curve

Fluorescence, plate mode
Evaluation type: Sum
Calculation: Start1: 1 Stop1: 1 Start2: 0 Stop2: 0
Selected: Range1
Table calculation: None
Curve fitting: Linear Regression; X-Axis log, Y-Axis log

m	9,732E-1
b	4,318E0
r	0,995830

Comment:

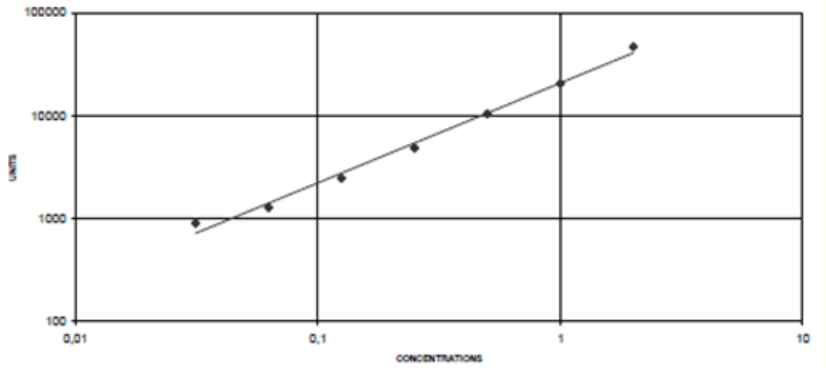

Test Run: PICOGREEN CHRISTA 2013.02.05 21:34:24 1431.dbf

	Sort contents		Sort sample IDs		Sort rows		Sort columns		Avg. of replicates
	Up / Down		Up / Down		Up / Down		Up / Down		
	Content	Sample ID	Well	Dilution factor	Raw data	Avg of replicates	SD of replicates	%CV	Calculated concentr.
	B		A08	1,000	57	65	8	11,6	2,33E-3
	B		B08		72				2,96E-3
	S1		A01	1,000	47320	46862	458	1,0	2,326
	S1		B01		46404				2,280
	S2		A02	1,000	20282	20518	236	1,2	0,974
	S2		B02		20754				0,997
	S3		A03	1,000	10095	10372	277	2,7	0,476
	S3		B03		10648				0,502
	S4		A04	1,000	4910	4834	77	1,6	0,227
	S4		B04		4757				0,220
	S5		A05	1,000	2388	2445	57	2,3	0,108
	S5		B05		2502				0,113
	S6		A06	1,000	1300	1268	33	2,6	57,88E-3
	S6		B06		1235				54,91E-3
	S7		A07	1,000	911	895	16	1,8	40,17E-3
	S7		B07		879				38,72E-3
	X1		C01	1,000	535	470	66	14,0	23,25E-3
	X1		D01		404				17,42E-3
	X2		C02	1,000	34277	34113	165	0,5	1,670
	X2		D02		33948				1,654
	X3		C03	1,000	33342	32665	677	2,1	1,623
	X3		D03		31988				1,556
	X4		C04	1,000	29574	29296	279	1,0	1,435
	X4		D04		29017				1,407
	X5		C05	1,000	5384	5258	126	2,4	0,249
	X5		D05		5132				0,237
	X6		C06	1,000	5987	5711	276	4,8	0,278
	X6		D06		5435				0,252
	X7		C07	1,000	10635	10146	490	4,8	0,502
	X7		D07		9656				0,454
	X8		C08	1,000	9531	9333	199	2,1	0,448
	X8		D08		9134				0,429
	X9		C09	1,000	3898	3858	41	1,0	0,179
	X9		D09		3817				0,175

Figure 45: Raw data of RG measurement on 05.02.2013

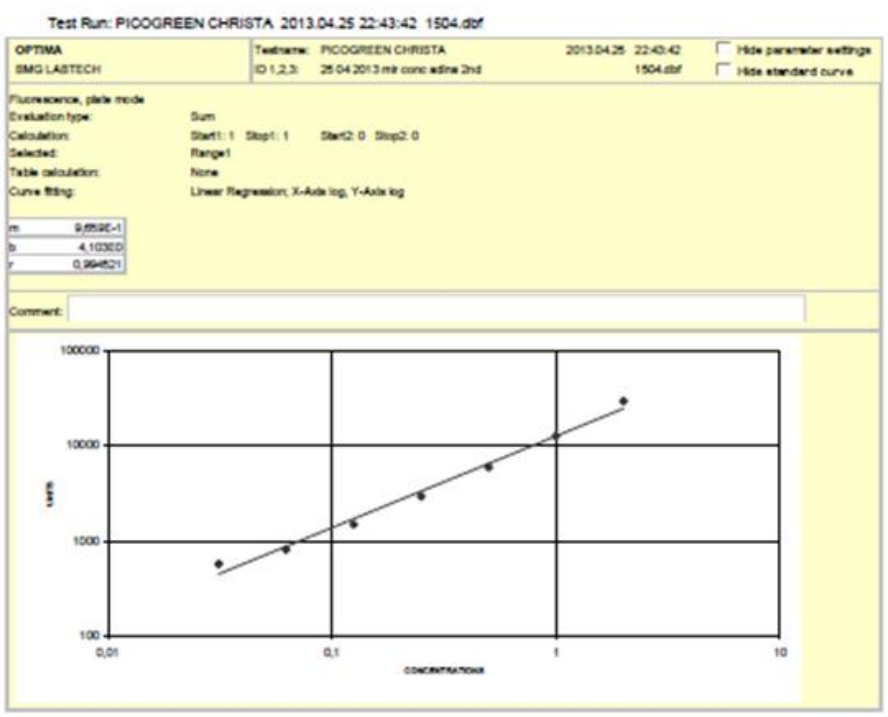

Test Run: PICOGREEN CHRISTA 2013.04.25 22:43:42 1504.dbf

Sort contents Up	Sort contents Down	Sort sample IDs Up	Sort sample IDs Down	Sort rows Up	Sort rows Down	Sort columns Up	Sort columns Down	Avg. of replicates
Content	Sample ID	Well	Dilution factor	Raw data	Avg. of replicates	SD of replicates	%CV	Calculated concentr.
S		A06	1,000	35	36	3	7,9	2,24E-3
S		B06		41				2,64E-3
S1		A01	1,000	28971	29618	647	2,2	2,350
S1		B01		30266				2,459
S2		A02	1,000	13016	12690	326	2,6	1,027
S2		B02		12364				0,973
S3		A03	1,000	5968	5954	36	0,6	0,460
S3		B03		5919				0,454
S4		A04	1,000	2962	2940	23	0,8	0,222
S4		B04		2917				0,218
S5		A05	1,000	1514	1486	28	1,9	0,111
S5		B05		1458				0,106
S6		A06	1,000	787	809	22	2,7	56,22E-3
S6		B06		830				59,40E-3
S7		A07	1,000	593	570	23	4,0	41,94E-3
S7		B07		547				38,57E-3
X1		C01	1,000	4396	4253	146	3,4	0,334
X1		D01		4107				0,311
X2		C02	1,000	2275	2404	129	5,4	0,169
X2		D02		2533				0,189
X3		C03	1,000	4666	4752	86	1,8	0,356
X3		D03		4837				0,368
X4		C04	1,000	5112	5709	403	7,1	0,469
X4		D04		5306				0,405
X5		C05	1,000	5996	6051	55	0,9	0,460
X5		D05		6106				0,469
X6		C06	1,000	10774	10341	433	4,2	0,844
X6		D06		9908				0,774
X7		C07	1,000	6461	6266	195	3,1	0,497
X7		D07		6071				0,466
X8		C08	1,000	4605	4391	296	6,7	0,356
X8		D08		4096				0,310
X9		C09	1,000	8522	8117	405	5,0	0,662
X9		D09		7711				0,597
X10		C10	1,000	5605	5327	279	5,2	0,429
X10		D10		5048				0,386
X11		C11	1,000	18562	17361	1202	7,1	1,464
X11		D11		16119				1,261
X12		C12	1,000	8757	8904	147	1,9	0,682
X12		D12		9100				0,709

Figure 46: Raw data of RG measurement on 05.02.2013

Test Run: PICOGREEN CHRISTA 2013.05.03 21:58:00 1505.dbf

OPTIMA BMG LABTECH	Testname: PICOGREEN CHRISTA ID 1,2,3: 03 05 2013 mir conc adina		2013.05.03 21:58:00 1505.dbf	Hide parameter settings Hide standard curve

Fluorescence, plate mode

Evaluation type:	Sum
Calculation:	Start1: 1 Stop1: 1 Start2: 0 Stop2: 0
Selected:	Range1
Table calculation:	None
Curve fitting:	Linear Regression; X-Axis log, Y-Axis log

m	9,668E-1
b	4,112E0
r	0,995015

Comment:

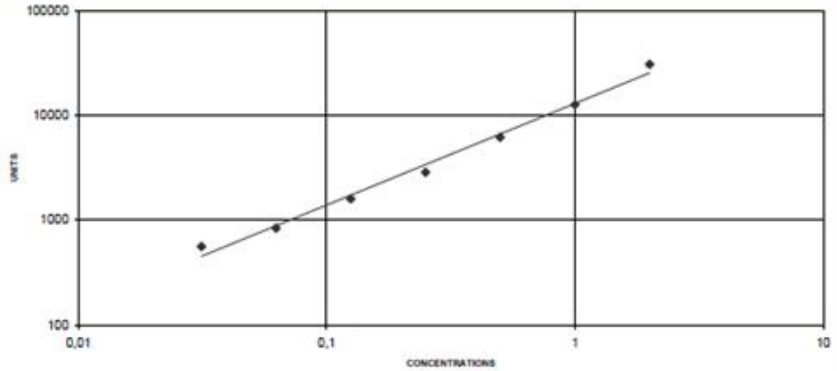

Test Run: PICOGREEN CHRISTA 2013.05.03 21:58:00 1505.dbf

Content	Sample ID	Well	Dilution factor	Raw data	Avg of replicates	SD of replicates	%CV	Calculated concentr.
B		A08	1,000	31	34	3	8,8	1,95E-3
B		B08		37				2,34E-3
S1		A01	1,000	32406	30607	1800	5,9	2,581
S1		B01		28807				2,285
S2		A02	1,000	12662	12622	41	0,3	0,977
S2		B02		12581				0,970
S3		A03	1,000	6370	6185	185	3,0	0,480
S3		B03		6000				0,451
S4		A04	1,000	2928	2862	66	2,3	0,215
S4		B04		2796				0,205
S5		A05	1,000	1644	1599	45	2,8	0,118
S5		B05		1554				0,112
S6		A06	1,000	868	838	30	3,6	61,06E-3
S6		B06		808				56,70E-3
S7		A07	1,000	578	563	15	2,7	40,10E-3
S7		B07		548				37,95E-3
X1		C01	1,000	2842	2660	182	6,8	0,208
X1		D01		2478				0,181
X2		C02	1,000	7866	7016	851	12,1	0,597
X2		D02		6165				0,464
X3		C03	1,000	4409	4134	276	6,7	0,328
X3		D03		3858				0,286
X4		C04	1,000	6963	6625	338	5,1	0,526
X4		D04		6287				0,473
X5		C05	1,000	4840	4484	356	7,9	0,361
X5		D05		4128				0,306
X6		C06	1,000	6391	6182	209	3,4	0,481
X6		D06		5973				0,449
X7		C07	1,000	8762	8409	354	4,2	0,667
X7		D07		8055				0,612
X8		C08	1,000	5812	5509	303	5,5	0,436
X8		D08		5206				0,389
X9		C09	1,000	5067	4867	200	4,1	0,379
X9		D09		4667				0,348

Figure 47: Raw data of RG measurement on 03.05.2013

Test Run: PICOGREEN CHRISTA 2013.06.12 20:46:40 1568.dbf

OPTIMA		Testname:	PICOGREEN CHRISTA	2013.06.12 20:46:40	Hide parameter settings
BMG LABTECH		ID 1,2,3:	12 06 2013 mir conc adina 2	1568.dbf	Hide standard curve

Fluorescence, plate mode
Evaluation type: Sum
Calculation: Start1: 1 Stop1: 1 Start2: 0 Stop2: 0
Selected: Range1
Table calculation: None
Curve fitting: Linear Regression; X-Axis log, Y-Axis log

m	8,496E-1
b	3,876E0
r	0,979065

Comment:

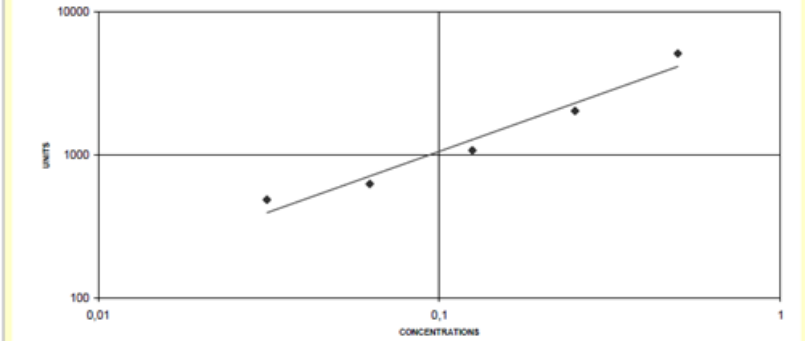

Test Run: PICOGREEN CHRISTA 2013.06.12 20:46:40 1568.dbf

	Sort contents		Sort sample IDs		Sort rows		Sort columns		Avg of replicates
	Up	Down	Up	Down	Up	Down	Up	Down	
	Content	Sample ID	Well	Dilution factor	Raw data	Avg of replicates	SD of replicates	%CV	Calculated concentr.
	B		A08	1,000	34	38	4	10,5	1,74E-3
	B		B08		42				2,23E-3
	s1		A01						
	s1		B01						
	s2		A02						
	s2		B02						
	S3		A03	1,000	5567	5153	414	8,0	0,702
	S3		B03		4739				0,581
	S4		A04	1,000	2510	2042	469	22,9	0,275
	S4		B04		1573				0,159
	S5		A05	1,000	1169	1083	87	8,0	0,112
	S5		B05		996				92,64E-3
	S6		A06	1,000	607	629	22	3,5	51,72E-3
	S6		B06		651				56,16E-3
	S7		A07	1,000	471	489	18	3,6	38,37E-3
	S7		B07		506				41,75E-3
	X1		C01	1,000	1273	946	327	34,6	0,124
	X1		D01		619				52,93E-3
	X2		C02	1,000	831	773	58	7,5	74,86E-3
	X2		D02		715				62,72E-3
	X3		C03	1,000	822	718	104	14,5	73,91E-3
	X3		D03		614				52,43E-3
	X4		C04	1,000	949	884	65	7,4	87,52E-3
	X4		D04		819				73,59E-3
	X5		C05	1,000	1047	1018	29	2,8	98,25E-3
	X5		D05		989				91,88E-3
	X6		C06	1,000	1255	1183	72	6,1	0,122
	X6		D06		1111				0,105
	X7		C07	1,000	1096	1066	30	2,8	0,104
	X7		D07		1036				97,04E-3
	X8		C08	1,000	1384	1352	32	2,4	0,136
	X8		D08		1320				0,129
	X9		C09	1,000	1126	1097	30	2,7	0,107
	X9		D09		1067				0,100
	X10		C10	1,000	2109	2288	179	7,8	0,224
	X10		D10		2467				0,269
	X11		C11	1,000	689	693	4	0,6	60,04E-3
	X11		D11		697				60,86E-3
	X12		C12	1,000	393	521	128	24,6	31,01E-3
	X12		D12		649				55,96E-3
	X13		E01	1,000	790	1027	237	23,1	70,53E-3
	X13		F01		1264				0,123

Gray fields contain deleted values.

Figure 48: Raw data of RG measurement on 12.06.2013

Test Run: PICOGREEN CHRISTA 2013.07.10 16:10:52 1672.dbf

OPTIMA BMG LABTECH	Testname: PICOGREEN CHRISTA ID 1,2,3: 10 07 2013 miRconc adina	2013.07.10 16:10:52 1672.dbf	☐ Hide parameter settings ☐ Hide standard curve	

Fluorescence, plate mode
Evaluation type: Sum
Calculation: Start1: 1 Stop1: 1 Start2: 0 Stop2: 0
Selected: Range1
Table calculation: None
Curve fitting: Linear Regression; X-Axis log, Y-Axis log

m	9,873E-1
b	3,560E0
r	0,995962

Comment:

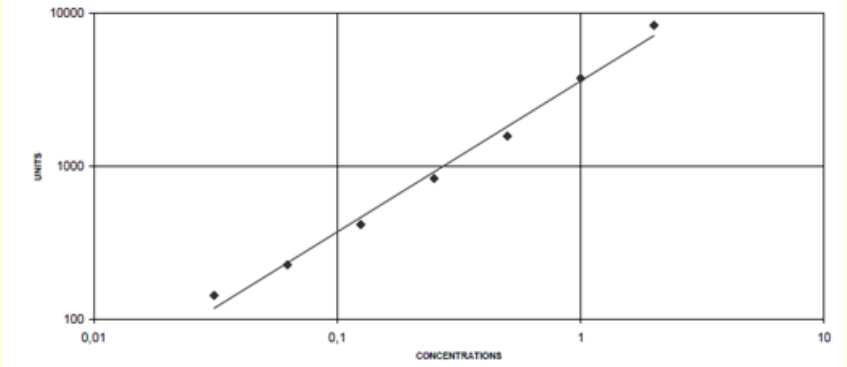

Test Run: PICOGREEN CHRISTA 2013.07.10 16:10:52 1672.dbf

	Sort contents		Sort sample IDs		Sort rows		Sort columns		☐ Avg. of replicates
	◉ Up ○ Down		○ Up ○ Down		○ Up ○ Down		○ Up ○ Down		
	Content	Sample ID	Well	Dilution factor	Raw data	Avg of replicates	SD of replicates	%CV	Calculated concentr.
	B		B10	1,000	19	18	2	8,6	4,89E-3
	B		C10		16				4,11E-3
	S1		B03	1,000	8359	8393	34	0,4	2,328
	S1		C03		8427				2,347
	S2		B04	1,000	3803	3787	16	0,4	1,049
	S2		C04		3771				1,040
	S3		B05	1,000	1630	1582	49	3,1	0,445
	S3		C05		1533				0,418
	S4		B06	1,000	883	835	49	5,8	0,239
	S4		C06		786				0,212
	S5		B07	1,000	416	418	2	0,5	0,111
	S5		C07		420				0,113
	S6		B08	1,000	226	228	2	0,7	60,09E-3
	S6		C08		229				60,90E-3
	S7		B09	1,000	132	144	12	8,0	34,85E-3
	S7		C09		155				41,01E-3
	X1		D02	1,000	785	741	45	6,0	0,212
	X1		E02		696				0,188
	X2		D03	1,000	3321	3008	314	10,4	0,914
	X2		E03		2694				0,739
	X3		D04	1,000	4074	3832	242	6,3	1,124
	X3		E04		3590				0,989
	X4		D05	1,000	1162	1071	91	8,5	0,316
	X4		E05		980				0,266
	X5		D06	1,000	387	369	19	5,0	0,104
	X5		E06		350				93,58E-3
	X6		D07	1,000	2290	2150	140	6,5	0,627
	X6		E07		2010				0,550
	X7		D08	1,000	3459	3220	239	7,4	0,953
	X7		E08		2981				0,819
	X8		D09	1,000	2270	2125	145	6,8	0,622
	X8		E09		1980				0,541
	X9		D10	1,000	2559	2466	94	3,8	0,702
	X9		E10		2372				0,650
	X10		D11	1,000	1744	1703	41	2,4	0,476
	X10		E11		1662				0,453

Figure 49: Raw data of RG measurement on 10.07.2013

5.3. miR-451expression levels normalized to U6 reference gene (Δct)

MiR-451 expression levels normalized to U6 reference gene as Δct values were calculated as a difference between the means of the threshold cycle's duplicates and are presented in Tab.15.

Table 15: miR-451expression levels normalized to U6 as Δct values

	Δct = mean ct (miR-451) – mean ct (U6)											
	Exp. date	**healthy**	**sh d1**	**sev d1**	**sh d4**	**sev d4**	**sh 1w**	**sev 1w**	**sh 2w**	**sev 2w**	**sh 3w**	**sev 3w**
set 1	30.04.13	10,04	11,47	10,69	12,25	10,54						9,96
	03.05.13	9,81	11,95	10,34	11,15	10,71						10,95
	14.05.13	10,72	12,23	11,76	12,49	12,18						11,36
	04.06.13	10,85			11,77	11,41						
	19.06.13	9,76					9,77	9,99	10,64	11,97		
	21.06.13	9,49					9,61	9,99	10,49	11,95		
set 2	02.05.13	9,18	12,76	10,30	10,88	12,61					10,64	13,54
	10.05.13	9,99	13,51	10,97	11,87	12,84					11,40	14,27
	04.06.13	10,85			10,86	12,27						
	19.06.13	9,76					11,02	11,41	9,50	11,85		
	21.06.13	9,49					11,00	11,49	9,48	11,72		
set 3	06.05.13	10,07	9,73	10,03	13,00	10,89					12,31	11,84
	10.05.13	10,34	9,75	10,00	13,08	11,34					12,34	11,53
	04.06.13	10,85			13,00	10,76						
	11.07.13	9,80					8,74	8,91	12,10	11,78		
	16.07.13	9,80					9,62	11,41	11,32	10,74		
set 4	08.05.13	9,91	11,92	9,08	12,95	14,71					11,32	11,28
	14.05.13	10,78	12,50	9,42	13,36	14,27					10,48	10,58
	04.06.13	10,85			13,17	14,83						
	11.07.13	9,80					9,07	11,62	10,17	10,78		
	16.07.13	9,80					10,31	12,99	10,25	12,14		
set 5	17.05.13	10,49									12,63	11,56
	11.07.13	9,80	8,29	9,77	11,69	12,11	8,36	11,43	8,53	12,03	12,09	11,05
	15.07.13	8,31	6,75	8,37	10,65	10,69	6,60	9,86	7,25	10,60	10,82	9,83

These values were used in Excel to generate the post-TBI miR451 temporal expression profile, illustrated in Fig.32.

5.4. miR-451expression alteration due to severe trauma (ΔΔct)

Alterations in miR-451 expression level due to "severe trauma" were represented as ΔΔct values, obtained by subtraction of "severe Δct" from "sham Δct", like Tab. 16 presents.

Table 16: ΔΔct, mean and SEM values for the five sets

		ΔΔct = Δct(sham) – Δct(severe)				
		1d	**4d**	**1w**	**2w**	**3w**
Set 1	30.04.2013	0,78	1,71			
	03.05.2013	1,61	0,43			
	14.05.2013	0,48	0,31			
	04.06.2013		0,36			
	19.06.2013			-0,22	-1,34	
	21.06.2013			-0,38	-1,46	
Set 2	02.05.2013	2,46	-1,73			-2,90
	10.05.2013	2,55	-0,97			-2,87
	04.06.2013		-1,41			
	19.06.2013			-0,39	-2,35	
	21.06.2013			-0,49	-2,24	
Set 3	06.05.2013	-0,31	2,12			0,47
	10.05.2013	-0,25	1,75			0,81
	04.06.2013		2,24			
	11.07.2013			-0,17	0,32	
	16.07.2013			-1,79	0,59	
Set 4	08.05.2013	2,84	-1,76			0,04
	14.05.2013	3,08	-0,91			-0,09
	04.06.2013		-1,66			
	11.07.2013			-2,55	-0,61	
	16.07.2013			-2,68	-1,89	
Set 5	17.05.2013					1,07
	11.07.2013	-1,48	-0,42	-3,07	-3,50	1,05
	15.07.2013	-1,63	-0,04	-3,27	-3,35	0,98
mean ΔΔct		**0,92**	**0,001**	**-1,50**	**-1,58**	**-0,16**
SEM		**0,51**	**0,37**	**0,41**	**0,44**	**0,53**
P values	p 1d & 1w	**0.0016**				
	P 1d & 2w	**0,0015**				

A positive ΔΔct value indicates an increase of miR-451 expression level, while a negative ΔΔct value reveals a miR-451 down-regulation, after severe brain trauma. In Excel were calculated also SEM and P values (see explanations at Chapter 2.5.3. and 2.5.4).

5.5. Raw data of qRT-PCRs

5.5.1. Amplification curves and melting peaks of the five sets

The amplification curves and related melting peaks for U6 reference gene and miR-451 target gene of the RT-PCR experiments, whose results were used to determine the post-TBI miR-451 expression profile (Fig.32), are presented in Fig.50-62. As already mentioned, U6 reference gene aimed to correct eventual sample-to-sample and run-to-run variations.

Following figures illustrate adequate amplification curves and single melting peaks of specific amplification products. No contamination are indicated via “green” (at amplification curves) or “blue” lines (at melting peaks) of the blank, RT(-) and MM samples.

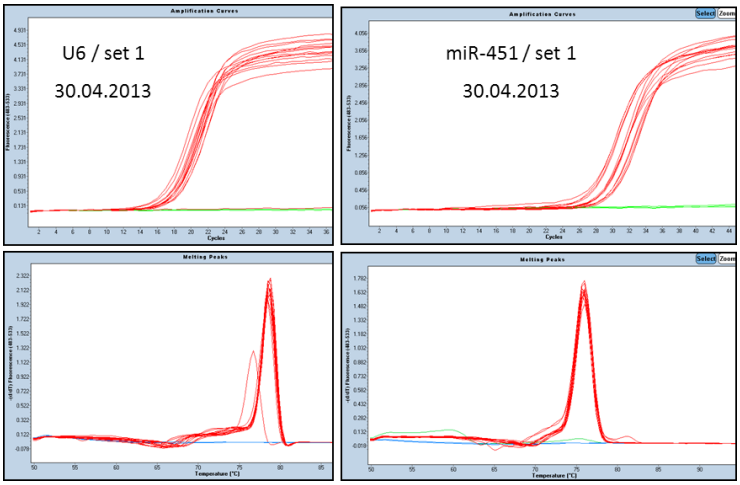

Figure 50: Amplification curves and melting peaks for set1 / 30.04.2013

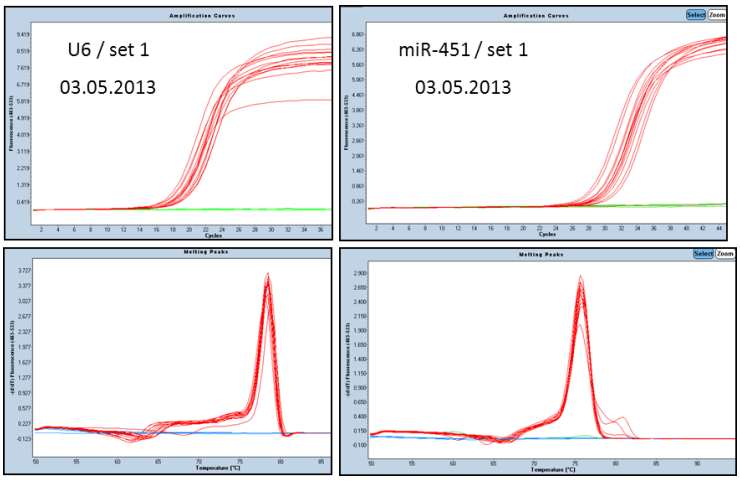

Figure 51: Amplification curves and melting peaks for set1 / 03.05.2013

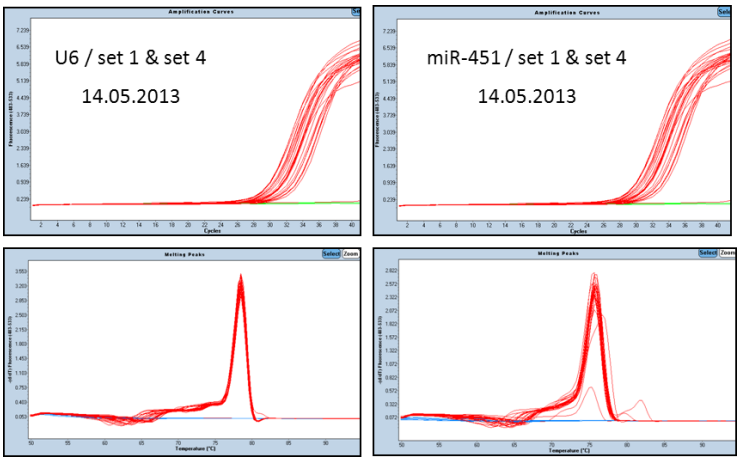

Figure 52: Amplification curves and melting peaks for set 1 & set 4 / 14.05.2013

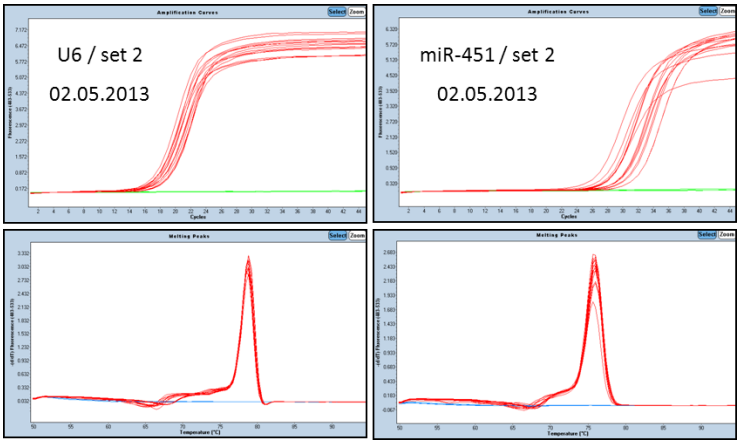

Figure 53: Amplification curves and melting peaks for set 2 / 02.05.2013

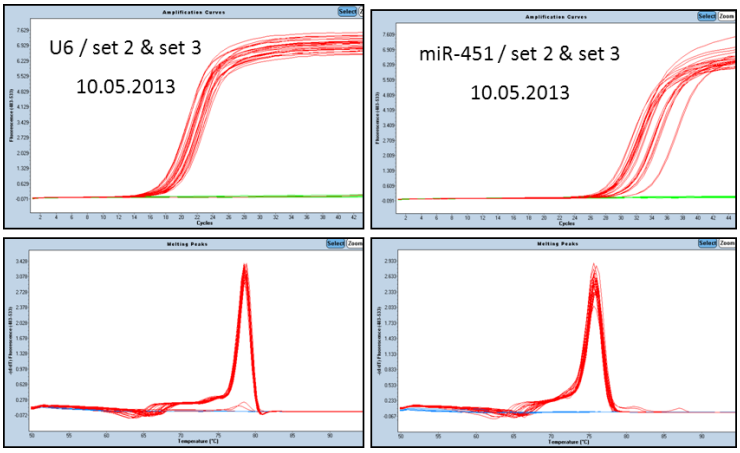

Figure 54: Amplification curves and melting peaks for set 2 & set 3 / 10.05.2013

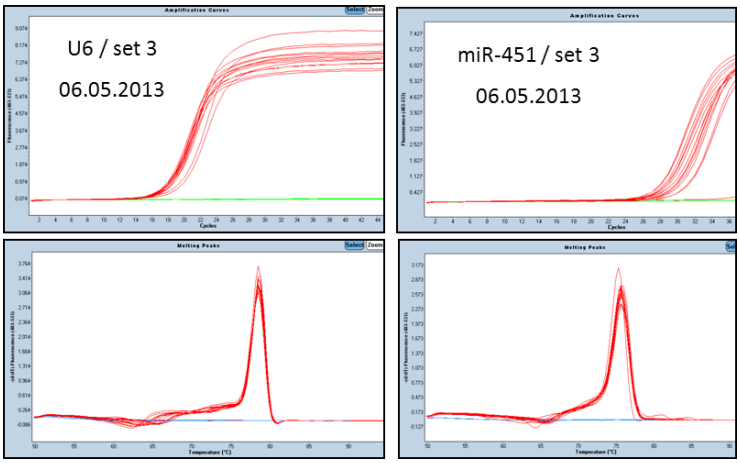

Figure 55: Amplification curves and melting peaks for set 3 / 06.05.2013

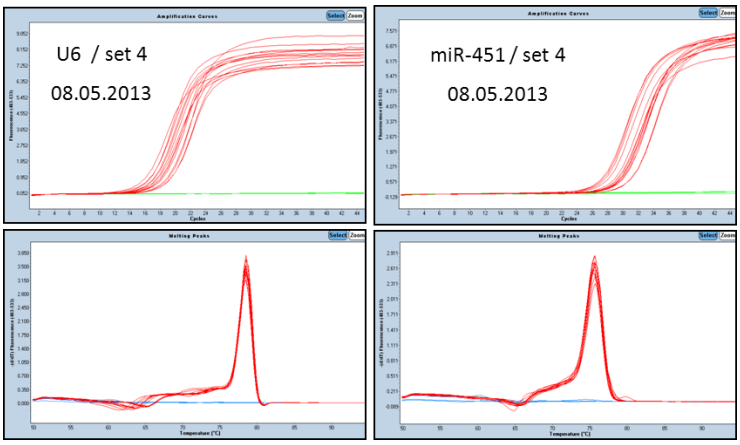

Figure 56: Amplification curves and melting peaks for set 2 & set 3 / 08.05.2013

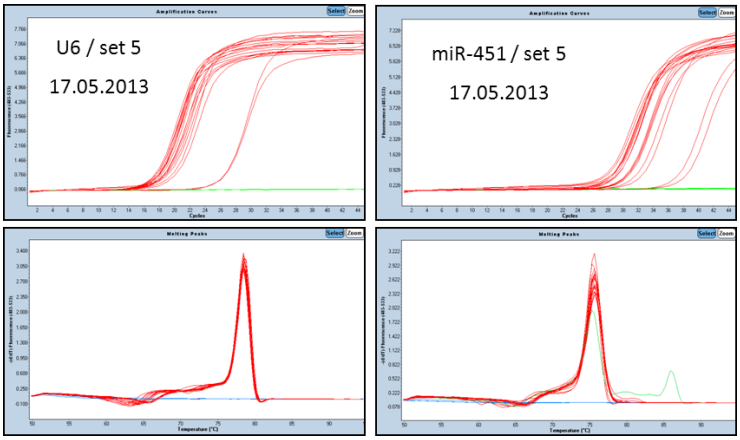

Figure 57: Amplification curves and melting peaks for set 5 / 17.05.2013

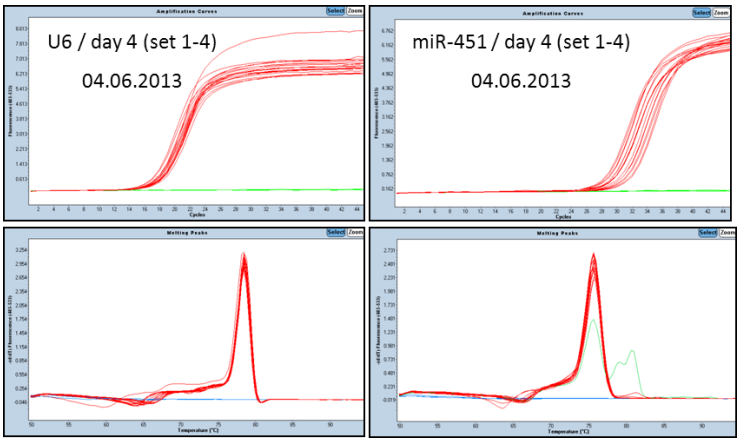

Figure 58: Amplification curves and melting peaks for day 4 (set 1-4) / 04.06.2013

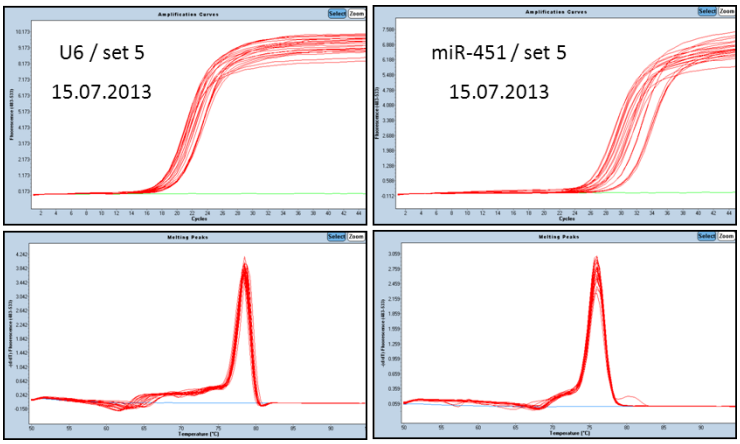

Figure 59: Amplification curves and melting peaks for set 5 / 15.07.2013

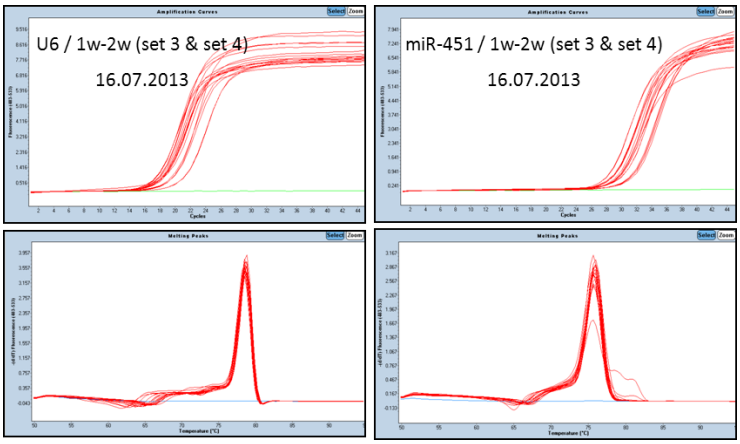

Figure 60: Amplification curves and melting peaks for 1w-2w (set 3 and set 4) /16.07.2013

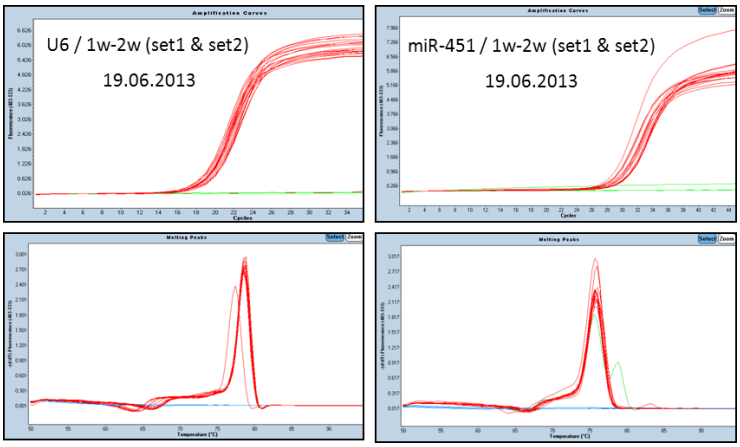

Figure 61: Amplification curves and melting peaks for 1w-2w (set 1 & set 2) /19.06.2013

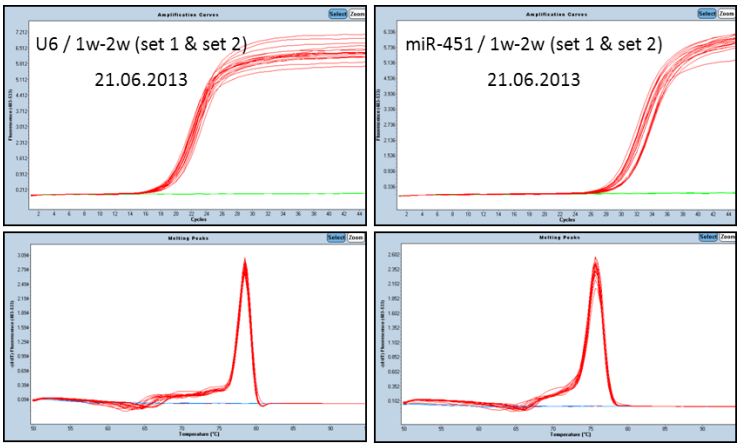

Figure 62: Amplification curves and melting peaks for 1w-2w (set 1 & set 2) / 21.06.2013

The RT-PCRs experiments (Fig.50-62), whose results (ct values) were used to determine the post-TBI miR-451 temporal expression profile of Fig.32, were operated at prior established RT-PCR conditions (see Chapter 3.3.).

“U6 for rat” and “human miR-451”, both from Exiqon, were used as primers.

The real-time PCR reactions were performed using “Roche Light-Cycler 480” at Qiagen cycling conditions (Tab.8), at which the annealing step was modified, according to the optimal annealing settings for the Exiqon primers (1min, 60°C / Tab.9).

5.5.2. Threshold cycle (ct) values of the five sets

Following tables (17 - 24) present the results of the qRT-PCR experiments (all measured threshold cycle “ct” values or crossing points “cp”) performed by “Roche Light-Cycler 480”, used to generate the post-TBI miR-451 temporal expression profile of Fig.32.

Table 17: ct values for set 1

set 1	**30.04.13**			**03.05.13**			**14.05.13**		
mir-451	**cp1**	**cp2**	**mean**	**cp1**	**cp2**	**mean**	**cp1**	**cp2**	**mean**
1450_h	28,63	28,30	28,47	29,68	29,65	29,67	30,99	30,88	30,94
1101_sh d1	29,30	29,32	29,31	-	30,52	30,52	32,67	32,72	32,70
763_sev d1	27,35	27,19	27,27	28,02	28,47	28,25	29,46	29,29	29,38
1080_sh d4	30,12	28,69	29,41	29,77	30,01	29,89	30,89	30,95	30,92
723_sev d4	28,88	28,59	28,74	30,10	30,16	30,13	31,80	31,62	31,71
1118_sh 3w	29,74	29,94	29,84	31,11	31,58	31,35	30,42	-	30,42
983_sev 3w	27,55	27,49	27,52	29,27	29,33	29,30	29,96	29,97	29,97
U6	**cp1**	**cp2**	**mean**	**cp1**	**cp2**	**mean**	**cp1**	**cp2**	**mean**
1450_h	18,28	18,58	18,43	19,78	19,93	19,86	20,02	20,42	20,22
1101_sh d1	17,76	17,93	17,85	19,02	18,13	18,58	20,66	20,27	20,47
763_sev d1	16,48	16,69	16,59	17,72	18,09	17,91	17,62	17,62	17,62
1080_sh d4	17,03	17,29	17,16	18,93	18,56	18,75	18,55	18,32	18,44
723_sev d4	17,86	18,53	18,20	18,94	19,9	19,42	19,56	19,50	19,53
1118_sh 3w	17,92	17,96	17,94	19,77	19,34	19,56	20,27	20,29	20,28
983_sev 3w	17,45	17,67	17,56	18,80	17,9	18,35	18,60	18,62	18,61

Table 18: ct values for set 2

set 2	02.05.13			10.05.13		
mir-451	**cp1**	**cp2**	**mean**	**cp1**	**cp2**	**mean**
1451_h	26,55	27,50	27,03	28,88	28,85	28,87
1100_sh d1	30,08	29,90	29,99	31,07	31,25	31,16
1188_sev d1	28,57	28,61	28,59	29,58	29,41	29,50
1083_sh d4	29,88	29,83	29,86	31,05	31,11	31,08
1258_sev d4	30,72	30,86	30,79	31,77	31,99	31,88
1119_sh 3w	27,92	28,16	28,04	29,15	29,34	29,25
976_sev 3w	31,81	31,81	31,81	33,83	33,98	33,91
U6	**cp1**	**cp2**	**mean**	**cp1**	**cp2**	**mean**
1451_h	17,62	18,08	17,85	18,76	18,99	18,88
1100_sh d1	17,00	17,46	17,23	17,48	17,82	17,65
1188_sev d1	18,16	18,42	18,29	18,23	18,83	18,53
1083_sh d4	18,98	18,97	18,98	18,97	19,45	19,21
1258_sev d4	17,80	18,56	18,18	19,00	19,09	19,05
1119_sh 3w	17,31	17,49	17,40	17,73	17,96	17,85
976_sev 3w	17,87	18,67	18,27	19,58	19,69	19,64

Table 19: ct values for set 3

set 3	06.05.13			10.05.13		
mir-451	**cp1**	**cp2**	**mean**	**cp1**	**cp2**	**mean**

1452_h	28,48	28,65	28,57	29,04	29,56	29,30
1103_sh d1	29,27	29,24	29,26	29,24	29,52	29,38
1189_sev d1	27,81	27,85	27,83	28,09	28,30	28,20
1082_sh d4	30,95	31,00	30,98	31,74	31,62	31,68
1245_sev d4	28,20	28,47	28,34	28,71	28,96	28,84
1120_sh 3w	29,82	30,20	30,01	30,86	30,78	30,82
1207_sev 3w	29,68	29,64	29,66	29,90	30,08	29,99
U6	**cp1**	**cp2**	**mean**	**cp1**	**cp2**	**mean**
1452_h	18,55	18,44	18,50	19,01	18,92	18,97
1103_sh d1	19,49	19,57	19,53	19,63	19,63	19,63
1189_sev d1	17,84	17,76	17,80	18,19	18,20	18,20
1082_sh d4	17,98	17,97	17,98	18,62	18,58	18,60
1245_sev d4	17,46	17,44	17,45	17,52	17,48	17,50
1120_sh 3w	17,69	17,72	17,71	18,48	18,49	18,49
1207_sev 3w	17,79	17,86	17,83	18,50	18,42	18,46

Table 20: ct values for set 4

set 4	**08.05.13**			**14.05.13**		
mir-451	**cp1**	**cp2**	**mean**	**cp1**	**cp2**	**mean**
1451_h	28,78	28,93	28,86	29,28	29,98	29,63
1032_sh d1	29,66	29,22	29,44	30,93	30,97	30,95

1187_sev d1	27,64	27,5	27,57	30,08	30,23	30,16
1038_sh d4	29,97	29,91	29,94	32,04	33,01	32,53
1256_sev d4	30,96	30,97	30,97	31,96	32,50	32,23
1152_sh 3w	29,53	27,23	28,38	-	29,86	29,86
1305_sev 3w	29,63	28,03	28,83	30,32	30,69	30,51
U6	**cp1**	**cp2**	**mean**	**cp1**	**cp2**	**mean**
1451_h	18,89	19,00	18,95	18,80	18,91	18,86
1032_sh d1	16,51	18,53	17,52	18,47	18,44	18,46
1187_sev d1	18,04	18,94	18,49	20,70	20,77	20,74
1038_sh d4	17,17	16,81	16,99	19,24	19,10	19,17
1256_sev d4	16,92	15,60	16,26	17,94	17,99	17,97
1152_sh 3w	16,53	17,59	17,06	19,47	19,29	19,38
1305_sev 3w	17,87	17,23	17,55	20,04	19,82	19,93

Table 21: ct values for set 5 and day 4 / set 1-4

samples	**17.05.13**			**day 4 / set 1 - 4**	**04.06.13**		
mir-451	**cp1**	**cp2**	**mean**	**mir-451**	**cp1**	**cp2**	**mean**
1450_h	28,64	28,74	28,69	1450_h	28,88	28,97	28,93
1102_sh d1_set5	28,03	28,11	28,07	1080_sh d4_set1	29,70	29,60	29,65
1103_sh d1_set3	29,03	29,19	29,11	723_sev d4_set1	29,60	29,56	29,58
763_sev d1_set1	28,59	28,57	28,58	1083_sh d4_set2	29,32	29,30	29,31

1081_sh d4_set5	30,65	30,49	30,57	1258_sev d4_set2	30,29	30,72	30,51
1256_sev d4_set5	31,61	32,55	32,08	1082_sh d4_set3	31,20	31,00	31,10
723_sev d4_set1	38,07	37,02	37,55	1245_sev d4_set3	28,31	28,49	28,40
1121_sh 3w_set5	30,42	30,46	30,44	1038_sh d4_set4	30,67	30,70	30,69
1206_sev 3w_set5	29,21	29,21	29,21	1256_sev d4_set4	31,84	31,73	31,79
U6	**cp1**	**cp2**	**mean**	**U6**	**cp1**	**cp2**	**mean**
1450_h	18,16	18,24	18,20	1450_h	18,07	18,08	18,08
1102_sh d1_set5	19,09	19,09	19,09	1080_sh d4_1	17,96	17,81	17,89
1103_sh d1_set3	19,76	19,87	19,82	723_sev d4_1	18,15	18,19	18,17
763_sev d1_set1	17,32	17,31	17,32	1083_sh d4_2	18,44	18,47	18,46
1081_sh d4_set5	18,48	18,49	18,49	1258_sev d4_2	18,23	18,25	18,24
1256_sev d4_set5	17,16	17,23	17,20	1082_sh d4_3	18,09	18,12	18,11
723_sev d4_set1	26,43	26,28	26,36	1245_sev d4_3	17,63	17,65	17,64
1121_sh 3w_set5	17,81	17,82	17,82	1038_sh d4_4	17,51	17,52	17,52
1206_sev 3w_set5	17,65	17,65	17,65	1256_sev d4_4	16,96	16,95	16,96

Table 22: ct values for set 1 and set 2 / 1w, 2w

set 1 and set 2	**19.06.13**			**21.06.13**		
mir-451	cp1	cp2	mean	cp1	cp2	mean
1452_H	29,19	29,54	29,37	29,24	29,07	29,16
1146_sh_1w_1	29,24	29,29	29,27	29,65	29,63	29,64

991_sev_1w_1	28,74	28,8	28,77	29,23	29,15	29,19
1148_sh_2w_1	29,42	29,49	29,46	29,54	29,71	29,63
985_sev_2w_1	30,21	30,26	30,24	30,54	30,62	30,58
1147_sh_1w_2	29,67	30,02	29,85	29,88	29,93	29,91
993_sev_1w_2	30,26	30,32	30,29	30,62	30,66	30,64
1150_sh_2w_2	28,56	28,63	28,60	28,85	29,2	29,03
987_sev_2w_2	30,32	30,46	30,39	30,55	30,72	30,64
U6	**cp1**	**cp2**	**mean**	**cp1**	**cp2**	**mean**
1452_H	19,62	19,60	19,61	19,64	19,69	19,67
1146_sh_1w_1	19,50	19,50	19,50	20,05	20,01	20,03
991_sev_1w_1	18,75	18,82	18,79	19,3	19,11	19,21
1148_sh_2w_1	18,78	18,86	18,82	19,14	19,13	19,14
985_sev_2w_1	18,27	18,26	18,27	18,58	18,68	18,63
1147_sh_1w_2	18,85	18,81	18,83	18,83	18,98	18,91
993_sev_1w_2	18,90	18,87	18,89	19,1	19,21	19,16
1150_sh_2w_2	19,07	19,12	19,10	19,53	19,57	19,55
987_sev_2w_2	18,55	18,53	18,54	18,95	18,88	18,92

Table 23: ct values for set 5

set 5	**11.07.13**			**15.07.13**		
mir-451	**cp1**	**cp2**	**mean**	**cp1**	**cp2**	**mean**

1450_h	28,65	28,83	28,74	27,16	27,12	27,14
1102_sh d1	27,64	27,73	27,69	26,93	26,84	26,89
765_sev d1	26,89	26,89	26,89	26,59	26,62	26,61
1081_sh d4	29,86	29,96	29,91	30,59	30,85	30,72
1242_sev d4	31,21	31,02	31,12	30,66	30,65	30,66
1459_sh 1w	26,54	26,53	26,54	25,79	25,96	25,88
1465_sev 1w	28,34	28,58	28,46	27,71	27,89	27,80
1284_sh 2w	26,94	26,78	26,86	26,5	26,47	26,49
1460_sev 2w	28,75	28,76	28,76	28,63	28,46	28,55
1121_sh 3w	29,58	29,74	29,66	29,61	29,53	29,57
1206_sev 3w	28,58	28,44	28,51	28,26	28,14	28,20
U6	**cp1**	**cp2**	**mean**	**cp1**	**cp2**	**mean**
1450_h	18,94	18,94	18,94	18,81	18,86	18,84
1102_sh d1	19,29	19,5	19,40	20,12	20,16	20,14
765_sev d1	17,09	17,16	17,13	18,28	18,19	18,24
1081_sh d4	18,20	18,25	18,23	20,14	20,00	20,07
1242_sev d4	18,99	19,02	19,01	20,04	19,9	19,97
1459_sh 1w	18,21	18,15	18,18	18,96	19,60	19,28
1465_sev 1w	17,02	17,05	17,04	18,02	17,86	17,94
1284_sh 2w	18,54	18,12	18,33	19,34	19,13	19,24
1460_sev 2w	16,71	16,74	16,73	17,88	18,01	17,95

1121_sh 3w	17,53	17,61	17,57	18,79	18,72	18,76
1206_sev 3w	17,30	17,63	17,47	18,32	18,42	18,37

Table 24: ct values for set 3 and set 4 / 1w, 2w

set 3 and set 4	**11.07.13**			**16.07.13**		
mir-451	cp1	cp2	mean	cp1	cp2	mean
1450_h	28,65	28,83	28,74	28,65	28,83	28,74
1288_sh 1w	27,52	27,84	27,68	28,77	29,78	29,28
1229_sev 1w	28,29	28,32	28,31	29,61	28,8	29,21
1151_sh 2w	29,23	29,21	29,22	29,63	31,24	30,44
1239_sev 2w	29,96	30,04	30,00	31,75	31,52	31,64
1458_sh 1w	28,08	28,06	28,07	27,97	28,86	28,42
1238_sev 1w	29,82	29,77	29,80	31,45	29,54	30,50
1283_sh 2w	27,18	27,22	27,20	27,98	28,89	28,44
1456_sev 2w	29,11	29,1	29,11	29,45	29,47	29,46
U6	**cp1**	**cp2**	**mean**	**cp1**	**cp2**	**mean**
1450_h	28,65	28,83	28,74	18,94	18,94	18,94
1288_sh1w	18,94	18,94	18,94	19,76	19,55	19,66
1229_sev 1w	19,29	19,5	19,40	17,78	17,82	17,80
1151_sh 2w	17,09	17,16	17,13	18,94	19,29	19,12
1239_sev 2w	18,2	18,25	18,23	20,86	20,94	20,90

1458_sh 1w	18,99	19,02	19,01	17,89	18,33	18,11
1238_sev 1w	18,21	18,15	18,18	17,9	17,12	17,51
1283_sh 2w	17,02	17,05	17,04	18,34	18,03	18,19
1456_sev 2w	18,54	18,12	18,33	17,46	17,18	17,32

5.6. Equipment

2720 Thermal Cycler	Applied BioSystems
Biofuge fresco centrifuge	Heraeus
Biofuge pico	Heraeus
Electrophoresis chamber Hoefer® HE33	Phamacia Biotech
Electrophoresis Power Supply Power Station 300	Labnet International
Fridge Premium No Frost	Liebherr
Heating block	HLC
Hera freeze	Heraeus

5.7. Consumpton of items, plastic ware, reagents, buffers

GelRed	Biotium	Cat No: 41002
LE Agarose	Biozym	Cat No: 340004

6x Gel Loading Buffer Stock:

Bromphenolblue 0.25%

Xylen Cyanol FF 0.25%

Glycerine in H2O 30%

Loading Buffer:

Gel Loading Buffer Stock	100µl
Glycerine	250µl
RNase free H2O	250µl

1x TBE Running Buffer (1000ml)

50ml 10xTBE Buffer (107.81g Tris, 55.03ml boric acid, 7.45ml Titriplex III)

950ml destilled water

1x TBE Buffer for Agarose Gels (1000ml)

50ml 10xTBE Buffer

950ml destilled water

100µl Gel Red

5.8. Marker

5.8.1. GeneRulerTM DNA Ladder Mix (0.1µg/µl, 50µg Fermentas)

5.9. Primers

5.9.1. U6 snRNA (has, mmu, rno) PCR primer set, UniRT (Exiqon)

(miRCURY LNA™ Universal RT microRNA PCR, reference gene primer set, 200 rxns)

Product No: 203907

5.9.2. hsa-miR-451a LNA™ PCR primer set, UniRT (Exiqon)

(target sequence: AAACCGUUACCAUUACUGAGUU)

Product No: 204734

5.10. Kits

5.10.1. Quant-iT™ RiboGreen® RNA Assay Kit (Invitrogen)

(Invitrogen Molecular Probes for 2000 reactions)

Ribosomal RNA-Standard	200µl
100µg/ml in TE-Buffer	
20x TE-Buffer	25ml
Quant-iT™ RiboGreen® RNA reagent	1ml

Cat. No: R11490

5.10.2. miScript PCR Starter Kit (80) (Qiagen)

For 10 x 20 µl RT reactions and 80 x 25 µl PCRs; miScript Reverse Transcriptase Mix, 10x miScript Nucleics Mix, 5x miScript HiSpec Buffer, 5x miScript HiFlex Buffer, 2x QuantiTect SYBR Green PCR Master Mix, 10x miScript Universal Primer, Human RNU6B (RNU6-2) miScript Primer Assay, Human miR-15a miScript Primer Assay, RNase-Free Water

Cat. No. 218193

5.10.3. miScript II RT Kit (50) (Qiagen)

(For 50 cDNA synthesis reactions: miScript Reverse Transcriptase Mix, 10x miScript Nucleics Mix, 5x miScript HiSpec Buffer, 5x miScript HiFlex Buffer, RNase-Free Water) / Cat. No: 218161

5.10.4. Universal cDNA Synthesis Kit II, 8-64 rxns (Exiqon)

(miRCURY LNA™ microRNA PCR, Polyadenylation and cDNA synthesis kit II (8-64 rxns)) / Product no.: 203301

5.10.5. miScript SYBR Green PCR Kit (200) (Qiagen)

(For 200 reactions: QuantiTect SYBR Green PCR Master Mix, miScript Universal Primer)

Cat. No: 218073

6. LITERATURE

1. Zhang Y, Liao Y, Wang D, He Y, Cao D, Zhang F, et al. Altered expression levels of miRNAs in serum as sensitive biomarkers for early diagnosis of traumatic injury. Journal of cellular biochemistry. 2011;112(9):2435-42.
2. <BlueBook_factsheet-a.pdf>.
3. Ghajar J. Traumatic brain injury. The Lancet. 2000;356(9233):923-9.
4. Werner C, Engelhard K. Pathophysiology of traumatic brain injury. British journal of anaesthesia. 2007;99(1):4-9.
5. Cook NL, Vink R, Donkin JJ, van den Heuvel C. Validation of reference genes for normalization of real-time quantitative RT-PCR data in traumatic brain injury. Journal of neuroscience research. 2009;87(1):34-41.
6. Goodlett CR, Horn KH. Mechanisms of alcohol-induced damage to the developing nervous system. Alcohol research & health : the journal of the National Institute on Alcohol Abuse and Alcoholism. 2001;25(3):175-84.
7. Van Cruchten S, Van Den Broeck W. Morphological and biochemical aspects of apoptosis, oncosis and necrosis. Anatomia, histologia, embryologia. 2002;31(4):214-23.
8. Lewis KM, Turner RJ, Vink R. Blocking neurogenic inflammation for the treatment of acute disorders of the central nervous system. International journal of inflammation. 2013;2013:578480.
9. Witt KA, Mark KS, Hom S, Davis TP. Effects of hypoxia-reoxygenation on rat blood-brain barrier permeability and tight junctional protein expression. American journal of physiology Heart and circulatory physiology. 2003;285(6):H2820-31.
10. Hawkins BT, Davis TP. The blood-brain barrier/neurovascular unit in health and disease. Pharmacological reviews. 2005;57(2):173-85.
11. Oliva AA, Jr., Kang Y, Sanchez-Molano J, Furones C, Atkins CM. STAT3 signaling after traumatic brain injury. Journal of neurochemistry. 2012;120(5):710-20.
12. Goldberg M, Gomez-Orellana I. Challenges for the oral delivery of macromolecules. Nature reviews Drug discovery. 2003;2(4):289-95.
13. <InTech-Excitotoxicity_and_oxidative_stress_in_acute_ischemic_stroke.pdf>.
14. Vink R, Nimmo AJ. Multifunctional drugs for head injury. Neurotherapeutics : the journal of the American Society for Experimental NeuroTherapeutics. 2009;6(1):28-42.

15. Potts MB, Koh SE, Whetstone WD, Walker BA, Yoneyama T, Claus CP, et al. Traumatic injury to the immature brain: inflammation, oxidative injury, and iron-mediated damage as potential therapeutic targets. NeuroRx : the journal of the American Society for Experimental NeuroTherapeutics. 2006;3(2):143-53.

16. Xiong Y, Mahmood A, Chopp M. Neurorestorative treatments for traumatic brain injury. Discovery medicine. 2010;10(54):434-42.

17. Xiong Y, Mahmood A, Chopp M. Angiogenesis, neurogenesis and brain recovery of function following injury. Current opinion in investigational drugs. 2010;11(3):298-308.

18. Varela-Nallar L, Inestrosa NC. Wnt signaling in the regulation of adult hippocampal neurogenesis. Frontiers in cellular neuroscience. 2013;7:100.

19. Oomen CA, Girardi CE, Cahyadi R, Verbeek EC, Krugers H, Joels M, et al. Opposite effects of early maternal deprivation on neurogenesis in male versus female rats. PloS one. 2009;4(1):e3675.

20. Doll H, Maegele M, Bohl J, Storkel S, Kipfmueller F, Schaefer U, et al. Pharyngeal selective brain cooling is associated with reduced CNS cortical lesion after experimental traumatic brain injury in rats. Journal of neurotrauma. 2010;27(12):2245-54.

21. Doll H, Truebel H, Kipfmueller F, Schaefer U, Neugebauer EA, Wirth S, et al. Pharyngeal selective brain cooling improves neurofunctional and neurocognitive outcome after fluid percussion brain injury in rats. Journal of neurotrauma. 2009;26(2):235-42.

22. Kulbatski I, Mothe AJ, Parr AM, Kim H, Kang CE, Bozkurt G, et al. Glial precursor cell transplantation therapy for neurotrauma and multiple sclerosis. Progress in histochemistry and cytochemistry. 2008;43(3):123-76.

23. Maegele M, Schaefer U. Stem cell-based cellular replacement strategies following traumatic brain injury (TBI). Minimally invasive therapy & allied technologies : MITAT : official journal of the Society for Minimally Invasive Therapy. 2008;17(2):119-31.

24. Richardson RM, Singh A, Sun D, Fillmore HL, Dietrich DW, 3rd, Bullock MR. Stem cell biology in traumatic brain injury: effects of injury and strategies for repair. Journal of neurosurgery. 2010;112(5):1125-38.

25. Shear DA, Tortella FC. A military-centered approach to neuroprotection for traumatic brain injury. Frontiers in neurology. 2013;4:73.

26. Sun D, Bullock MR, McGinn MJ, Zhou Z, Altememi N, Hagood S, et al. Basic fibroblast growth factor-enhanced neurogenesis contributes to cognitive recovery in rats following traumatic brain injury. Experimental neurology. 2009;216(1):56-65.

27. Wei HJ, Jiang RC, Liu L, Zhang JN. Circulating endothelial progenitor cells in traumatic brain injury: an emerging therapeutic target? Chinese journal of traumatology = Zhonghua chuang shang za zhi / Chinese Medical Association. 2010;13(5):316-8.

28. Christensen M, Schratt GM. microRNA involvement in developmental and functional aspects of the nervous system and in neurological diseases. Neuroscience letters. 2009;466(2):55-62.

29. Hu Z, Yu D, Almeida-Suhett C, Tu K, Marini AM, Eiden L, et al. Expression of miRNAs and their cooperative regulation of the pathophysiology in traumatic brain injury. PloS one. 2012;7(6):e39357.

30. Kosik KS. The neuronal microRNA system. Nature reviews Neuroscience. 2006;7(12):911-20.

31. Mestdagh P, Derveaux S, Vandesompele J. Whole-genome RT-qPCR microRNA expression profiling. Methods in molecular biology. 2012;815:121-30.

32. Olde Loohuis NF, Kos A, Martens GJ, Van Bokhoven H, Nadif Kasri N, Aschrafi A. MicroRNA networks direct neuronal development and plasticity. Cellular and molecular life sciences : CMLS. 2012;69(1):89-102.

33. Papapetrou EP, Korkola JE, Sadelain M. A genetic strategy for single and combinatorial analysis of miRNA function in mammalian hematopoietic stem cells. Stem cells. 2010;28(2):287-96.

34. Redell JB, Liu Y, Dash PK. Traumatic brain injury alters expression of hippocampal microRNAs: potential regulators of multiple pathophysiological processes. Journal of neuroscience research. 2009;87(6):1435-48.

35. Small EM, Olson EN. Pervasive roles of microRNAs in cardiovascular biology. Nature. 2011;469(7330):336-42.

36. Sundermeier TR, Palczewski K. The physiological impact of microRNA gene regulation in the retina. Cellular and molecular life sciences : CMLS. 2012;69(16):2739-50.

37. Thounaojam MC, Kaushik DK, Basu A. MicroRNAs in the brain: it's regulatory role in neuroinflammation. Molecular neurobiology. 2013;47(3):1034-44.

38. Xiao Y, Xu C, Guan J, Ping Y, Fan H, Li Y, et al. Discovering dysfunction of multiple microRNAs cooperation in disease by a conserved microRNA co-expression network. PloS one. 2012;7(2):e32201.

39. Liu NK, Xu XM. MicroRNA in central nervous system trauma and degenerative disorders. Physiological genomics. 2011;43(10):571-80.

40. Fineberg SK, Kosik KS, Davidson BL. MicroRNAs potentiate neural development. Neuron. 2009;64(3):303-9.

41. Hutchison ER, Okun E, Mattson MP. The therapeutic potential of microRNAs in nervous system damage, degeneration, and repair. Neuromolecular medicine. 2009;11(3):153-61.

42. Schratt G. Fine-tuning neural gene expression with microRNAs. Current opinion in neurobiology. 2009;19(2):213-9.

43. Dueck A, Ziegler C, Eichner A, Berezikov E, Meister G. microRNAs associated with the different human Argonaute proteins. Nucleic acids research. 2012;40(19):9850-62.

44. Yang JS, Maurin T, Lai EC. Functional parameters of Dicer-independent microRNA biogenesis. RNA. 2012;18(5):945-57.

45. Hui A, How C, Ito E, Liu FF. Micro-RNAs as diagnostic or prognostic markers in human epithelial malignancies. BMC cancer. 2011;11:500.

46. Bhalala OG, Srikanth M, Kessler JA. The emerging roles of microRNAs in CNS injuries. Nature reviews Neurology. 2013;9(6):328-39.

47. Ruberti F, Barbato C, Cogoni C. Targeting microRNAs in neurons: tools and perspectives. Experimental neurology. 2012;235(2):419-26.

48. Hebert SS, Nelson PT. Studying microRNAs in the brain: technical lessons learned from the first ten years. Experimental neurology. 2012;235(2):397-401.

49. O'Carroll D, Schaefer A. General principals of miRNA biogenesis and regulation in the brain. Neuropsychopharmacology : official publication of the American College of Neuropsychopharmacology. 2013;38(1):39-54.

50. Presutti C, Rosati J, Vincenti S, Nasi S. Non coding RNA and brain. BMC neuroscience. 2006;7 Suppl 1:S5.

51. Kinjo ER, Higa GS, de Sousa E, Casado OA, Damico MV, Britto LR, et al. A possible new mechanism for the control of miRNA expression in neurons. Experimental neurology. 2013.

52. Nowak JS, Michlewski G. miRNAs in development and pathogenesis of the nervous system. Biochemical Society transactions. 2013;41(4):815-20.

53. Shi Y, Sun G, Zhao C, Stewart R. Neural stem cell self-renewal. Critical reviews in oncology/hematology. 2008;65(1):43-53.

54. Barbato C, Giorgi C, Catalanotto C, Cogoni C. Thinking about RNA? MicroRNAs in the brain. Mammalian genome : official journal of the International Mammalian Genome Society. 2008;19(7-8):541-51.

55. Bian S, Sun T. Functions of noncoding RNAs in neural development and neurological diseases. Molecular neurobiology. 2011;44(3):359-73.

56. Bian S, Xu TL, Sun T. Tuning the cell fate of neurons and glia by microRNAs. Current opinion in neurobiology. 2013.

57. Hansen KF, Sakamoto K, Wayman GA, Impey S, Obrietan K. Transgenic miR132 alters neuronal spine density and impairs novel object recognition memory. PloS one. 2010;5(11):e15497.

58. He X, Yu Y, Awatramani R, Lu QR. Unwrapping myelination by microRNAs. The Neuroscientist : a review journal bringing neurobiology, neurology and psychiatry. 2012;18(1):45-55.

59. Nelson PT, Dimayuga J, Wilfred BR. MicroRNA in Situ Hybridization in the Human Entorhinal and Transentorhinal Cortex. Frontiers in human neuroscience. 2010;4:7.

60. Satterlee JS, Barbee S, Jin P, Krichevsky A, Salama S, Schratt G, et al. Noncoding RNAs in the brain. The Journal of neuroscience : the official journal of the Society for Neuroscience. 2007;27(44):11856-9.

61. Wang W, Kwon EJ, Tsai LH. MicroRNAs in learning, memory, and neurological diseases. Learning & memory. 2012;19(9):359-68.

62. Ziats MN, Rennert OM. Identification of differentially expressed microRNAs across the developing human brain. Molecular psychiatry. 2013.

63. Barca-Mayo O, Lu QR. Fine-Tuning Oligodendrocyte Development by microRNAs. Frontiers in neuroscience. 2012;6:13.

64. Zhao X, He X, Han X, Yu Y, Ye F, Chen Y, et al. MicroRNA-mediated control of oligodendrocyte differentiation. Neuron. 2010;65(5):612-26.

65. McKiernan RC, Jimenez-Mateos EM, Bray I, Engel T, Brennan GP, Sano T, et al. Reduced mature microRNA levels in association with dicer loss in human temporal lobe epilepsy with hippocampal sclerosis. PloS one. 2012;7(5):e35921.

66. Tao J, Wu H, Lin Q, Wei W, Lu XH, Cantle JP, et al. Deletion of astroglial Dicer causes non-cell-autonomous neuronal dysfunction and degeneration. The Journal of neuroscience : the official journal of the Society for Neuroscience. 2011;31(22):8306-19.

67. Gal-Ben-Ari S, Kenney JW, Ounalla-Saad H, Taha E, David O, Levitan D, et al. Consolidation and translation regulation. Learning & memory. 2012;19(9):410-22.

68. Fiore R, Khudayberdiev S, Saba R, Schratt G. MicroRNA function in the nervous system. Progress in molecular biology and translational science. 2011;102:47-100.

69. Lambert TJ, Storm DR, Sullivan JM. MicroRNA132 modulates short-term synaptic plasticity but not basal release probability in hippocampal neurons. PloS one. 2010;5(12):e15182.

70. Parsons MJ, Grimm CH, Paya-Cano JL, Sugden K, Nietfeld W, Lehrach H, et al. Using hippocampal microRNA expression differences between mouse inbred strains to characterise miRNA function. Mammalian genome : official journal of the International Mammalian Genome Society. 2008;19(7-8):552-60.

71. Pham JT, Gallicano GI. Specification of neural cell fate and regulation of neural stem cell proliferation by microRNAs. American journal of stem cells. 2012;1(3):182-95.

72. Sempere LF, Freemantle S, Pitha-Rowe I, Moss E, Dmitrovsky E, Ambros V. Expression profiling of mammalian microRNAs uncovers a subset of brain-expressed microRNAs with possible roles in murine and human neuronal differentiation. Genome biology. 2004;5(3):R13.

73. Luikart BW, Perederiy JV, Westbrook GL. Dentate gyrus neurogenesis, integration and microRNAs. Behavioural brain research. 2012;227(2):348-55.

74. Ming GL, Song H. Adult neurogenesis in the mammalian central nervous system. Annual review of neuroscience. 2005;28:223-50.

75. Muradov JM, Ewan EE, Hagg T. Dorsal column sensory axons degenerate due to impaired microvascular perfusion after spinal cord injury in rats. Experimental neurology. 2013;249C:59-73.

76. Saugstad JA. MicroRNAs as effectors of brain function with roles in ischemia and injury, neuroprotection, and neurodegeneration. Journal of cerebral blood flow and

metabolism : official journal of the International Society of Cerebral Blood Flow and Metabolism. 2010;30(9):1564-76.

77. Ziu M, Fletcher L, Rana S, Jimenez DF, Digicaylioglu M. Temporal differences in microRNA expression patterns in astrocytes and neurons after ischemic injury. PloS one. 2011;6(2):e14724.

78. Redell JB, Moore AN, Ward NH, 3rd, Hergenroeder GW, Dash PK. Human traumatic brain injury alters plasma microRNA levels. Journal of neurotrauma. 2010;27(12):2147-56.

79. Liu DZ, Tian Y, Ander BP, Xu H, Stamova BS, Zhan X, et al. Brain and blood microRNA expression profiling of ischemic stroke, intracerebral hemorrhage, and kainate seizures. Journal of cerebral blood flow and metabolism : official journal of the International Society of Cerebral Blood Flow and Metabolism. 2010;30(1):92-101.

80. Laterza OF, Lim L, Garrett-Engele PW, Vlasakova K, Muniappa N, Tanaka WK, et al. Plasma MicroRNAs as sensitive and specific biomarkers of tissue injury. Clinical chemistry. 2009;55(11):1977-83.

81. Kaur P, Armugam A, Jeyaseelan K. MicroRNAs in Neurotoxicity. Journal of toxicology. 2012;2012:870150.

82. Lei P, Li Y, Chen X, Yang S, Zhang J. Microarray based analysis of microRNA expression in rat cerebral cortex after traumatic brain injury. Brain research. 2009;1284:191-201.

83. Truettner JS, Alonso OF, Bramlett HM, Dietrich WD. Therapeutic hypothermia alters microRNA responses to traumatic brain injury in rats. Journal of cerebral blood flow and metabolism : official journal of the International Society of Cerebral Blood Flow and Metabolism. 2011;31(9):1897-907.

84. Truettner JS, Motti D, Dietrich WD. MicroRNA overexpression increases cortical neuronal vulnerability to injury. Brain research. 2013.

85. O'Connor RM, Grenham S, Dinan TG, Cryan JF. microRNAs as novel antidepressant targets: converging effects of ketamine and electroconvulsive shock therapy in the rat hippocampus. The international journal of neuropsychopharmacology / official scientific journal of the Collegium Internationale Neuropsychopharmacologicum. 2013;16(8):1885-92.

86. Patz S, Trattnig C, Grunbacher G, Ebner B, Gully C, Novak A, et al. More than cell dust: microparticles isolated from cerebrospinal fluid of brain injured patients are

messengers carrying mRNAs, miRNAs, and proteins. Journal of neurotrauma. 2013;30(14):1232-42.

87. Svasti S, Masaki S, Penglong T, Abe Y, Winichagoon P, Fucharoen S, et al. Expression of microRNA-451 in normal and thalassemic erythropoiesis. Annals of hematology. 2010;89(10):953-8.

88. Kouhkan F, Soleimani M, Daliri M, Behmanesh M, Mobarra N, Mossahebi Mohammadi M, et al. miR-451 Up-regulation, Induce Erythroid Differentiation of CD133+cells Independent of Cytokine Cocktails. Iranian journal of basic medical sciences. 2013;16(6):756-63.

89. Tsuchiya S, Oku M, Imanaka Y, Kunimoto R, Okuno Y, Terasawa K, et al. MicroRNA-338-3p and microRNA-451 contribute to the formation of basolateral polarity in epithelial cells. Nucleic acids research. 2009;37(11):3821-7.

90. Bianchi N, Zuccato C, Finotti A, Lampronti I, Borgatti M, Gambari R. Involvement of miRNA in erythroid differentiation. Epigenomics. 2012;4(1):51-65.

91. Bruchova-Votavova H, Yoon D, Prchal JT. miR-451 enhances erythroid differentiation in K562 cells. Leukemia & lymphoma. 2010;51(4):686-93.

92. Masaki S, Ohtsuka R, Abe Y, Muta K, Umemura T. Expression patterns of microRNAs 155 and 451 during normal human erythropoiesis. Biochemical and biophysical research communications. 2007;364(3):509-14.

93. Rathjen T, Nicol C, McConkey G, Dalmay T. Analysis of short RNAs in the malaria parasite and its red blood cell host. FEBS letters. 2006;580(22):5185-8.

94. Zhan M, Miller CP, Papayannopoulou T, Stamatoyannopoulos G, Song CZ. MicroRNA expression dynamics during murine and human erythroid differentiation. Experimental hematology. 2007;35(7):1015-25.

95. Rasmussen KD, Simmini S, Abreu-Goodger C, Bartonicek N, Di Giacomo M, Bilbao-Cortes D, et al. The miR-144/451 locus is required for erythroid homeostasis. The Journal of experimental medicine. 2010;207(7):1351-8.

96. Patrick DM, Zhang CC, Tao Y, Yao H, Qi X, Schwartz RJ, et al. Defective erythroid differentiation in miR-451 mutant mice mediated by 14-3-3zeta. Genes & development. 2010;24(15):1614-9.

97. Yu D, dos Santos CO, Zhao G, Jiang J, Amigo JD, Khandros E, et al. miR-451 protects against erythroid oxidant stress by repressing 14-3-3zeta. Genes & development. 2010;24(15):1620-33.

98. Kirschner MB, Kao SC, Edelman JJ, Armstrong NJ, Vallely MP, van Zandwijk N, et al. Haemolysis during sample preparation alters microRNA content of plasma. PloS one. 2011;6(9):e24145.

99. Podolska A, Anthon C, Bak M, Tommerup N, Skovgaard K, Heegaard PM, et al. Profiling microRNAs in lung tissue from pigs infected with Actinobacillus pleuropneumoniae. BMC genomics. 2012;13:459.

100. Hsieh CH, Yang JC, Jeng JC, Chen YC, Lu TH, Tzeng SL, et al. Circulating microRNA signatures in mice exposed to lipoteichoic acid. Journal of biomedical science. 2013;20:2.

101. Rosenberger CM, Podyminogin RL, Navarro G, Zhao GW, Askovich PS, Weiss MJ, et al. miR-451 regulates dendritic cell cytokine responses to influenza infection. Journal of immunology. 2012;189(12):5965-75.

102. Stoecklin-Wasmer C, Guarnieri P, Celenti R, Demmer RT, Kebschull M, Papapanou PN. MicroRNAs and their target genes in gingival tissues. Journal of dental research. 2012;91(10):934-40.

103. Wang H, Peng W, Ouyang X, Li W, Dai Y. Circulating microRNAs as candidate biomarkers in patients with systemic lupus erythematosus. Translational research : the journal of laboratory and clinical medicine. 2012;160(3):198-206.

104. Ning P, Liu DW, Mao YG, Peng Y, Lin ZW, Liu DM. [Differential expression profile of microRNA between hyperplastic scar and normal skin]. Zhonghua yi xue za zhi. 2012;92(10):692-4.

105. Chen H, Untiveros GM, McKee LA, Perez J, Li J, Antin PB, et al. Micro-RNA-195 and -451 regulate the LKB1/AMPK signaling axis by targeting MO25. PloS one. 2012;7(7):e41574.

106. Zhang X, Wang X, Zhu H, Zhu C, Wang Y, Pu WT, et al. Synergistic effects of the GATA-4-mediated miR-144/451 cluster in protection against simulated ischemia/reperfusion-induced cardiomyocyte death. Journal of molecular and cellular cardiology. 2010;49(5):841-50.

107. Wang X, Zhu H, Zhang X, Liu Y, Chen J, Medvedovic M, et al. Loss of the miR-144/451 cluster impairs ischaemic preconditioning-mediated cardioprotection by targeting Rac-1. Cardiovascular research. 2012;94(2):379-90.

108. Pan X, Wang R, Wang ZX. The potential role of miR-451 in cancer diagnosis, prognosis, and therapy. Molecular cancer therapeutics. 2013;12(7):1153-62.

109. Wu LN, Wei XW, Fan Y, Miao JN, Wang LL, Zhang Y, et al. Altered expression of 14-3-3zeta protein in spinal cords of rat fetuses with spina bifida aperta. PloS one. 2013;8(8):e70457.

110. Tian Y, Nan Y, Han L, Zhang A, Wang G, Jia Z, et al. MicroRNA miR-451 downregulates the PI3K/AKT pathway through CAB39 in human glioma. International journal of oncology. 2012;40(4):1105-12.

111. Nan Y, Han L, Zhang A, Wang G, Jia Z, Yang Y, et al. MiRNA-451 plays a role as tumor suppressor in human glioma cells. Brain research. 2010;1359:14-21.

112. Gal H, Pandi G, Kanner AA, Ram Z, Lithwick-Yanai G, Amariglio N, et al. MIR-451 and Imatinib mesylate inhibit tumor growth of Glioblastoma stem cells. Biochemical and biophysical research communications. 2008;376(1):86-90.

113. Godlewski J, Bronisz A, Nowicki MO, Chiocca EA, Lawler S. microRNA-451: A conditional switch controlling glioma cell proliferation and migration. Cell Cycle. 2010;9(14):2742-8.

114. Godlewski J, Nowicki MO, Bronisz A, Nuovo G, Palatini J, De Lay M, et al. MicroRNA-451 regulates LKB1/AMPK signaling and allows adaptation to metabolic stress in glioma cells. Molecular cell. 2010;37(5):620-32.

115. Xie Z, Chen G, Zhang X, Li D, Huang J, Yang C, et al. Salivary microRNAs as promising biomarkers for detection of esophageal cancer. PloS one. 2013;8(4):e57502.

116. Wang T, Zang WQ, Li M, Wang N, Zheng YL, Zhao GQ. Effect of miR-451 on the biological behavior of the esophageal carcinoma cell line EC9706. Digestive diseases and sciences. 2013;58(3):706-14.

117. Li C, Liu T, Qi F, Li F, Zhu L, Wang P, et al. Analysis of intragraft MicroRNA expression in a mouse-to-rat cardiac xenotransplantation model. Microsurgery. 2013.

118. Wang Z, Zhang H, Zhang P, Li J, Shan Z, Teng W. Upregulation of miR-2861 and miR-451 expression in papillary thyroid carcinoma with lymph node metastasis. Medical oncology. 2013;30(2):577.

119. Li X, Sanda T, Look AT, Novina CD, von Boehmer H. Repression of tumor suppressor miR-451 is essential for NOTCH1-induced oncogenesis in T-ALL. The Journal of experimental medicine. 2011;208(4):663-75.

120. Brenner B, Hoshen MB, Purim O, David MB, Ashkenazi K, Marshak G, et al. MicroRNAs as a potential prognostic factor in gastric cancer. World journal of gastroenterology : WJG. 2011;17(35):3976-85.

121. Konishi H, Ichikawa D, Komatsu S, Shiozaki A, Tsujiura M, Takeshita H, et al. Detection of gastric cancer-associated microRNAs on microRNA microarray comparing pre- and post-operative plasma. British journal of cancer. 2012;106(4):740-7.

122. Ali S, Saleh H, Sethi S, Sarkar FH, Philip PA. MicroRNA profiling of diagnostic needle aspirates from patients with pancreatic cancer. British journal of cancer. 2012;107(8):1354-60.

123. Li HY, Zhang Y, Cai JH, Bian HL. MicroRNA-451 inhibits growth of human colorectal carcinoma cells via downregulation of Pi3k/Akt pathway. Asian Pacific journal of cancer prevention : APJCP. 2013;14(6):3631-4.

124. Bitarte N, Bandres E, Boni V, Zarate R, Rodriguez J, Gonzalez-Huarriz M, et al. MicroRNA-451 is involved in the self-renewal, tumorigenicity, and chemoresistance of colorectal cancer stem cells. Stem cells. 2011;29(11):1661-71.

125. Bian HB, Pan X, Yang JS, Wang ZX, De W. Upregulation of microRNA-451 increases cisplatin sensitivity of non-small cell lung cancer cell line (A549). Journal of experimental & clinical cancer research : CR. 2011;30:20.

126. Wang R, Wang ZX, Yang JS, Pan X, De W, Chen LB. MicroRNA-451 functions as a tumor suppressor in human non-small cell lung cancer by targeting ras-related protein 14 (RAB14). Oncogene. 2011;30(23):2644-58.

127. Caruso P, MacLean MR, Khanin R, McClure J, Soon E, Southgate M, et al. Dynamic changes in lung microRNA profiles during the development of pulmonary hypertension due to chronic hypoxia and monocrotaline. Arteriosclerosis, thrombosis, and vascular biology. 2010;30(4):716-23.

128. Li HP, Zeng XC, Zhang B, Long JT, Zhou B, Tan GS, et al. miR-451 inhibits cell proliferation in human hepatocellular carcinoma through direct suppression of IKK-beta. Carcinogenesis. 2013.

129. Redova M, Poprach A, Nekvindova J, Iliev R, Radova L, Lakomy R, et al. Circulating miR-378 and miR-451 in serum are potential biomarkers for renal cell carcinoma. Journal of translational medicine. 2012;10:55.

130. Zhang Z, Luo X, Ding S, Chen J, Chen T, Chen X, et al. MicroRNA-451 regulates p38 MAPK signaling by targeting of Ywhaz and suppresses the mesangial hypertrophy in early diabetic nephropathy. FEBS letters. 2012;586(1):20-6.

131. Dai N, Zhong ZY, Cun YP, Qing Y, Chen C, Jiang P, et al. Alteration of the microRNA expression profile in human osteosarcoma cells transfected with APE1 siRNA. Neoplasma. 2013;60(4):384-94.

132. Namlos HM, Meza-Zepeda LA, Baroy T, Ostensen IH, Kresse SH, Kuijjer ML, et al. Modulation of the osteosarcoma expression phenotype by microRNAs. PloS one. 2012;7(10):e48086.

133. Jones KB, Salah Z, Del Mare S, Galasso M, Gaudio E, Nuovo GJ, et al. miRNA signatures associate with pathogenesis and progression of osteosarcoma. Cancer research. 2012;72(7):1865-77.

134. Bergamaschi A, Katzenellenbogen BS. Tamoxifen downregulation of miR-451 increases 14-3-3zeta and promotes breast cancer cell survival and endocrine resistance. Oncogene. 2012;31(1):39-47.

135. Ng EK, Li R, Shin VY, Jin HC, Leung CP, Ma ES, et al. Circulating microRNAs as specific biomarkers for breast cancer detection. PloS one. 2013;8(1):e53141.

136. Yang JS, Lai EC. Dicer-independent, Ago2-mediated microRNA biogenesis in vertebrates. Cell Cycle. 2010;9(22):4455-60.

137. Yang JS, Maurin T, Robine N, Rasmussen KD, Jeffrey KL, Chandwani R, et al. Conserved vertebrate mir-451 provides a platform for Dicer-independent, Ago2-mediated microRNA biogenesis. Proceedings of the National Academy of Sciences of the United States of America. 2010;107(34):15163-8.

138. Cheloufi S, Dos Santos CO, Chong MM, Hannon GJ. A dicer-independent miRNA biogenesis pathway that requires Ago catalysis. Nature. 2010;465(7298):584-9.

139. Cifuentes D, Xue H, Taylor DW, Patnode H, Mishima Y, Cheloufi S, et al. A novel miRNA processing pathway independent of Dicer requires Argonaute2 catalytic activity. Science. 2010;328(5986):1694-8.

140. Fanselow MS, Dong HW. Are the dorsal and ventral hippocampus functionally distinct structures? Neuron. 2010;65(1):7-19.

141. <EN-miScript-PCR-System-Handbook.pdf>.

142. <Einführung in Statistik.pdf>.